Versatile Approaches to Engineering and Applied Sciences: **Materials and Methods**

Dr. Arif Hikmet Çakoğlu
Dr. Muhammet Raşit Sancar

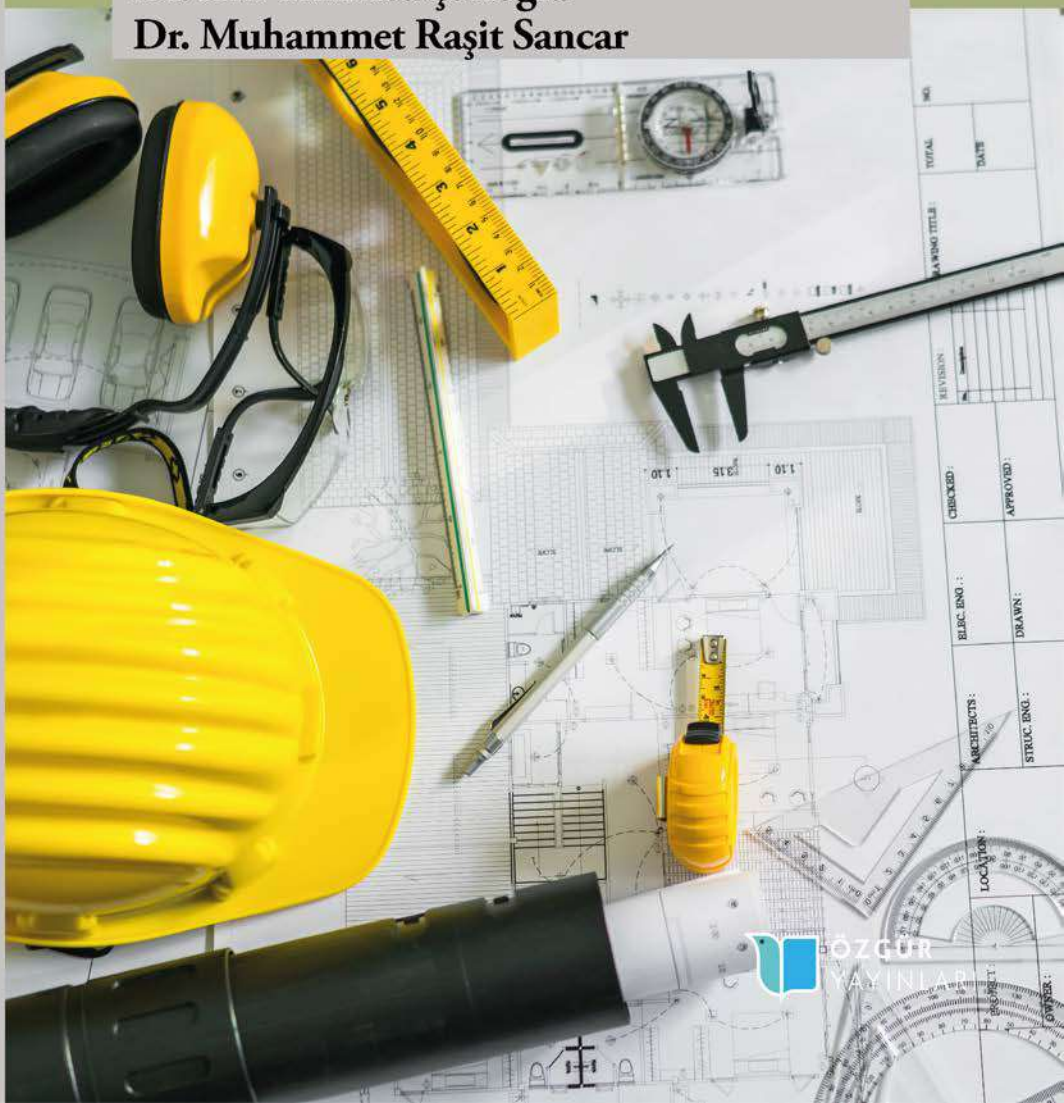

ÖZGÜR YAYINLARI

Versatile Approaches to Engineering and Applied Sciences: Materials and Methods

Dr. Arif Hikmet Çakoğlu
Dr. Muhammet Raşit Sancar

ÖZGÜR YAYINLARI

Published by
Özgür Yayın-Dağıtım Co. Ltd.
Certificate Number: 45503

15 Temmuz Mah. 148136. Sk. No: 9 Şehitkamil/Gaziantep
+90.850 260 09 97
+90.532 289 82 15
www.ozguryayınlari.com
info@ozguryayinlari.com

Versatile Approaches to Engineering and Applied Sciences: Materials and Methods

Dr. Arif Hikmet Çakoğlu • Dr. Muhammet Raşit Sancar

Language: Turkish
Publication Date: 2023
Cover design by Mehmet Çakır
Cover design and image licensed under CC BY-NC 4.0
Print and digital versions typeset by Çizgi Medya Co. Ltd.

ISBN (PDF): 978-975-447-569-2

DOI: https://doi.org/10.58830/ozgur.pub50

This work is licensed under the Creative Commons Attribution-NonCommercial 4.0 International (CC BY-NC 4.0). To view a copy of this license, visit https://creativecommons.org/licenses/by-nc/4.0/ This license allows for copying any part of the work for personal use, not commercial use, providing author attribution is clearly stated.

Suggested citation:
Çakoğlu, A.H., (2023). *Versatile Approaches to Engineering and Applied Sciences: Materials and Methods.* Özgür Publications. DOI: https://doi.org/10.58830/ozgur.pub50. License: CC-BY-NC 4.0

The full text of this book has been peer-reviewed to ensure high academic standards. For full review policies, see https://www.ozguryayinlari.com/

ÖZGÜR YAYINLARI

Ön Söz

Mühendislik ve fen alanında yapılan çalışmalar, insan hayatını kolaylaştıran, refah seviyesini yükseltmeyi amaç edinmiştir. Geçtiğimiz yüzyıllardaki tarım toplumlarından sanayi devrimleri sonrası bulunan icatlara, dünyada özellikle son 40-50 yıldaki yenilikler; cep telefonundan akıllı telefonlara, drone teknolojisi, sağlık hizmetlerindeki gelişmeler örnek olarak verilebilir. Dünyamız nüfusunun 1950'lerde 3 milyardan günümüzde 8 milyara çıktığını düşünürsek; kara parçalarının yani toprağın sabit olduğunu da dikkate aldığımızda, var olan kaynakların en verimli şekilde değerlendirilmesi zaruret arz etmektedir. Küresel iklim değişikliğinin artık daha fazla hissedilmesi tüm mühendislik ve fen bilim dalları arasında disiplinler arası çalışmaların önemini artırmıştır. Artık var olan en küçük maddeden en iyi sonucu alabilmek, insanların gelecek nesillere bırakacağı en değerli miras olarak kabul edilecektir. Bu nedenle, temelinde deneysel, araştırmacı düşünceler olan ve farklı disiplinler arasında da ilişkilendirilebilen tüm çalışmaların, insan hayatına ve doğanın sürdürülebilirliğine katkı sağlaması beklentisi daima olacaktır. Elinizdeki kitapta, bilim insanlarımızın alanlarıyla ilgili ve disiplinler arası yeni gelişmelere açık çalışmalarını bulacaksınız.

Bilimsel çalışmalarıyla kitaba ve mühendislik bilimine yapmış oldukları katkılarından dolayı değerli bilim insanlarımıza teşekkür eder, başta fen ve mühendislik olmak üzere disiplinler arası çalışmalar yapmakta olan araştırmacı ve tüm bilim severlere hayırlı olmasını dilerim.

Dr. Öğr. Üyesi Arif Hikmet ÇAKOĞLU

Ocak, 2023

Preface

Studies in the field of engineering and science aim to increase the level of welfare and facilitate human life. From the agricultural societies of the past centuries to the inventions after the industrial revolutions, innovations in the world, especially in the last 40-50 years; From mobile phones to smart phones, drone technology and developments in healthcare can be given as examples. Considering that the population of our world increased from 3 billion in the 1950s to 8 billion today; Considering that the land is fixed, it is necessary to use the existing resources in the most efficient way. The fact that global climate change is felt more and more has increased the importance of interdisciplinary studies among all engineering and science branches. Getting the best out of the smallest material that exists now will be considered the most valuable legacy that people will leave to future generations. For this reason, there will always be an expectation that all studies, which are based on experimental and research ideas and can be associated between different disciplines, will contribute to human life and the sustainability of nature. In the book in your hand, you will find the works of our scientists that are open to new developments in their fields and interdisciplinary.

I would like to thank our esteemed scientists for their contributions to the book and engineering science with their scientific studies, and I wish good luck to researchers and all science lovers who are doing interdisciplinary studies, especially science and engineering

Asst. Prof. Dr. Arif Hikmet ÇAKOĞLU

January, 2023

Değerli okuyucular,

Bu kitap, mühendislik disiplininde önemli bir yer tutan konuları ele almaktadır. Mühendislik, doğal kaynakların ve fiziksel süreçlerin bilimsel prensiplerle kullanılması ve işlenmesi yoluyla teknolojik çözümler üretmek için kullanılan bir disiplindir. Mühendisler, zorlu mühendislik problemlerini çözmek, yenilikçi teknolojiler geliştirmek ve sürdürülebilir çözümler sağlamak için birçok farklı disiplinden yararlanır.

Bu kitap, mühendisliğin temel ilkelerine odaklanmaktadır. Okuyucular, bir çok alanda temel ve detaylandırılmış bilgilere ulaşabileceklerdir. Kitapta, mühendislik problemlerinin çözümünde kullanılan matematiksel ve bilimsel yöntemler de ele alınmaktadır.

Mühendislik, teknolojik ilerlemenin itici gücüdür. Geliştirilen teknolojiler, tıp, çevre, enerji ve birçok farklı alanlarda insanların hayatını kolaylaştırmakta ve iyileştirmektedir. Mühendisler, dünya çapında yapılan çalışmalar sayesinde birçok zorlu mühendislik probleminin üstesinden gelmektedirler.

Bu kitap, öğrencilerin, araştırmacıların ve mühendislerin mühendislik disiplininin temellerini anlamalarına yardımcı olacak bir kaynak olarak tasarlanmıştır. Umarız bu kitap, mühendislik kariyeri hedefleyenler için ilham verici olur ve mühendisliğin önemini anlamalarına yardımcı olur.

Saygılarımla,

Muhammet Raşit SANCAR

Dear readers,

This book covers the important topics in the field of engineering. Engineering is a discipline that uses scientific principles to process and utilize natural resources and physical processes to create technological solutions. Engineers draw from many different disciplines to solve challenging engineering problems, develop innovative technologies, and provide sustainable solutions.

This book focuses on the fundamental principles of engineering. Readers will have access to basic and detailed information in many different areas. The book also covers the mathematical and scientific methods used to solve engineering problems.

Engineering is the driving force behind technological progress. The technologies developed in the field make life easier and better for people in areas such as medicine, the environment, energy, and many others. Engineers are able to overcome many challenging engineering problems thanks to work done worldwide.

This book is designed as a resource to help students, researchers, and engineers understand the fundamentals of the engineering discipline. We hope that this book will inspire those who aspire to a career in engineering and help them understand the importance of engineering.

Sincerely,

Muhammet Raşit SANCAR

Contents

CHAPTER 1

Analysis of the Conditions for Issuing Work Experience Documents in Construction Work Tenders

Lecturer Dr. Arif Hikmet ÇAKOĞLU[1]

INTRODUCTION

In our country, the State Procurement Law No. 2886 and the Public Procurement Law No. 4734 are in force in order to eliminate the construction and major maintenance and repair needs of public institutions. Of these, the State Procurement Law No. 2886 has not been repealed since the Public Procurement Law No. 4734 began to be applied as of 01.01.2003, but its scope has been limited. according to Law No. 4734; public administrations within the scope of general budget, special budget administrations, special provincial administrations, municipalities and revolving affiliated organizations, associations (except in the form of higher professional organization involved with their bodies), legal persons; economic institutions of state economic enterprises public enterprises public; social security institutions, funds, or private law was established by Presidential Decree, and the public entities with legal personality has been given the task themselves (professional organizations, and higher education institutions (excluding foundations) with the-budget, independent organizations, directly or indirectly, separately or together with the above-mentioned authorities given to the capital, where

1 Department of Real Estate Development and Management Boyabat Faculty of Economics and Administrative, Sinop University ORCID : 0000 0002 8055 7858 acakoglu@sinop.edu.tr

more than half of any kind of organization, institution, community, business and companies; 4603 within the scope of the law is more than half of the banks with the banks directly or indirectly, separately or together, while companies where capital construction procurement is being done; according to Law No. 2886, apartments with annexed included in the general budget, special provincial administrations and municipalities can make you tender. In other words, Law No. 4734 provides for the provision of services directly from the source, while Law No. 2886 provides for the sale, leasing, exchange, etc. it is preferred in service procurement works as it is applied in mutual exchange-based and transportation education. For example; works such as building construction, choosing canteens and small businesses of schools and dormitories in exchange for the land of municipalities are also tendered in accordance with Law No. 2886. dec.

MATERIALS AND METHODS

The law constituting the tender legislation, the relevant implementing regulations, as well as the building inspection implementing regulation, using the old and new regulations published by the Ministry of Environment and Urbanization, formerly the Ministry of Public Works and Housing, have been tried to be examined through different approaches. Also the Metropolitan law, the resulting numbers to 30, but of our country's population is 78% of the cities, which constitutes 22/D, and it ceased to be made pursuant to execution of construction works procurement and tender through direct individual experience with the contractor or legal persons that do not have to be opened were asked to show the way. In addition, the types of work experience documents, which are one of the most important documents in the construction works tenders, and the conditions for their issuance were also mentioned.

FINDINGS

18 of the Public Procurement Law No. 4734. According to the article, the types of tenders are listed as follows.

a) Open Tender

b) Negotiable Tender

c) Decommissioning Between Certain Bidders

The conditions for the implementation of all three types of tenders have been explained in the Law, but it has also been stated that it is an open tender that is aslolan; other procedures can be applied if special conditions such as

urgency, technological products occur. Also, with Article 22/d, known as the direct procurement procedure, the method that allows administrations to meet their needs up to a certain limit has been jul-tered from being a tender procedure by law No. 4964.

An open tender is a tender procedure in which all bidders can bid (Law Art.19).The tender procedure among certain bidders is that as a result of preliminary evaluation, those invited by the decommissioning administration can submit an offer (Art. Law).20), if it is a bargaining procedure; 21 of the Law. According to paragraphs (a), (b), (c), (d) and (e) of the article, it is decomposed according to the formation of different conditions.

In all construction work tenders, bidders are asked to determine their professional qualifications in addition to their financial and economic qualifications, and a work experience certificate requirement is required for this purpose. There are different types of work experience certificate under the names of completion of work, job status, job supervision and job management. Of these, the certificate of completion of work is issued to individuals or legal entities that have completed construction work before, but their subcontractors can also use this document, albeit at a different rate. Certificate of completion of work; it must be regulated by the administration performing the work at the request of the contractor. The governor also for construction of private individuals or legal entities on the environment, urbanization and climate change after applying to this institution designated by the Provincial Directorate of review, depending on the commission can be given. A certificate of employment status can be issued for work that has completed at least 80% of the commitment and is ongoing, but there is a condition that it will be issued within fifteen years from the date of the first announcement or invitation. Business management and business audit documents are; work experience institution or organization authorized to edit document who served in an Engineer, Architect, Project Manager, Construction Manager, Control Engineer, District Manager, Regional Director at the entities in positions such as those in the private sector commitments in again, Engineer, Architect, Project Manager, Construction Manager, Field Engineer, as well as to employees are provided. Details such as how to take into account the labor regulations and labor inspection documents and how much of the amount of the work is explained in the construction works implementation regulation.

39 of the Construction Works Implementation Regulation. In the article, the conditions for issuing a work experience certificate and institutions with regulatory authority are mentioned. Accordingly, at

least 80% of the jobs that individuals or legal entities have completed with temporary or final acceptance in the last fifteen years or again with temporary acceptance in the last fifteen years can be arranged for completed jobs. In business partnerships; pilot partner work experience desired minimum rate of at least 80% of each of the other partners at least 20%, at terms that are required to provide when positioned on the other hand, if the minimum desired rate of work experience to meet all of the pilot partner, the other partners work experience desired minimum rate is 40% less than similar non-construction work is allowed to provide documentation of work experience in the case that contractors also gain a lot of similar work finished. For example, in a building construction tender, if the pilot partner provides the required work experience amount alone, the other partner can bid if they provide at least 40% of the required work experience document amount, regardless of whether they have done installation work. Moreover, after the winning of the tender and the completion of the work, the small partner who has not built a building before gets the right to participate in other building construction tenders with a new work experience certificate. Another method of participation in tenders is to ensure that more than one legal entity participates by creating a business partnership. All legal entities can be companies, as well as individuals. Here; Those who have a work experience certificate in different fields are given the opportunity to obtain a new work experience certificate at the rate of their shares in the established business partnership. Administrations will decide which works will be considered as similar works depending on the relevant communiqué. In addition, those who perform duties such as building supervision officer, control supervisor, related directorate in the public sector may also issue work supervision or work management documents on their behalf for the construction works for which they have been personally assigned. Meanwhile, engineers and architects, graduation and job if construction work has been completed the certificate of completion documents as if fifteen years more than fifteen years will be able to use to be able to use if desired if within fifteen years after graduation is the condition of construction work being completed. The corresponding figure for each year is updated on February 1 of each year and has been determined as TL 808,172.00 for 2022.

Again, legal entities have been granted the right to use the graduation certificates of technical personnel as a work experience certificate by Law, provided that at least 51% of the shareholders are engineers and architects. By taking advantage of this, companies that do not have a lot of experience can participate in construction work tenders, win the tender and have a new

completion certificate after finishing the job. There is also a requirement in the Law that the share of the technical staff in such legal entities be protected for at least 5 years. However, even if the technical staff transfers the report card to a legal entity in the contracting documents replacing the work experience issued before the Law No. 4734, it is mandatory to work in that company, and if the employment contract expires, the validity of the contractor report card disappears.

A similar situation, 28/3/1981 17293 published in the Official Gazette numbered, dated, construction, installation and repair works in accordance with the regulation on technical engineers and architects to participate in tenders for the amount of technicians who study outside being limited to, technical officers, technicians and even the right to have work experience, which can be transmitted to the contracting document instead of stamps are given. In fact, the unrealized report cards of those who do construction work using the aforementioned contracting report card are updated every year with a communique published in the Official Gazette in March. But; these rights of technicians, science officers and technicians are not valid for tenders conducted in accordance with Law No. 4734. However, with the communiqué published in the Official Gazette dated March 2, 1995 and numbered 22215, the contracting report cards were divided into six groups as A, B, C, D, G and H, and depending on their branches, technicians were provided with the opportunity to receive a report card from a subgroup of engineers or architects. For example, if a civil engineer, a higher engineer or an architect can receive a group B contracting certificate, a construction technician, a science officer, a higher technician, and graduates of technical teaching have been granted this right from group C.

According to the regulation mentioned, ended up in the hands of contractors and contractor who will participate in the tender validity report cards, 24 March 2021 Updated at the date and 31433 published in the official gazette the rates as indicated in Table 1 and the following was published by the group, it was stated that it would be adopted and transferred on the condition that stay the same.

Table 1. Coefficients of updating contractor report cards (2021)

Years	coefficients to be applied in 2021	Years	coefficients to be applied in 2021	Years	coefficients to be applied in 2021
1953 and before	4.958.008,970	1981	69,823,255	2002	7,646
1954	4.472.152,496	1982	58.056,744	2003	5,870
1955	3.960.681,315	1983	50.467,385	2004	5,064
1956	3.244.849,040	1984	40.375,518	2005	4,536
1957	2.838.643,484	1985	27.833,207	2006	4,279
1958	2.596.570,816	1986	20.158,969	2007	3,817
1959-1966	2.205.707,322	1987	15.537,993	2008	3,583
1967	2.001.100,153	1988	10.329,896	2009	3,273
1968	1.836.894,921	1989	6.266,785	2010	3,193
1969	1.749.814,136	1990	3.801,181	2011	2,964
1970	1.633.055,267	1991	2.439,124	2012	3,016
1971	1.469.244,367	1992	1.464,708	2013	2,869
1972	1.245.187,938	1993	883,562	2014	2,626
1973	1.101.499,522	1994	529,371	2015	2,448
1974	817.538,191	1995	240,620	2016	2,277
1975	651.940,676	1996	133,316	2017	2,069
1976	556.068,442	1997	68,480	2018	1,797
1977	407.882,142	1998	39,683	2019	1,461
1978	291.672,175	1999	25,613	2020	1,241
1979	215.955,513	2000	15,490	2021	1,000
1980	100.876,963	2001	12,653		

Direct Procurement Procedure (22/d)

The first metropolitan cities in Turkey were Istanbul, Ankara and Izmir with the law issued in 1984, while in 1988 this number increased to 8 (eight), in 1993 to 15 and in 2000 to 16 with Sakarya. At the time of the entry into force of the Public Procurement Law, there were a total of 16 metropolitan municipalities, but there were several first-tier municipalities in each of them, and these first-tier municipalities were transformed into district municipalities by the law passed in 2008. On November 12, 2012, with the Metropolitan Law No. 6360, this number increased to 30 with the addition of provinces with a total population exceeding 750,000. moreover, the metropolitan municipality borders have been extended to the property

administration borders by transferring the villages to the neighborhood status and including the districts.

Table 2. Some monetary limits in the Public Procurement Law (excluding VAT)

Some monetary limits set by Law No. 4734
Article 22 / d of the Law No. 4734
Administrations within the boundaries of the
Metropolitan Municipality amount to 218.395 TL*
Administrations in other provinces 72.752 TL*
Article 62 (h) of Law No. 4734
Certificate of work experience for
Engineers and Architects in the account 808.172 TL*

* Limits for the topics mentioned in the content of this article

the population residing within the boundaries of 30 metropolitan municipalities is 66,092,128. In other words, the population residing within the boundaries of the metropolitan municipality is about 78.05% of the total population of the country. In comparison, the ratio of the population in the other 51 provinces to the total population is about 21.95%. (TUIK, 2021)

Public institutions within the metropolitan borders can be built up to JUL 218,395.00, excluding VAT, in accordance with Article 22 / d, by direct procurement procedure. This figure, which is updated every year as of February 1, is one third in the provinces other than the metropolitan ones. Although it has ceased to be a tender procedure, a completion certificate for this work can be issued after the completion of the work recorded on the Electronic Public Procurement Platform (EKAP). In addition, individuals or legal entities with this completion certificate can participate in another construction work tender and bid up to twice the amount of the document. In this way, the amount of completion documents increases. However, due to the lack of tender type, the lack of a work experience certificate in the direct procurement procedure and the subsequent issuance of a work completion certificate at the end of the work to individuals or legal entities who have not completed the construction work before may cause a decrease in the qualification as a contractor. jul. In a total of 51 provinces other than metropolitan cities, this is unlikely to be possible due to the low limit. Because it is mandatory to tender for construction works exceeding 72.752,00 TL excluding VAT with the figures of 2022.

Construction Supervision Officer (Control Officer)

4.4 of the Regulation on the Control of Public Works published in the Official Gazette No. 16745 dated September 5, 1979, entitled "control organization". in its article, when defining a control officer, it mentions that this task can also be assigned to engineers, architects and technicians in mandatory cases. This regulation remained in force until 2018.

4. The regulation issued by the Ministry of Environment and Urbanization published in the Official Gazette No. 30442 dated March 5, 2018 is entitled audit service. Item (C) in accordance with the engineer's control, depending on the control of the technician as an engineer's assistant (D) in paragraph depending on the nature of the work and the property control under the responsibility of more than one Engineer, Technician, Technician, Laboratory Assistant, it is stated that can be assigned [5].

4 of the Regulation published in the Official Gazette by the Ministry of Environment and Urbanization. Article (e) of the subparagraph "Construction site supervisor: Technical personnel with a diploma of an engineer, architect or technical teacher or technician related to them who manages and implements construction works on behalf of a building contractor in accordance with its subject and nature" contains the phrase. 6 Of the same regulation. article 2 / c also says that the construction site supervisor "must be a construction, mechanical, electrical, construction supervision technician or technical teacher related to them".

According to the regulation published in the Official Gazette dated 29.12.2018 and numbered 30640 in the Building Inspection Application Regulation, technicians can also be assigned as auxiliary control personnel.

Table 3. Limits of authority of technical personnel in building inspection companies

Technical personnel	Inspection authority limit (m^2)
Civil Engineer or Architect	30.000
Mechanical Engineer	60.000
Electrical Engineer	120.000
Technical Teacher (Construction, Machinery, Electricity)	13.500
Technician (Construction, Machinery, Electricity, Building Inspection)	8.500
Technicians (Construction, Machinery, Electricity)	3.500

Technical personnel are a member of the commission for construction work tenders, they perform an audit role during construction, and all members of the inspection and acceptance commissions are required to be technical

personnel. Technicians and Technicians can also take part in temporary and final admissions. In the same way, the contractor company also needs to have engineers and technicians who should be employed in such positions as field officer and construction site chief in the construction business. If members of the committee of inspection and acceptance of construction work with building control officials to the detriment of one of the parties will be subjected to disciplinary action if it is found that neglect will lead to the criminal prosecution will be in accordance with the legislation also stated that it is entitled to compensation of material damage(Construction ISL. Examination and Admission Regulations, 2009).

As can be seen, other technical personnel, especially technicians, perform almost the same tasks as engineers and architects, but, like them, they do not have the right to use graduation certificates as a certificate of work experience.

RESULTS

The lack of a work experience certificate in construction works commissioned by the administrations within the Metropolitan Municipalities in accordance with Article 22 / d of the Law may seem like a method in terms of the emergence of new contractors, but it may also lead to a shift away from a professional quality qualification.

Jul construction works that can be carried out with direct procurement in 30 metropolitan cities where 78.05% of the population of our country lives cannot be carried out due to the fact that the limit in other provinces has been reduced to one third. Raising this rate in other provinces will make it easier to meet the needs of institutions.

The granting of the right to use the graduation certificates as a work experience certificate to technical personnel who have graduated from associate degree, as well as engineers and architects, will contribute to the improvement of qualifications in the contracting profession. Although the limit is not as high as engineers and architects - as in the previous contracting report card - granting rights will allow more technical staff to do work related to their field in the sector.

REFERENCES

The Law on State Procurement. (1983, September 8). The Official Gazette (Issue:18161). Access address : https://www.mevzuat.gov.tr/Mevzuat-Metin/1.5.2886.pdf

Regulation on Public Structures Supervision Services. (2018, June 5). Ministry of Environment and Urbanization. The Official Gazette (Issue:30442). Access address: https://www.resmigazete.gov.tr/eskiler/2018/06/20180605-8.htm

K.I.K., The Law on Public Procurement. (2002, January 22). The Official Gazette (number:24648). Access address: https://www.resmigazete.gov.tr/eskiler/2002/01/20020122.htm#1

Regulation on Construction Site Chiefs. (2019, March 2). Ministry of Environment and Urbanization. The Official Gazette (Issue:30702). Access address: https://www.resmigazete.gov.tr/eskiler/2019/03/20190302-2.htm

TUIK., Turkish Statistical Institute. Access Address:https://data.tuik.gov.tr/Bulten/Index?p=Address-Based-Nufus-Registration-System-Results-2021

The Regulation on Amendments to the Regulation on the Implementation of Building Supervision. (2018, December 29). The Official Gazette (Issue: 30640). Access address: https://www.resmigazete.gov.tr/eskiler/2018/12/20181229-2.htm

Regulation on the Implementation of Construction Works Tenders. (2009, March 4). The Official Gazette (Issue: 27159 (Duplicate)). Access address: https://www.resmigazete.gov.tr/eskiler/2009/03/20090304M1-2.htm

Inspection and Acceptance Regulations of Construction Works. (2009, March 4). The Official Gazette (Issue: 27159 (Duplicate)). Access address: https://www.resmigazete.gov.tr/eskiler/2009/03/20090304M1-2.htm

The Regulation on Participation in Tenders for Construction, Plant and Repair Works (1981, March 28) Official Gazette (Issue: 17293) Access address: https://www.resmigazete.gov.tr/arsiv/17293.pdf

The Regulation on Amendments to the Regulation on the Implementation of Construction Works. (2018, August 13). The Official Gazette (Issue: 30508). Access address : https://www.resmigazete.gov.tr/eskiler/2018/08/20180813-12.htm

CHAPTER 2

The Effect of Dust Deposition on Photovoltaic Systems' Electricity Generation and its Economical Analysis

Muhammet Raşit SANCAR[1]

INTRODUCTION

Energy production from renewable energy sources has become very important due to increasing energy demand and global warming. Electricity production from solar energy, which is one of the renewable sources, can be achieved by harnessing both its thermal energy and photovoltaic potential. Turkey has a great potential for electricity generation from solar energy. Global radiation and sunshine durations values for Turkey are presented in Figure 1 and Figure 2 respectively. In order to benefit from this potential, photovoltaic systems have increasingly become widely used. Today, many studies are carried out on electricity generation from photovoltaic panels, and there is a continuous development and improvement. With these developments, the efficiency of photovoltaic panels increases and it is observed that there is a serious opportunity to benefit from solar energy. As important as it is to increase efficiency with the advancement of technological studies, it is also important to minimize the losses in the photovoltaic panels in the field.

1 Isparta University of Applied sciences,Institute of Postgraduate Education, Energy Systems Engineering, Isparta, Turkiye, ORCID Code: (0000-0002-4488-8393) d1840640001@isparta.edu.tr. Muhammet Raşit SANCAR is a priority field researcher of YÖK 100/2000.

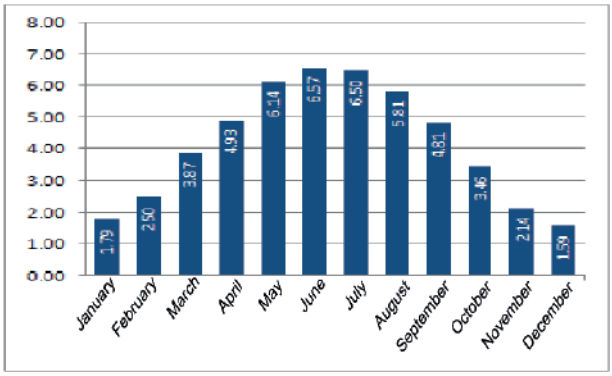

Figure 1. Global radiation values for Turkiye(KWh/m2-day)(GEPA)

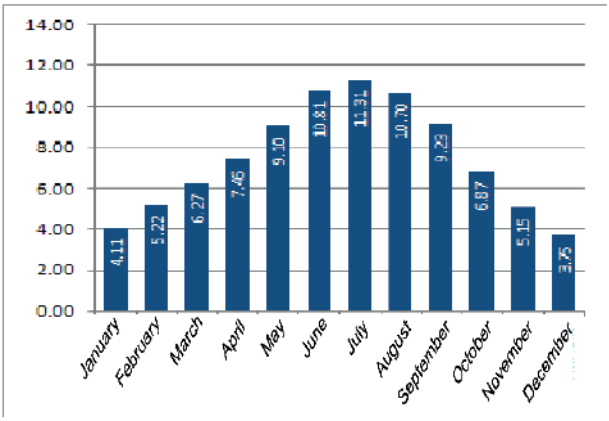

Figure 2. Sunshine duration for Turkiye(hours)(GEPA)

If a conventional silicon crystal photovoltaic panel is lined up from the front surfaces to the inner parts; It consists of an aluminum frame, glass, encapsulant (EVA film), solar cells, encapsulant (EVA film), backsheet and junction box elements. As seen in Figure 3, glass is used on the front surfaces of the panels that meet the sun. Electricity generation in the panels occurs when the sun rays coming to the surface of the panel pass through the transparent protective glass and reach the cells and convert into electrical energy with the photoelectric effect. During this process, the permeability of the protective glass on the top surface is of great importance. Due to environmental conditions, accumulated dust on the surface of the panel causes the glass permeability to decrease and subsequently cause a decrease in the energy obtained.

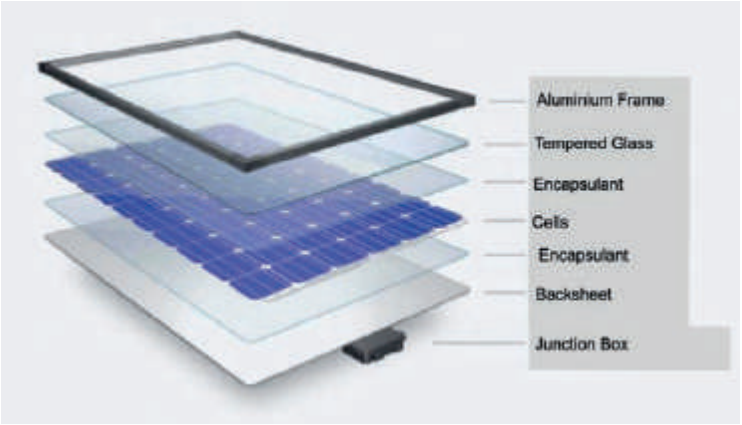

Figure 3. General elements of a photovoltaic panel (Tevı vd.,2018)

There have been many studies done within the scope of the effect of dust deposition on photovoltaic panels. In a study conducted in Iraq, an experiment was done on the surface of the panel with sand, cement, white cement, gypsum and technical gypsum powder samples at a density of 35 g/m2 and a permeability decrease of the glass of 40, 45, 55, 50 and 52 percent was observed for each of the samples used respectively (Alnasser, et al. 2020). As for a study carried out in Algeria, samples of ash, cement, gypsum, salt, soil and sand dust samples with densities of 1.02 g/m2, 1.01 g/m2, 1.01 g/m2, 1.2 g/m2, 1.02 g/m2 and 1 g/m2 showed a decrease in permeability of 73.71 ,74.62, 65.52, 62.79 ,20.02 and 19.11 percent. (Abderrezek ve Fathi 2017)

Table 1 below presents the results of a study conducted in the west of Rajasthan which was aimed to investigate the effect of bird droppings on permeability photovoltaic panels and its relation to different tilt angles in the years 2015, 2016, and 2017. According to the data, the highest permeability reduction was observed at 0° angles by 31% in 2015 and 2017, while the highest power generation reduction was observed at 0° and 10° angles by 23.8%.

Table 1. Loss in permeability and loss power generation with inclination angle β (Sisodia ve Mathur 2019)

angle	year			Power generation loss (%)
β°	2015	2016	2017	
0°	31	30	31	23,8
10°	28	29	29	23,8
20°	27	26	27	21
25°	15	14	14	11,5
30°	14	13	13	10,8
40°	13	13	13	10,5
50°	14	14	15	10,8
60°	15	16	16	10,8
70°	18	19	19	15,8
80°	21	22	21	16
90°	24	23	23	16,5

In Table 2, the calculated permeability reduction and power generation reduction data of a study conducted in Belgium are presented. In this study, measurements were made using two different photovoltaic panel brands, Sanyo and Eurosolare panels and glass samples. In the study carried out with different densities of artificially deposited white sand, clay and cement powder samples, the parameters with the highest loss of permeability was determined to be at 66.66% with the 60 g/m2 density cement powder sample while the highest loss in panel power generation was 65.68% in the Eurosolare brand panel with cement dust.

Table 2. Production losses of Sanyo and Eurosolare brand panels under different dustiness samples (Appels, et al. 2013)

(g/m²)	White sand (250μm)		
	T(%)	P_{max} (%)	
		Sanyo HIP-210 NKHE1	Eurosolare PL160
10	1,05	1,78	0,08
20	4,02	4,84	5,46
40	9,18	9,77	9,1
60	15,03	14,74	13,76
(g/m²)	Clay (68μm)		
	T(%)	P_{max} (%)	
		Sanyo HIP-210 NKHE1	Eurosolare PL160
10	9,97	8,16	9,7
20	20,03	19,38	20,36
40	39,56	38,86	37,12
60	48,42	48,77	47,21
(g/m²)	Cement (10μm)		
	T(%)	P_{max} (%)	
		Sanyo HIP-210 NKHE1	Eurosolare PL160
10	18,41	20,92	19,06
20	40,61	40,65	39,78
40	53,48	51,24	52,44
60	66,66	64,16	65,68

In the experiments conducted on five different powder samples with densities of 100 g/m2, it was determined that the effect of sand, cement, white cement, gypsum and technical gypsum powder samples on panel power generation loss was 12, 14, 15, 9, and 10 percent respectively. (Alnasser, et al. 2020)In a different study, experiments on five different dust types with a density ratio of 10 g/m2, the effect of red soil, ash, sand, calcium carbonate

and silica gel samples on panel power generation loss was found to occur at 7, 25, 4, 5 and 5, and 4.5 percent respectively (Kazem ve Chaichan 2016).

In Table 3, the experimental data of the losses in photovoltaic panel power generation of the coal dust sample with different particle sizes and weights made in the Aegean region of Turkey are presented. In this study which to kinds of photovoltaic cells were used, monocrystalline silicon (m-Si) and polycrystalline silicon (p-Si), it was determined that the maximum reduction occurred at the size of 38 μm and the weight of 15 g.

Table 3. Effect of coal dust with different particle sizes on panel power generation loss (Adıgüzel, et al. 2019)

Particle size	Mass (g)	Type of photovoltaic panel	
		m-Si	p-Si
38 μm	5	%39,61	%38,52
	10	%52,15	%47,79
	15	%62.05	%60,07
38-53 μm	5	%36,64	%31,08
	10	%47,86	%43,67
	15	%55,78	%57,03
53-75 μm	5	%32,42	%26,78
	10	%42,91	%40,07
	15	%50,83	%52,15
75-106 μm	5	%26,43	%22,21
	10	%37,96	%30,3
	15	%44,23	%43,67
106-250 μm	5	%20,8	%17,28
	10	%29,25	%20,34
	15	%36,97	%28,93
250-500 μm	5	%15,17	%10,94
	10	%20,1	%11,72
	15	%28,9	%14,96

In Table 4, data of a study carried out in Athens that examined the effect of red soil, limestone and fly ash dust samples at different densities on the panel yield is presented. According to the observed results, it was determined that the highest decrease in panel efficiency occurred in the fly ash dust sample at 1.5% with a density of 3.71 g/m2.

Table 4. Effect of various dust types on panel efficiency

Dust samples	density (g/m^2)	%
red soil	0,12	0,5
	0,35	0,75
limestone	0,28	0,4
	1,51	0,95
fly ash	0,63	0,1
	3,71	1,5

Two identical photovoltaic panels were used in an experiment on the roof of a building in Shanghai. To test the effect of the accumulated dust on the panel efficiency, one of the photovoltaic panels was artificially dusted with a sand dust sample. Spreading the dust samples on the panel surface at densities of 2.199 g/m2, 6.29 g/m2, 17.37 g/m2, 21.067 g/m2 and 30.18 g/m2, the losses in panel efficiency were 5.296, 12.027, 34.332, 38.981 and 43.216 percent respectively. (Wang, Meng ve Chen 2020)

Another experiment investigating the effect of dust on production loss in photovoltaic panels was carried out in Doha, Qatar. Two arrays were used in this experiment, one which was cleaned weekly and the other one which was cleaned every two months. The monthly panel performance loss measured was found to vary between 6% and 23% per month depending on the current environmental conditions and dust characteristics. (Javed, et al. 2021)

In another study conducted in Mauritania, dirty and clean panels were used to determine the effect of dust on electricity generation on photovoltaic panels. The panels defined as clean were cleaned with two different methods, with and without water. According to the results obtained, it was observed that the output power of dusty photovoltaic panels was lost by 21.57% compared to the clean panels. The modules that had a power value of 2.88 kW and 2.95 kW at the beginning showed an increase in power output of up to 3.29 kW and 3.26 kW, respectively after cleaning. (Lasfar, et al. 2021)

A study in Senegal investigated the performance of photovoltaic panels when their surfaces get dry cleaned. Two identical polycrystalline solar panels were used, one of the panels was cleaned daily while the other was not cleaned. After a month, the dirty panel experienced a maximum loss of 17.13% compared to the clean panel. When compared with the data in the initial conditions, a deterioration of 10.16% and 24.09% was detected for the dry-cleaned and the uncleaned panels, respectively. (Aidara, et al. 2018)

A study carried out on a part of a solar power station with an installed power of 1 MW in Zahrani, a coastal region of Lebanon, a water-based robotic on-wheel device was used to remove the dust accumulated on the panels. The detected results showed that the cleaning procedure can effectively minimize the dust effect on the power output of the solar panel. It was calculated that an average increase of 32.27% was achieved in electricity production. (Hammoud, et al. 2019)

The effect of dust accumulation on the performance of photovoltaic panels under outdoor conditions was experimentally investigated in the city of Ouargla, southeast of Algeria. One of the panels, which was taken as a reference, was cleaned regularly using a soft wiper and distilled water at the beginning of each measurement while the other was left uncleaned to examine the effect of dust accumulation on the output power of the solar panels. As a result of the observations, it was determined that 4.36 g/m2 dust accumulated on the surface of the panel which was exposed to external environmental conditions for 8 weeks without cleaning. Due to this deposit, it was concluded that the dirty panel caused a decrease of 8.41%, 6.10% and 0.51%, in the maximum power output, short circuit current and open circuit voltage in energy production respectively, compared to the cleaned panel.

MATERIALS AND METHOD

In this study, a power plant simulation study with an installed power of 1 MW was carried out for the province of Isparta using PVsyst software. In this simulation study, the effects of five different powder samples, namely sand, cement, white cement, gypsum and technical gypsum, on power generation were investigated. An article study conducted by Tamadher and his friends which investigated the effect of the dust samples on power generation of a panel in 5 different cleaning periods was used as a source. Cleaning periods were performed as weekly, bi-weekly, monthly, bi-monthly and quarterly. The first simulation study was carried out without dust loss, while the other simulation studies were carried out according to the yield loss values in the article.

The article used as a source

The study was carried out to determine the effect of different dust samples on photovoltaic panel power generation at different cleaning periods. In the study, white cement, cement, sand, gypsum and technical gypsum powders were used as different powder samples. (Alnasser, et al. 2020). Sand, which is one of these dust samples, is a type of dust that rises as a result of the movement of vehicles and is collected and accumulated from the environment. A sample of gypsum powder, whose chemical compound is CaSO4·2H2O, is a substance sometimes added to lime to change soil acidity and can be found in different colors. Cement consists of various compounds, primarily lime, silica, alumina and iron oxide. White cement and ordinary cement types were used for this study of this powder sample, which has different types and types. The physical properties of these different powder samples were investigated by different methods.

In this study, power generation reductions as a result of cleaning the panel were measured at 1-week, 2-week, 1-month, 2-month and 3-month cleaning periods using sand, gypsum, technical plaster, cement and white cement powder types. The power drop graph of the cleaning periods is given in Figure 4.

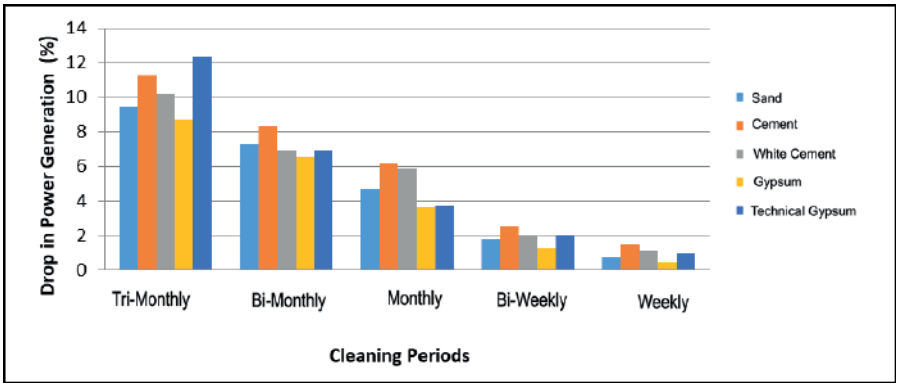

Figure 4. Power drop values according to cleaning periods for used data

2.2 Climate of Isparta province

Isparta province is located in the Mediterranean region. The climate characteristics of the transition zone between the Mediterranean climate and the continental climate are observed. Isparta has a semi-arid climate with less humid winters and hot summers. The hottest months in Isparta are July and August, and the coldest months are January and February. According to

meteorological data, the annual average temperature of Isparta province is 12.3 ºC, the annual average highest temperature is 18.4 ºC and the annual average minimum temperature is 6 ºC. Average temperature values of Isparta province are given in Figure 5.

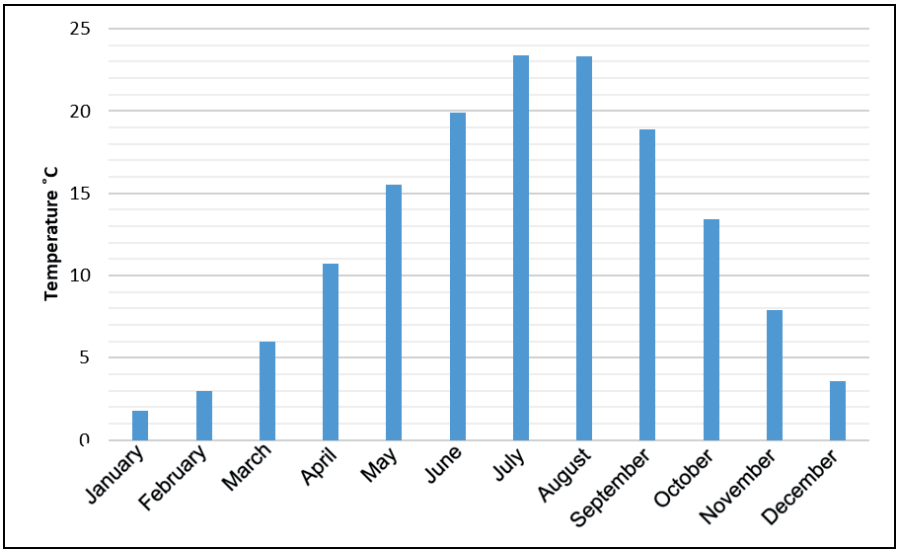

Figure 5. Monthly temperature values of Isparta province

When the monthly average radiation values of Isparta province were examined, it was determined that the highest radiation value observed was 6.80 (kWh/m2day) in June, and the lowest radiation value was 1.82 (kWh/m2day) in December. When the sunshine durations are examined, it is observed that the monthly average maximum sunshine duration is 11.72 hours in July, and the lowest sunshine duration is 4.00 hours in December. The graph of global radiation values of Isparta province is given in Figure 6 and the graph showing the sunshine durations is given in Figure 7.

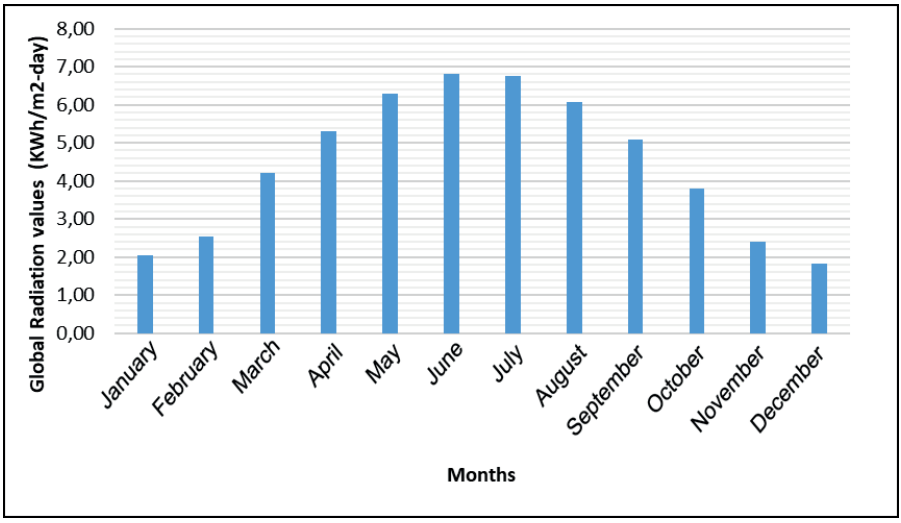

Figure 6. Global radiation values graph of Isparta province

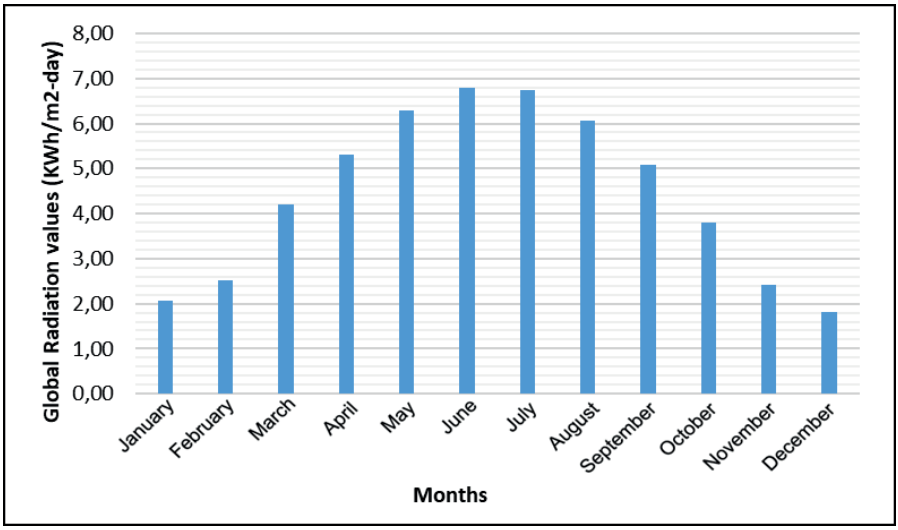

Figure 7. Sunshine duration of Isparta Province

2.3. The power plant

The analyzes were carried out with a simulation study of a photovoltaic power plant with an installed power of 1 MW in Isparta province, which was made on the PVsyst software. The simulation image of the power plant is given in Figure 8.

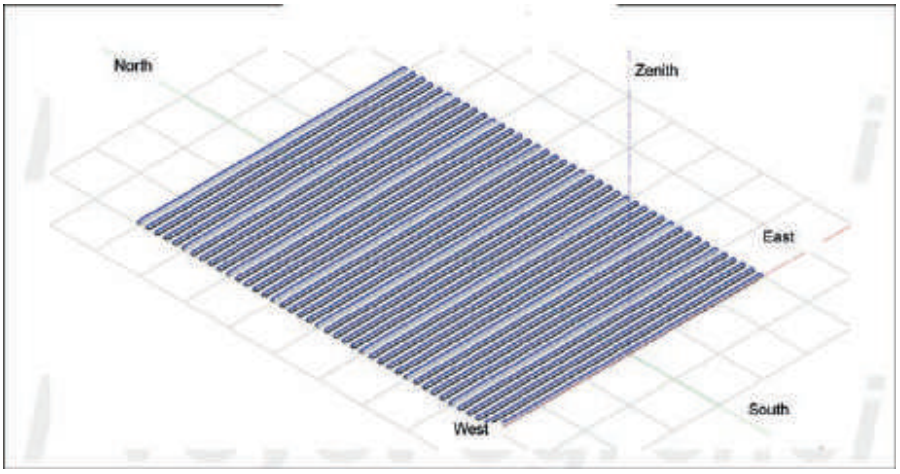

Figure 8. Simulated image of the power plant (PVsyst, 2022)

In the simulation study analyzed, the photovoltaic plant has a single slope and an azimuth angle. This tilt angle is 37.9º and the azimuth angle is 0º. The characteristics of the simulated power plant are given in Table 5. 8 inverters are used in the plant and the technical specifications of these inverters are presented in Table 6.

Table 5. Properties of the panels used in the power plant simulation

Parameters used in simulating the Power Plant	
Numer of series in the system	41 Adet
Numer of panels in each series	203 Adet
Total number of panels	8323 Adet
Tilt angle	37.9°
Per per unit	120Wp
Pmpp (operating conditions 50 ° C)	875kWp
Umpp (operating conditions 50 ° C)	627 V
Immp (operating conditions 50 ° C)	1394 A
Total PV nominal power(STC)	999 kWp

Table 6. Properties of the inverters used in the power plant simulation

Properties of the inverters used	
Model	SUN2000-100KTL-INM0-415Vac
Rated power per unit	100kWac
Number of inverters used	8 adet
Total power	800kWac
Operating voltage	200-1000V
Maximum power(=>35°C)	110kWac
Nominal power ratio (DC:AC)	1.25

THE SIMULATION

Simulation of the power plant

In the simulation study, the 7.2.14 version of the PVsyst software, which enables the simulation and analysis of grid-connected and off-grid systems, was used. Thanks to the software, results related to factors such as electricity generation, system losses and shading of the photovoltaic systems planned to be installed can be obtained. The weather database of this software can be used and the files of the prepared weather data can be added to the interface of the software and then simulated. The interface of the mentioned PVsyst software is presented in Figure 9.

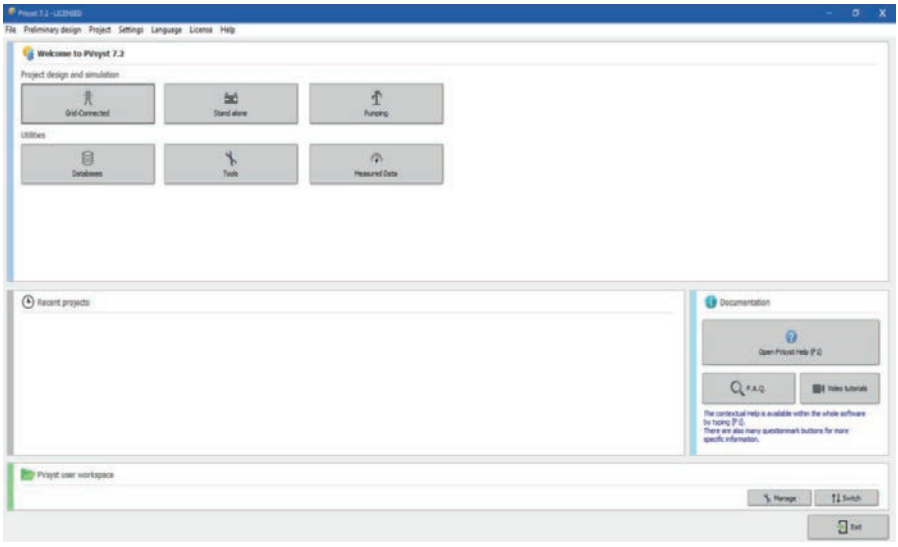

Figure 9. The user interface of the Pvsyst software (PVsyst, 2022)

Since the 1MW installed power system modeled in the simulation studies is planning to produce electricity from a grid-connected solar energy, the "Grid Connected" button in the software interface specified in Figure 9 was selected. The main purpose of the study is to obtain electricity generation data and evaluate it in terms of production. The simple diagram of the grid-connected photovoltaic system belonging to the software is presented in Figure 10.

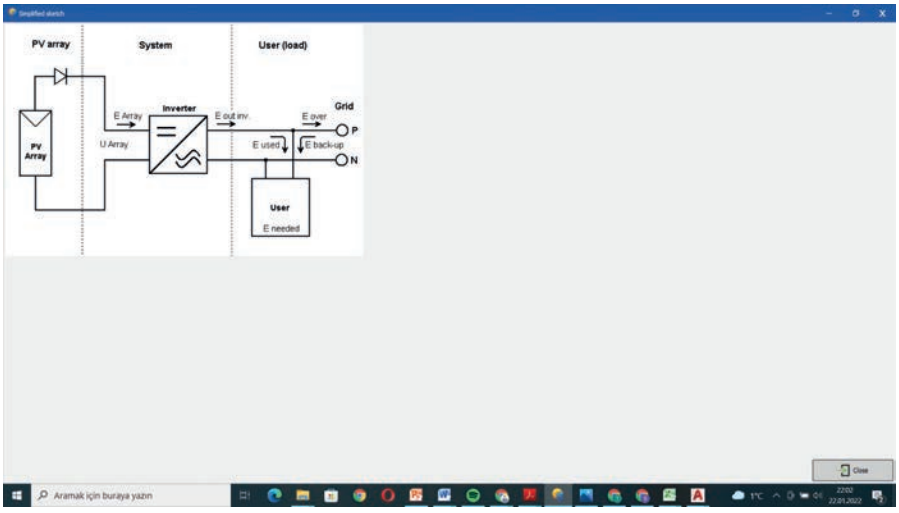

Figure 10. A schematic diagram of a simple Grid-connected photovoltaic system (PVsyst, 2022)

The simulation study was carried out using Meteonorm 8.0 (2003-2013) – Synthetic climate data in the data pool found in the software interface. Some graphics of the data obtained from the software are presented in Figure 11, Figure 12 and Figure 13.

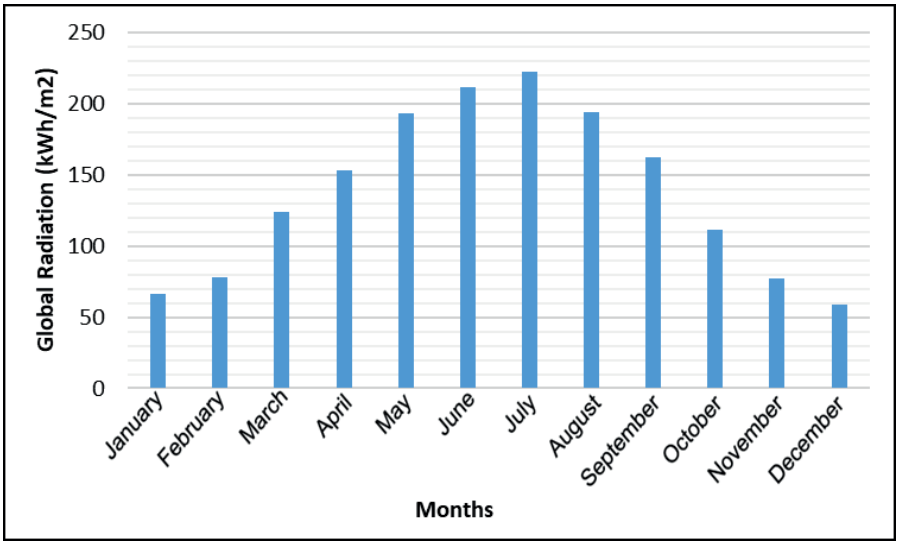

Figure 11. Monthly global radiation values (PVsyst, 2022)

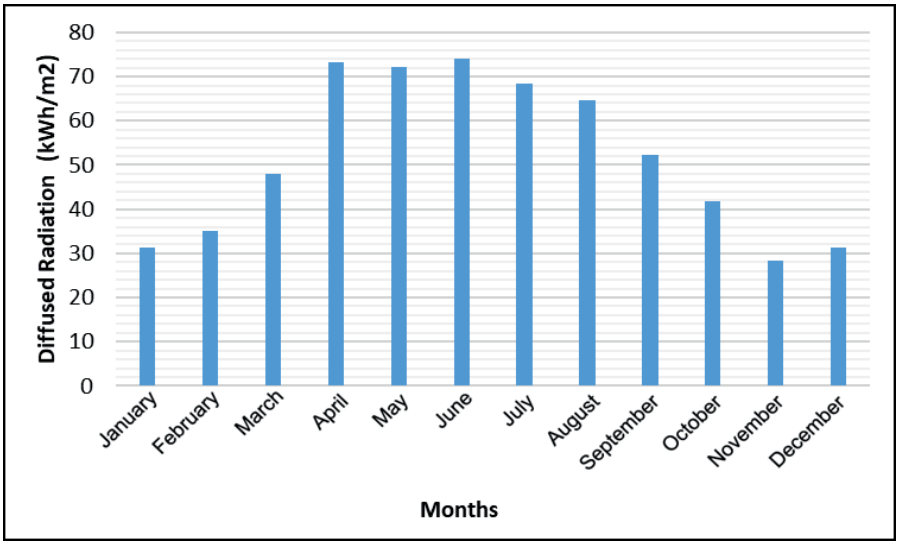

Figure 12. Monthly diffused radiation values (PVsyst, 2022)

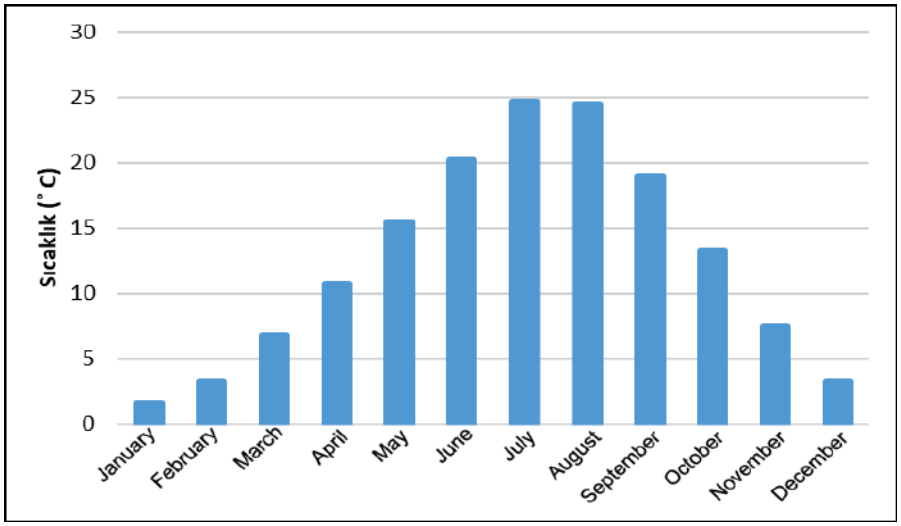

Figure 13. Monthly average temperature values (PVsyst, 2022)

By using the "Orientation" button in Figure 14, the values of the simulated power plant were determined and these values were defined by the software as 0° for the azimuth angle and 37.9° for tilt angle.

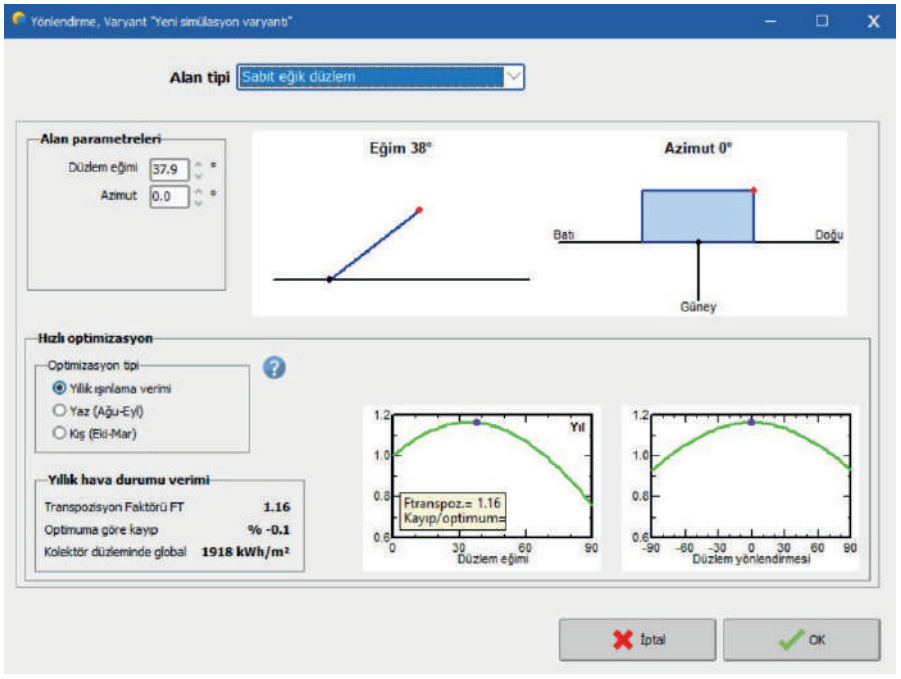

Figure 14. "Orientation" button interface (PVsyst, 2022)

The panel and inverter properties used while performing the plant simulation are defined by the software from the "System" button interface. The "System" interface is presented in Figure 15.

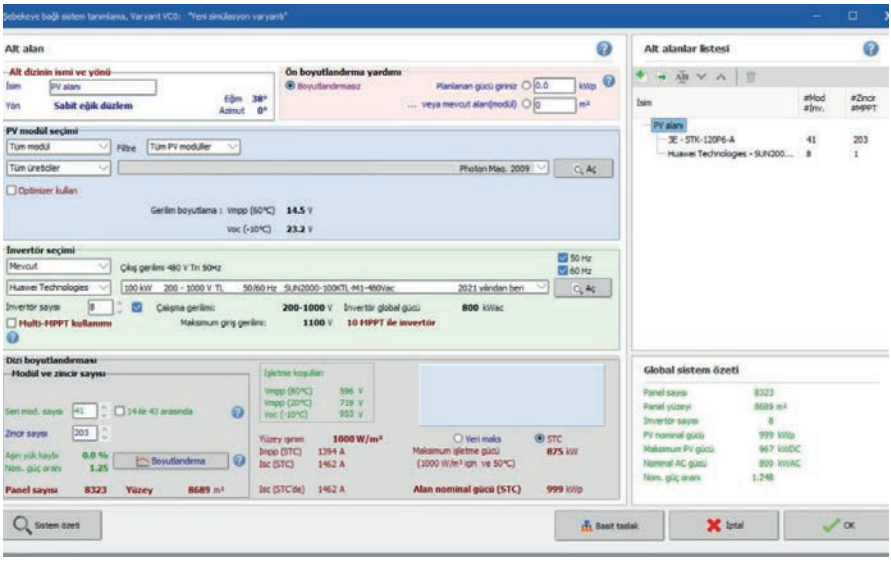

Figure 15. "System" button interface (PVsyst, 2022)

Using the tables of "Activity-based tariffs approved by EMRA(Energy Market Regulatory Authority) are to be applied as of June 1, 2022", the kWh unit price values of "Industry", "public and private services sector and other" and the sub-fields "agricultural activities" using binary and single term subheadings under the main title of medium voltage are given in Table 7.

Table 7. Table of The EMRA tariff on June 1st (EPDK, 2022)

	Activity-based tariffs approved by EMRA(Energy Market Regulatory Authority) are to be applied as of June 1, 2022					
	1/6/2022	Activity-based consumer tariffs (kr/kWh)				
Users of the Transmission system	Users of the Transmission system	Retail Monomial Energy Price	Retail Day-time Energy Price	Retail Peak Demand Energy Price	Retail Night-time Energy Price	Distribution Price
	Medium voltage					
	Binary					
	Industry	248.3714	251.3801	395.2221	135.2853	14.7972
	Public and private services sector and other	230.2455	232.5236	363.0085	128.7021	23.0611
	Agricultural activities	157.6777	159.2914	251.4048	85.6839	18.9925
	Monomial					
	Industry	256.6870	259.8001	408.5735	139.7250	16.3448
	Public and private services sector and other	235.0787	237.3568	367.8417	133.5347	28.7660
	Agricultural activities	159.7360	161.3497	253.4633	87.7413	23.6477

Research Findings

Presented Figure 16 is annual total electricity generation data of 25 different simulation studies in total created in the PVsyst program based on the power reduction values predetermined for 5 different dust samples according to 5 different cleaning periods. According to the data obtained, the highest value of electricity production was attained with 1-week cleaning periods. In addition to this, simulations in which the cleaning process was applied every 3 months achieve the lowest values in terms of electricity generation. As seen in Figure 16, it was observed that the highest electricity production in all cleaning applications was in the gypsum powder sample. In total, the highest electricity generation was 1470.9 MWh in the gypsum

powder sample and the lowest electricity generation was 1392.9 MWh in the technical gypsum powder sample.

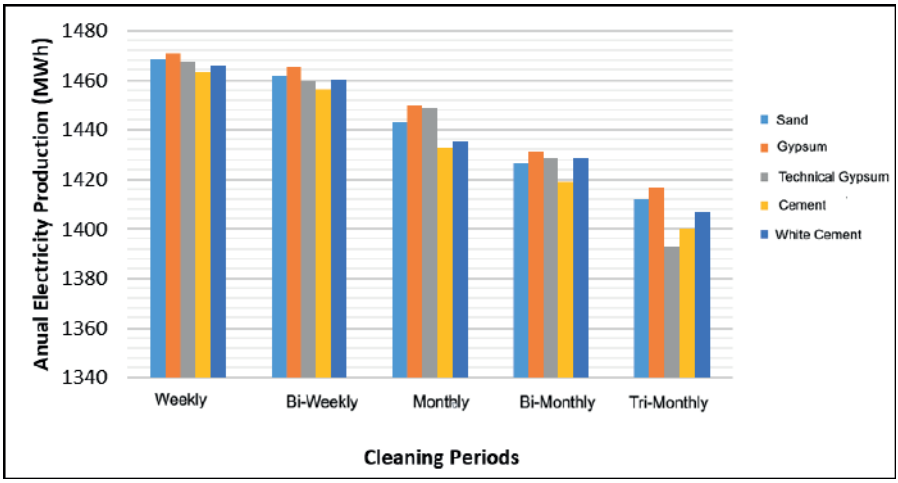

Figure 16. Annual electricity production values as a result of cleaning different dust samples at varying intervals

The annual electricity generation data of the simulation studies carried out for different dust samples and variable cleaning intervals were analyzed in the light of the data in Figure 16. These calculations were made for the data belonging to the industrial sub-field, and are given in Table 8 and Table 9 for the binomial and monomial titles respectively.

In Table 8, it is seen that the highest loss, ₺189 428.68, occurred with the technical gypsum powder sample which had a three-month cleaning interval while the lowest loss was ₺7 240.80 in the gypsum powder sample, which had a weekly cleaning interval.

Table 8. Economic analysis in which dust loss data is applied to the medium voltage and binary tariff of the "Industry" sub-field, in the light of EMRA values (Annual)

Cleaning intervals	Weekly	Weekly	Monthly	Bi-monthly	Tri-monthly
Sand	₺12 613.01	₺29 430.35	₺72 174.43	₺ 111 414.89	₺145 049.58
Gypsum	₺7 240.80	₺20 320.96	₺56 291.38	₺99 502.61	₺133 370.87
Technical Gypsum	₺15 649.47	₺32 933.96	₺56 291.38	₺105 575.54	₺189 428.68
Cement	₺24 992.44	₺40 875.49	₺96 466.14	₺128 465.81	₺ 172 377.76
White Cement	₺18 685.94	₺31 999.67	₺90 393.22	₺105 575.54	₺ 157 429.01

In Table 9, it was seen that the highest economic loss value was ₺194 918.17 in the technical gypsum powder sample during the three-month cleaning period while the lowest economic loss value, ₺7 450.63, occurred in the gypsum powder sample during a one-week cleaning period.

Table 9. Economic analysis in which dust loss data is applied to the "Industry" sub-field of the medium voltage and monomial tariff in the light of EMRA values (Annual)

Cleaning intervals	Weekly	Weekly	Monthly	Bi-monthly	Tri-monthly
Sand	₺12 978.52	₺30 283.22	₺74 265.99	₺ 114 643.61	₺149 253.00
Gypsum	₺7 450.63	₺20 909.84	₺57 922.66	₺ 102 386.12	₺137 235.85
Technical Gypsum	₺16 102.98	₺33 888.36	₺57 922.66	₺108 635.04	₺194 918.17
Cement	₺25 716.70	₺42 060.03	₺99 261.66	₺132 188.65	₺177 373.13
White Cement	₺19 227.44	₺32 926.99	₺93 012.74	₺108 635.04	₺161 991.18

According to the data obtained Table 8 and Table 9 presented, it was observed that the highest the lowest economic losses were experienced in the samples with a 3-month cleaning interval and a 1-week cleaning interval in both tables respectively.

In Figure 16, Calculations made for the data belonging to the "Public and Private Services Sector and Other" sub-field of EMRA is presented in Table 10 and Table 11 for the binomial and monomial titles, respectively.

In Table 10, we can see that the highest economic loss was experienced at ₺168 027.44 in the technical gypsum powder sample with a three-month cleaning period and the lowest economic loss was ₺6 422.75 in the gypsum powder type with a weekly cleaning interval. Considering the sand dust sample separately, it was seen that while a loss of ₺11 188.02 was experienced in the one-week cleaning period, this loss was ₺ 128 662.20 in the tri-monthly cleaning period.

Table 10. Economic analysis in which dust loss data are applied to the "Public and Private Services Sector and Other" sub-field of the medium voltage and binary tariff in the light of EMRA values (Annual)

Cleaning intervals	Weekly	Weekly	Monthly	Bi-monthly	Tri-monthly
Sand	₺11 188.02	₺26 105.37	₺64 020.32	₺ 98 827.48	₺128 662.20
Gypsum	₺6 422.75	₺18 025.14	₺49 931.71	₺88 261.02	₺118 302.92
Technical Gypsum	₺13 881.43	₺29 213.16	₺49 931.71	₺93 647.85	₺ 168 027.44
Cement	₺22 168.85	₺36 257.46	₺85 567.61	₺113 952.03	₺152 902.90
White Cement	₺16 574.84	₺28 384.41	₺80 180.79	₺93 647.85	₺139 643.03

In Table 11, it can be seen that the highest economic loss was experienced at ₺167 319.60 in the technical gypsum powder sample with a three-month(tri-monthly) cleaning period and the lowest economic loss was ₺6 395.69 in the gypsum powder type with a one-week(weekly) cleaning period.

Table 11. Economic analysis in the light of EMRA values, where dust loss data are applied to the "Public and Private Services Sector and Other" sub-field of the medium voltage and monomial tariff (Annual)

Cleaning intervals	Weekly	Weekly	Monthly	Bi-monthly	Tri-monthly
Sand	₺11 140.89	₺25 995.40	₺63 750.62	₺98 411.16	₺ 128 120.19
Gypsum	₺6 395.69	₺17 949.20	₺ 49 721.36	₺87 889.21	₺ 117 804.55
Technical Gypsum	₺13 822.95	₺29 090.09	₺49 721.36	₺93 253.34	₺ 167 319.60
Cement	₺22 075.46	₺36 104.72	₺85 207.15	₺113 471.99	₺ 152 258.77
White Cement	₺16 505.02	₺28 264.84	₺79 843.01	₺93 253.34	₺ 139 054.76

Finally, calculations made for the data in Figure 16 belonging to the "Agricultural Activities" sub-field of EMRA are presented in Table 12 and Table 13 for the binomial and monomial headings, respectively.

In Table 12, it was observed that the highest economic loss value was at ₺112 475.72 in the technical gypsum powder sample during the three-month cleaning interval and the lowest economic loss value at ₺4 299.32, occurred in the gypsum powder sample during a one-week cleaning interval.

Table 12. Economic analysis in which dust loss data is applied to the "Agricultural Activities" sub-field of the medium voltage and binary tariff in the light of EMRA values (Annual)

Cleaning intervals	Weekly	Weekly	Monthly	Bi-monthly	Tri-monthly
Sand	₺ 7 489.14	₺17 474.65	₺42 854.50	₺66 154.03	₺86 125.06
Gypsum	₺ 4 299.32	₺12 065.83	₺33 423.74	₺59 080.96	₺79 190.68
Technical Gypsum	₺ 9 292.08	₺19 554.97	₺33 423.74	₺62 686.84	₺112 475.72
Cement	₺14 839.58	₺24 270.35	₺57 278.02	₺76 278.24	₺102 351.52
White Cement	₺11 095.02	₺19 000.21	₺53 672.14	₺62 686.84	₺ 93 475.51

In Table 13, it was observed that the highest economic loss value was ₺110 368.18 in the technical gypsum powder sample during the three-month cleaning period while the lowest economic loss value, ₺4 218.76, occurred in the gypsum powder sample during a one-week cleaning period.

Table 13. Economic analysis in which dust loss data is applied to the "Agricultural Activities" sub-field of the medium voltage and monomial tariff in the light of EMRA values (Annual)

Cleaning intervals	Weekly	Weekly	Monthly	Bi-monthly	Tri-monthly
Sand	₺7 348.81	₺17 147.21	₺42 051.50	₺64 914.45	₺84 511.27
Gypsum	₺4 218.76	₺11 839.74	₺32 797.45	₺57 973.91	₺ 77 706.82
Technical Gypsum	₺ 9 117.96	₺19 188.55	₺32 797.45	₺61 512.23	₺ 110 368.18
Cement	₺14 561.52	₺23 815.58	₺56 204.76	₺74 848.95	₺100 433.68
White Cement	₺10 887.12	₺18 644.19	₺52 666.44	₺61 512.23	₺91 723.99

In Figure 17, a graph was created to show the annual total loss of electricity production under the exposure of different dust samples of the power plant simulation with variable cleaning periods. In order to create this graph, firstly, the dust deposition factor of the power plant was removed and annual electricity production values were accepted as reference.

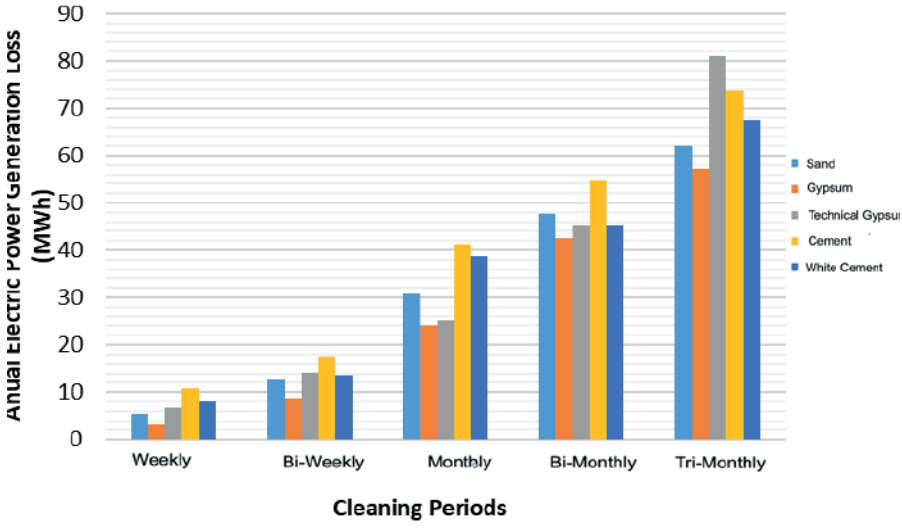

Figure 17. The effect of different dust samples on annual electricity production with variable cleaning periods

When the values calculated by eliminating the dusting factor are taken as reference; It was determined that the highest electricity production loss was 81.1MWh with the technical gypsum dust sample in the 3-month cleaning period, and the lowest electricity production loss was 3.1MWh with the gypsum dust sample in the 1-week cleaning period.

3.CONCLUSION

Electricity generation using photovoltaic panels from solar energy is a known, continuous, renewable and common method. Considering the effects of dusting factor, which is one of the biggest losses that can be encountered in the electricity generation process with photovoltaic panels, the decrease in efficiency and energy production results have been by use of simulations and analyzes. Electricity production loss due to loss of permeability of solar panels caused by settlement of various types of dust on the surface of the panel was investigated.

In this study, energy production losses due to the cleaning of sand, gypsum, technical plaster, cement and white cement powder samples accumulated on the surface of photovoltaic panels at different intervals were investigated. According to the data obtained as a result of cleaning the 5 dust samples mentioned above off the panel surfaces in 1 week, 2 weeks, 1 month, 2 months and 3 months' intervals, it was calculated that the highest amount of production loss occurred in the 3-month cleaning interval, with the technical gypsum powder sample at a total of 81.1 MWh per year.

The calculated losses were examined economically in the light of EMRA data; In binomial tariffs the losses were 189 428.68 TL, 168 027.44 TL and 112 475.72 TL for "Industry", "Public-Private Services Sector and Other" and "Agricultural Activities" respectively, and in the same order 194 918.17 TL, 167 319.60 TL and 110 368.18 TL for Monomial tariffs.

Table 14. Annual financial loss caused by dust deposition with a 3-month cleaning interval.

EMRA sub sectors	Binomial	Monomial
Industry	189 428.68TL	194 918.17TL
Public-Private Services Sector and Others	168 027.44TL	167 319.60TL
Agricultural activities	112 475.72TL	110 368.18 TL

In the calculations made with all cleaning periods, gypsum caused the lowest loss, while the highest loss was observed with cement in all cleaning intervals except for the three-month cleaning interval. In the three-month cleaning interval, it was determined that the highest loss occurred with the technical gypsum. For this reason, it has been determined that cement powder causes higher losses in cleaning intervals of two months or less, while higher losses occur with technical gypsum powder in long-term cleaning intervals such as three months.

In this study, guiding information is given in terms of the decrease in electricity production and material damage that may be experienced in case of establishing a power plant near the enterprises that produce the dust samples. Considering the calculated values, the importance of solar panel surface cleaning has been demonstrated by using numerical data in order to minimize the losses in electricity production. The use of cleaning machines and surface coating methods that prevent dust collection, which are some of the methods that can provide panel surface cleaning, are effective methods that can be used in order to minimize the losses that may occur.

In addition, many studies have been carried out on the effect of different dust types on photovoltaic panel electricity production, except for the dust samples used in this study. By using the data obtained from these studies, the effect of different dust types on the electricity production of the photovoltaic system can be investigated and an economic analysis can be carried out with the help of the method applied in the article. If the dust types can be spatially determined in our country, the dust-related losses could also be spatially calculated using the existing data, and as a result, a comprehensive study can be carried out on which region the dust-related losses will occur and at what level. As a result of these studies, data can be provided to guide commercial investments and academic studies.

REFERENCES

Abderrezek, M., & Fathi, M. (2017). Experimental study of the dust effect on photovoltaic panels' energy yield. Solar Energy, 142, 308-320.

Adıgüzel, E., Özer, E., Akgündoğdu, A., & Yılmaz, A. E. (2019). Prediction of dust particle size effect on efficiency of photovoltaic modules with ANFIS: An experimental study in Aegean region, Turkey. Solar Energy, 177, 690-702.

Aıdara, M. C., Ndıaye, M. L., Mbaye, A., Sylla, M., Ndıaye, P. A., & Ndıaye, A. (2018). Study of the performance of a system for dry cleaning dust deposited on the surface of solar photovoltaic panels. International Journal of Physical Sciences, 13(2), 16-23.

Alnasser, T. M., Mahdy, A. M., Abass, K. I., Chaichan, M. T., & Kazem, H. A. (2020). Impact of dust ingredient on photovoltaic performance: An experimental study. Solar Energy, 195, 651-659.

Appels, R., Lefevre, B., Herteleer, B., Goverde, H., Beerten, A., Paesen, R., ... & Poortmans, J. (2013). Effect of soiling on photovoltaic modules. Solar energy, 96, 283-291.

Dida, M., Boughali, S., Bechki, D., & Bouguettaia, H. (2020). Output power loss of crystalline silicon photovoltaic modules due to dust accumulation in Saharan environment. Renewable and Sustainable Energy Reviews, 124, 109787.

Enerji, T. C., & Bakanlığı, T. K. Yenilenebilir Enerji Genel Müdürlüğü,"Güneş enerjisi potansiyeli atlası (GEPA)".

EPDK, E. P. D. K. (2022). Elektrik piyasasında lisanssız elektrik üretimi.

Hammoud, M., Shokr, B., Assi, A., Hallal, J., & Khoury, P. (2019). Effect of dust cleaning on the enhancement of the power generation of a coastal PV-power plant at Zahrani Lebanon. Solar Energy, 184, 195-201.

Javed, W., Guo, B., Figgis, B., & Aïssa, B. (2021). Dust potency in the context of solar photovoltaic (PV) soiling loss. Solar Energy, 220, 1040-1052.

Kaldellis, J. K., Fragos, P., & Kapsali, M. (2011). Systematic experimental study of the pollution deposition impact on the energy yield of photovoltaic installations. Renewable energy, 36(10), 2717-2724.

Kazem, H. A., & Chaichan, M. T. (2016). Experimental analysis of the effect of dust's physical properties on photovoltaic modules in Northern Oman. Solar Energy, 139, 68-80.

Lasfar, S., Haidara, F., Mayouf, C., Abdellahi, F. M., Elghorba, M., Wahid, A., & Kane, C. S. E. (2021). Study of the influence of dust deposits on photovoltaic solar panels: case of Nouakchott. Energy for Sustainable Development, 63, 7-15.

MGM, M. G. M. (2018). İklim verileri bülteni.

PVsyst, 2022. Software for Photovoltaic Systems, www.pvsyst.com/7.2/Index

Sisodia, A. K. (2019). Impact of bird dropping deposition on solar photovoltaic module performance: a systematic study in Western Rajasthan. Environmental Science and Pollution Research, 26(30), 31119-31132.

Tevı, G. J. P., Faye, M. E., Moustapha, S. E. N. E., Issa, F. A. Y. E., Blieske, U., & Maiga, A. S. (2018, May). Solar photovoltaic panels failures causing power losses: a review. In 2018 7th International Energy and Sustainability Conference (IESC) (pp. 1-9). IEEE.

Wang, H., Meng, X., & Chen, J. (2020). Effect of air quality and dust deposition on power generation performance of photovoltaic module on building roof. Building Services Engineering Research and Technology, 41(1), 73-85.

CHAPTER 3

A Popular Dietary Supplement: Chlorella

Elif ÇİL[1]

INTRODUCTION

What is a dietary supplement?

The definition of food supplement was first mentioned in the Dietary Supplement Health and Education Act (DSHEA) in 1994. According to the FDA (Food & Drug Administration), food supplements are used for products that are recommended to be taken with nutrition, which is beneficial for the body but not in the definition of medicine, which can be in pills, tablets, capsules, powder, gel or liquid form. Generally, food supplements come in the form of vitamins, minerals, amino acids, or plant extracts. However, in some cases, for example, herbal teas and protein bars, these products are also labeled as food supplements and offered for sale because they are not provided as a meal or as a single member of the diet.

It has been reported in various studies that the use of supplements is higher in people with higher education levels and older people (Chen et al., 2011; Doğan et al., 2020; Çağındı et al., 2022). Reasons for this include suffering from various diseases or using drugs that reduce food absorption in people who cannot eat healthily enough or eat primarily fast food due to intense work tempo. Even if a balanced and high-quality diet is consumed, the absorption of vitamins, minerals, etc., in foods decreases with advancing

1 Institute of Science, Education Faculty, Department of Mathematics & Science Education, Ordu, Turkiye. ORCID Code: 0000-0003-1420-8729

age. As this increases the supply in the market, new products are added to the products marketed as food supplements every day. Although microalgae such as *Chlorella* have been used for years in the Far East for nutrition, drug production, etc., the spread of this microalgae as a food supplement to the world corresponds to recent years.

What is *Chlorella*?

Although algae are similar to plants in their ability to perform photosynthesis, they differ from plants in that they store photosynthesis products differently as starch, contain chlorophyll c and other pigments that are not found in plants, and are unable to form embryos. Algae are taxonomically divided into microalgae and macroalgae. Microalgae is a term used for algae smaller than 2 micrometers in diameter. A single-celled green freshwater algae *Chlorella* that originates in Korea, Taiwan, and Japan has rich in protein, dietary fiber, lipid-soluble vitamins, choline, and essential minerals. *Chlorella* mainly contains approximately 60% protein, and the amino acid quantity is regarded as the perfect protein except for methionine and tyrosine (Lee et al., 2008).

The genus *Chlorella* was discovered in 1890 by Beijerinck, and C. vulgaris is the type species of the genus. The culture of *Chlorella*, one of the green algae, was first made by Otto Warburg in 1919. This single-celled organism was tried to be grown under laboratory conditions, and in 1931, this study brought the German biochemist a Nobel Prize in medicine and physiology. Chlorella's popularity increased after it was heard that it was used on space stations and was known as "space algae" among the people. It is used to produce oxygen and biofuel required for astronauts in spacecraft. *Chlorella* vulgaris-assisted trials continue in hybrid life support unit tests at the International Space Station (Detrell, 2021).

Chlorella is known as a "superfood" because of its impressive nutrient profile. According to the study by Lee et al., 100 g of C. vulgaris powder contains 60.6 g of protein, 13 g of dietary fiber, 12.8 g of fat, 3.7 g of carbohydrates, 2400 mg of chlorophyll, 106 mg of carotene, 22.8 mg of vitamin E, 0.74 mg of vitamin c. and 100g is only 372kcal (Lee et al., 2008). It has a valuable biomass containing amino acids and bioactive peptides, mono and polyunsaturated fatty acids, chlorophyll, xanthophyll and beta carotene, beta1,3 glucan, and exopolysaccharides causes them to be used for various purposes (Figure 1-2). *Chlorella* is a good source of iron. It meets between 6-40% of your daily need. It is also an excellent source of vitamin C—this aids in the absorption of iron. *Chlorella* contains small amounts of magnesium, zinc, copper, potassium, calcium, folic acid, and other B

vitamins. These small green cells provide a rich content of antioxidants. Like other seaweeds, *Chlorella* has a high omega-3 content. Just 3 grams of *Chlorella* provides 100 mg of omega-3s.

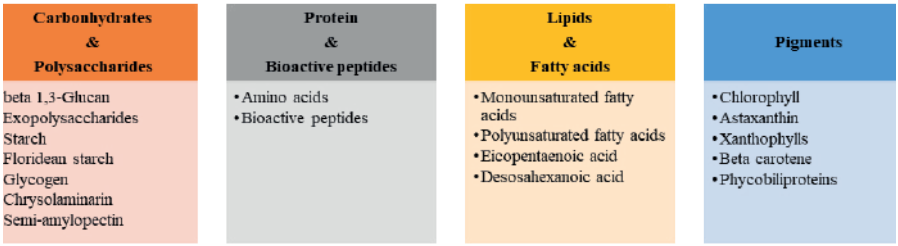

Figure 1. Chlorella Biomass Content

Figure 2. Chlorella application fields

Studies on the biological activity of *Chlorella* are generally related to *C. vulgaris, C. zofingiensis, C. sorokiniana, C. pyrenoidosa* species. There are studies about strengthening the immune system by *Chlorella* (An et al., 2008; Kang et al., 2013). *C. pyrenoidosa*, a single-celled microalga that grows in freshwater, is widely used in Japan and is consumed as a food supplement known to have beneficial effects on immune function. *Chlorella* is rich in antioxidants (Hernayanti & Simanjuntak, 2019; Yu et al., 2019; Wan et al., 2021). It was reported that *Chlorella* extract has an anticancer effect on hepatocellular cancer cell line (HepG2) and Ehrlich ascites carcinoma cell (Adzahar et al., 2021). It has been reported by Zhang et al. that *Chlorella* has an antitumoral effect on human colon cancer cells. In the same articles,

it has been reported that the exopolysaccharides of *Chlorella* have this effect (Zhang et al., 2019a; Zhang et al., 2019b).

Chlorella intake was adequate for blood glucose regulation in rats fed a high-fat diet. *Chlorella* intake may prevent insulin resistance in Wistar rats fed a high-fat diet. Lee & Kim, in their article published in 2009, reported that 10% *Chlorella* intake was effective in blood sugar regulation in Wistar rats fed a high-fat diet. This study has a promising result in preventing insulin resistance (Lee& Kim, 2009).

Chlorella helps regulate total cholesterol and LDL_C levels in Wistar rats and human adults (Lee et al., 2008; Sherafati et al., 2022). It has been reported that *C. vulgaris* decreases total lipid in the liver and serum and increases the amount of lipid excreted in feces in Wistar rats. Therefore, the consumption of *Chlorella* is promising in preventing dyslipidemia (Lee et al., 2008). Sherefati et al., In a systematic review study published in 2022, reported that *C. vulgaris* dietary supplements had beneficial effects on total cholesterol and LDL-C levels. They stated that the most effective dosage should be lower than 1500 mg per day (Sherefati et al., 2022).

Lower the risk of anemia in pregnant women: In the article Nakano et al. in 2010, they gave 6 grams of *Chlorella* dietary supplement to 32 pregnant women from the 12th week to the 18th week. In the control group trial conducted on 70 pregnant women, the anemia rate of pregnant women in the experimental group was found to be significantly lower than those in the control group (Nakano et al., 2010).

C. vulgaris has the potential to be an alternative antidepressant (Soetantyo & Sarto 2019; Dome et al 2019). Dietary supplements can be used to support drug therapy in standard antidepressant treatment. There are limited experimental studies in which Chlorella dietary supplement is used in addition to drug therapy in the antidepressant treatment, and positive results are obtained (Panahi et al., 2015).

Chlorella contains lutein and zeaxanthin, two carotenoids that protect the eye and reduce the risk of cataracts and macular degeneration. It has been mentioned in various studies that *Chlorella* primarily supports the nervous system with its high content of carotenoids and antioxidants. They also have potent anti-inflammatory effects. Due to these properties, it has been reported that it has a protective effect, especially in tissues exposed to intense oxygen and, therefore, oxidative stress. We can add hepatoprotective to this protective effect (Hernayanti & Simanjuntak, 2019; Zafar et al., 2021; Zhang et al., 2019c; Capek et al., 2020).

Antimicrobial effect of *Chlorella*: The first antibacterial studies on *Chlorella* were made in 1944 by Pratt et al. in his work. They reported that *Chlorella* has an antibacterial content, which they call Chlorellin. Najdenski et al. In the antimicrobial activity study, they applied to some microalgae they selected in 2013, reported that the water extract of *Chlorella* sp. was effective only against *Stahylococcus aureus* and *S. pyogenes*, but not on *Pseudomonas aeroginosa* and *Candida albicans*. Mashhadinejad et al., in their study published in 2017, affect the effects of *C. vulgaris* microalgae growing conditions and extraction solvent on antimicrobial activity on *S. aureus, B. subtilis, E. coli, P. aeroginosa*, and *C. albicans* agar well diffusion and minimum inhibitory concentration. Research method. Among the acetone, chloroform, and ethyl acetate solvents, the most effective solvent was chloroform, and the least effective was acetone. Velichkova et al. (2018) investigated the antimicrobial activity of ethanolic extracts of *Spirulina* sp., *Chlorella* vulgaris, and *Lemna minuta* by agar well diffusion method. *S. aureus* ATCC 25923, *E. coli* ATCC 25922, *P. aeruginosa* ATCC 27853), *Bacillus cereus*, *Salmonella typhimurium*, *C. albicans*, Malassezia pachydermatis were used as a pathogen. they were reported to be effective. In the study conducted by Dineshkumar et al. in 2017, *K. pneumoniae*, *P. mirabilis*, *V. cholerae*, *S. typhi, E. coli, S. aureus, B. subtilis, Enterococcus* sp., *Clostridium botulini*, *Nocardia* sp. They tried the antimicrobial effect of ethanolic, methanolic chloroform, and diethylether *Chlorella* extracts on ethanolic extracts by disc diffusion method and found low antimicrobial activity (Syed et al., 2015; Pradhan et al., 2021).

In which forms is Chlorella used as a dietary supplement?

Chlorella has supplements in liquid, tablet, and powder form. Its nutritional value can be increased when the powder form is added to salads, cheese, sauces, smoothies or other beverages.

Diprat et al., in their study in 2020, *C. sorokiniana* was used to make gluten-free-beta carotene-rich bread. Bread with 2.5% microalgae had an acceptance rate of over 70% (Diprat et al., 2020). *Chlorella* has also been used by adding organic energy bars, noodles, and yogurt (Raja et al. 2018). *Chlorella* is also used in the famous Japanese wasabi.

Points to consider about *Chlorella*

It is vital to consult a physician, pharmacist, or other healthcare professional before starting to use a food supplement. A product that is "natural" may also not be "safe." Because an allergic situation may develop against the nutritional supplement that is planned to be taken, or it may interact with the drug or other food supplements being used. For this reason, it is an

essential point at which age, condition, etc., to use the food supplement. It should not be ignored that vitamin and mineral supplements are made into packaged products today. When nutritional supplements, multivitamins, and a diet rich in vitamins and minerals come together, the intake of a mineral such as iron may exceed the recommended dose.

Like plants, the chemical composition of algae is affected by the habitat in which it grows. In recent years it has been reported that *C. vulgaris* can absorb heavy metals, and it has been widely used in wastewater treatment and advanced biological treatment systems (Manzoor et al., 2019; Blosi et al., 2022). In this context, if *Chlorella* is to be used as a food or nutritional supplement, it is very important to provide a product with clean ingredients.

Another point to be considered is to control the purity, quality, and potency of the nutritional supplement. The FDA in the United States and the Ministry of Agriculture and Forestry in the Republic of Turkey are responsible for the implementation of laws and regulations governing dietary supplements. The current list of approved supplements or restricted substances in Turkey can be accessed from the food safety information system on the official website of the Ministry of Agriculture and Forestry (https://ggbs.tarim.gov.tr/).

REFERENCES

Adzahar, N. S., Basri, D. F., Latif, E. S., & Sallehudin, N. J. (2021). In Vitro and in Vivo Cytotoxic Effects of Chlorella Against Various types of Cancer. *IIUM Medical Journal Malaysia*, *20*(1).

An, H. J., Rim, H. K., Lee, J. H., Seo, M. J., Hong, J. W., Kim, N. H., ... & Kim, H. M. (2008). Effect of Chlorella vulgaris on immune-enhancement and cytokine production in vivo and in vitro. *Food Science and Biotechnology*, *17*(5), 953-958.

Blosi, M., Brigliadori, A., Zanoni, I., Ortelli, S., Albonetti, S., & Costa, A. L. (2022). Chlorella vulgaris meets TiO2 NPs: effective sorbent/photocatalytic hybrid materials for water treatment application. *Journal of Environmental Management*, *304*, 114187.

Capek, P., Matulová, M., Šutovská, M., Barboríková, J., Molitorisová, M., & Kazimierová, I. (2020). Chlorella vulgaris α-L-arabino-α-L-rhamno-α, β-D-galactan structure and mechanisms of its anti-inflammatory and anti-remodelling effects. *International Journal of Biological Macromolecules*, *162*, 188-198.

Chen, S. Y., Lin, J. R., Chen, T. H., Guo, S. G., Kao, M. D., & Pan, W. H. (2011). Dietary supplements usage among elderly Taiwanese during 2005-2008. *Asia Pacific journal of clinical nutrition*, *20*(2), 327-336.

Çağındı, Ö., Yeyinli, N., İnce C., Dedeoğlu, M., & Köse E. (2022). Covıd-19 Hastalığını Önlemede Kullanılan Takviye Edici Gıdalar ve Sağlık Üzerine Etkileri. *Gıda*, *47*(2), 183-198.

Detrell, G. (2021). Chlorella vulgaris photobioreactor for oxygen and food production on a moon base—potential and challenges. *Frontiers in Astronomy and Space Sciences*, *8*, 700579.

Dineshkumar, R., Narendran, R., Jayasingam, P., & Sampathkumar, P. (2017). Cultivation and chemical composition of microalgae *Chlorella vulgaris* and its antibacterial activity against human pathogens. *J Aquac Mar Biol*, *5*(3), 00119.

Doğan, S., Okumuş, E., Bakkalbaşı, E., & Cavidoğlu, İ. (2020). Van İli Kentsel Alanda Takviye Edici Gıdaların Kullanımı ve Tüketicilerin Bilinç Düzeyi. *Yüzüncü Yıl Üniversitesi Fen Bilimleri Enstitüsü Dergisi*, *25*(2), 75-84.

Dome, P., Tombor, L., Lazary, J., Gonda, X., & Rihmer, Z. (2019). Natural health products, dietary minerals and over-the-counter medications as add-on therapies to antidepressants in the treatment of major depressive disorder: a review. *Brain Research Bulletin*, *146*, 51-78.

Diprat, A. B., Thys, R. C. S., Rodrigues, E., & Rech, R. (2020). Chlorella sorokiniana: A new alternative source of carotenoids and proteins for gluten-free bread. *Lwt*, *134*, 109974.

Kang, H. K., Salim, H. M., Akter, N., Kim, D. W., Kim, J. H., Bang, H. T., ... & Suh, O. S. (2013). Effect of various forms of dietary Chlorella supplementation on growth performance, immune characteristics, and intestinal microflora population of broiler chickens. *Journal of Applied Poultry Research*, *22*(1), 100-108.

Hernayanti, H., & Simanjuntak, S. B. I. (2019). Antioxidant effect of Chlorella vulgaris on physiological response of rat induced by carbon tetrachloride. *Biosaintifika: Journal of Biology & Biology Education*, *11*(1), 84-90.

Lee, H. S., Park, H. J., & Kim, M. K. (2008). Effect of Chlorella vulgaris on lipid metabolism in Wistar rats fed high fat diet. *Nutrition research and practice*, *2*(4), 204-210.

Lee, H. S., & Kim, M. K. (2009). Effect of Chlorella vulgaris on glucose metabolism in Wistar rats fed high fat diet. *Journal of medicinal food*, *12*(5), 1029-1037.

Manzoor, F., Karbassi, A., & Golzary, A. (2019). Removal of heavy metal contaminants from wastewater by using Chlorella vulgaris beijerinck: a review. *Current Environmental Management (Formerly: Current Environmental Engineering)*, *6*(3), 174-187.

Mashhadinejad, A., Zamani, H., Sarmad. J. (2017). Effect of growth conditions and extraction solvents on enhancement of antimicrobial activity of the microalgae *Chlorella vulgaris.* Pharm Biomed Res 2016; 2(4): 65-73.

Nakano, S., Takekoshi, H., & Nakano, M. (2010). Chlorella pyrenoidosa supplementation reduces the risk of anemia, proteinuria and edema in pregnant women. *Plant foods for human nutrition*, *65*(1), 25-30.

Najdenski, H. M., Gigova, L. G., Iliev, I. I., Pilarski, P. S., Lukavský, J., Tsvetkova, I. V., Ninova, M. S. & Kussovski, V. K. (2013). Antibacterial and antifungal activities of selected microalgae and cyanobacteria. *International journal of food science & technology, 48*(7), 1533-1540.

Nicoletti, M. (2016). Microalgae nutraceuticals. *Foods*, *5*(3), 54.

Panahi, Y., Badeli, R., Karami, G. R., Badeli, Z., & Sahebkar, A. (2015). A randomized controlled trial of 6-week Chlorella vulgaris supplementation in patients with major depressive disorder. *Complementary therapies in medicine*, *23*(4), 598-602.

Panahi, Y., Darvishi, B., Jowzi, N., Beiraghdar, F., & Sahebkar, A. (2016). Chlorella vulgaris: a multifunctional dietary supplement with diverse medicinal properties. *Current pharmaceutical design*, *22*(2), 164-173.

Pradhan, B., Patra, S., Dash, S. R., Nayak, R., Behera, C., & Jena, M. (2021). Evaluation of the antibacterial activity of methanolic extract of Chlorella vulgaris Beyerinck [Beijerinck] with special reference to antioxidant modulation. *Future Journal of Pharmaceutical Sciences*, *7*(1), 1-11.

Raja, R., Coelho, A., Hemaiswarya, S., Kumar, P., Carvalho, I. S., & Alagarsamy, A. (2018). Applications of microalgal paste and powder as food and feed: An update using text mining tool. *Beni-Suef University journal of basic and applied sciences*, *7*(4), 740-747.

Sherafati, N., Bideshki, M. V., Behzadi, M., Mobarak, S., Asadi, M., & Sadeghi, O. (2022). Effect of supplementation with Chlorella vulgaris on lipid profile in adults: a systematic review and dose-response meta-analysis of randomized controlled trials. *Complementary Therapies in Medicine*, 102822.

Soetantyo, G. I., & Sarto, M. (2019). The antidepressant effect of Chlorella vulgaris on female Wistar rats (Rattus norvegicus Berkenhout, 1769) with chronic unpredictable mild stress treatment. *J Trop Biodivers Biotechnol*, *4*, 72-81.

Syed, S., Arasu, A., & Ponnuswamy, I. (2015). The uses of Chlorella vulgaris as antimicrobial agent and as a diet: the presence of bio-active compounds which caters the vitamins, minerals in general. *International Journal of Bio-Science and Bio-Technology*, *7*(1), 185-190.

Velichkova, K., Sirakov, I., Rusenova, N., Beev, G., Denev, S., Valcheva, N., Dinev, T. (2018). In vitro antimicrobial activity on *Lemna minuta, Chlorella vulgaris* and *Spirulina* sp. extracts, *Fresenius Enviromental Bulletin, 27*(8), 5736-5741.

Wan, X., Li, X., Liu, D., Gao, X., Chen, Y., Chen, Z., ... & Zhao, C. (2021). Physicochemical characterization and antioxidant effects of green microalga Chlorella pyrenoidosa polysaccharide by regulation of microRNAs and gut microbiota in Caenorhabditis elegans. *International Journal of Biological Macromolecules*, *168*, 152-162.

Yu, M., Chen, M., Gui, J., Huang, S., Liu, Y., Shentu, H., ... & Zhang, Y. (2019). Preparation of Chlorella vulgaris polysaccharides and their antioxidant activity in vitro and in vivo. *International journal of biological macromolecules*, *137*, 139-150.

Zafar, J., Aqeel, A., Shah, F. I., Ehsan, N., Gohar, U. F., Moga, M. A., ... & Chicea, R. (2021). Biochemical and Immunological implications of Lutein and Zeaxanthin. *International Journal of Molecular Sciences*, *22*(20), 10910.

Zhang, J., Liu, L., Ren, Y., & Chen, F. (2019a). Characterization of exopolysaccharides produced by microalgae with antitumor activity on human colon cancer cells. *International journal of biological macromolecules*, *128*, 761-767.

Zhang, J., Liu, L., & Chen, F. (2019b). Production and characterization of exopolysaccharides from Chlorella zofingiensis and Chlorella vulgaris with anti-colorectal cancer activity. *International journal of biological macromolecules*, *134*, 976-983.

Zhang, R., Chen, J., Mao, X., Qi, P., & Zhang, X. (2019c). Anti-inflammatory and anti-aging evaluation of pigment–protein complex extracted from Chlorella pyrenoidosa. *Marine drugs*, *17*(10), 586.

CHAPTER 4

Al Doping Influence on Structural, Morphological and Optical Properties of CuO Films

Şilan BATURAY[1]

Canan AYTUĞ AVA[2]

1. Introduction

Copper oxide nanostructured materials is very interesting semiconductor material. Characteristically, copper oxide can be originated different forms as cuprous oxide (Cu_2O) and copper monoxide (CuO), and it shows crystal form of Cu_4O_3 (Suda et al., 1992). These crystal properties are encouraging materials owing to their excellent optical and electrical properties, environmentally friendly, richness in environment, low-cost, strong absorption coefficient in the region of UV-Vis, etc (Sultana et al., 2017).

While copper oxide compound is a characteristic *n*-type conductivity, cuprous oxide is a monoclinic *p*-type conductivity. Copper oxide nanostructured materials are generally used in application of

1 Dicle University, Faculty of Science, Department of Physics, 21280, Diyarbakir, Turkey. Bu çalışmanın bir bölümü X. INTERNATIONAL ISTANBUL SCIENTIFIC RESEARCH CONGRESS de "STRUCTURAL AND OPTICAL PROPERTIES OF AL DOPED CuO FILMS" başlığı altında tam metin olarak sunulmuştur.

2 Dicle University, Science and Technology Application and Research Center, 21280, Diyarbakir, Turkey, Dicle University, Department of Physics, Institute of Natural Sciences, 21280, Diyarbakir, Turkey

microelectronics (Zhen et al., 2018), field-emission instruments (Chen et al., 2005) biotechnology (Hassan et al., 2019), catalysts (Prasad and Rattan, 2010), photovoltaic application (Wang et al., 2011), super-capacitors application (Nandhini et al., 2019), *p-n* junctions (Zhao et al., 2021), lithium ion battery anodes (Ko et al., 2012), high-temperature superconductors sensors (Cava et al., 1987) because of the fact that it have important structural, electrical, magnetic and optical properties related to those of conventional bulk materials. In general, CuO has monoclinic *p*-type electrical conductivity for fabricating variety of procedures owing to the holes which is seen in the valence band of the nanostructured material. Additionally, the material of nanostructured has an indirect optical energy band value which allows it to fold extra energy (Masudy-Panah et al., 2016). The informed optical energy band value for CuO material changes between 1.2 and 2.1 eV (Venkateswari et al., 2017; Zheng and Liu, 2007). In the Cu_2O nanostructured materials, the direct energy band value changes between 2.1 and 2.6 eV and the crystal configuration of this nanostructured material was given as cubic; it is similarly given as cuprite in the works (Dolai et al., 2017). Similarly, the Cu_2O nanostructured material has indicated a *p*-type conductivity due to negative vacancies and strong electronegativity value of the copper element.

Shape controlled topologies have an important role in the properties of the transition metal oxides films in the nanoscale region. Also, a number of metals can be used as doping elements to improve quality of crystalline properties of thin films with excellent physical and chemical properties of CuO thin films. Ramyaet et al. (2016) have synthesized Ni:CuO nanostructured materials using precipitation technique and reported that metal doping has tailored the structure of energy band gap and luminescence properties which in turn improved the antibacterial activity of CuO materials. Shaikh et al. (2011) demonstrated that Ru doped CuO film has an important role in improving green chemistry approach for more efficient supercapacitors. Huang et al. (2012) reported that Ag particle loaded on the CuO nanosheet arrays affected the electrical conductivity of the electrode and increased the electrical interaction among the used substrate using a template-free fabrication technique and silver mirror reactions.

The effects of various parameters such as annealing methods, storage temperature, film thickness, distance from solution spray head, solvent property and storage time were investigated so far. These parameters have changed the physical properties including crystal parameters, absorbance and transmittance value of the thin films, and this has led the researchers to improve the both chemical and physical properties of the CuO samples to be

obtained by using different metals. While the physical and chemical properties of nanostructured CuO thin films have been examined by groups (Bae and Choi, 1999; Chaudhary et al., 2004; Mageshwari and Sathyamoorthy, 2013; Morales et al., 2005; Tamaki et al., 1998), Al:CuO thin films fabricated by using spin-coating method have not comprehensively been studied to date.

Metal doping has a great influence on the crystal parameters and optical properties of the CuO nanostructured film. However, there are few experimental studies on Al contribution. Therefore, further experimental studies are needed to better understand the effect of Al doping on the physical properties of the pure CuO. There is limited information about the effects on the crystal parameters, absorbance and transmittance value of Al:CuO samples prepared by method of spin coating, and Al:CuO films obtained by this technique have not been extensively investigated until now. In this study, Al:CuO thin films of were obtained by using the spin coating technique, which is an efficient, cost-effective and simple preparation method, and the crystal and optical properties of these thin films were investigated. The effect of the variation of the Al doping on the crystal structure and structural properties on thin film was evaluated using XRD. The transmittance, absorption properties the films in the visible region were analyzed using the UV-Vis device.

2. Experimental details

In the present study, Al doped CuO samples with three unlike weight ratios (0, 2 and 4 at wt% of Al) were fabricated on SLG substrate by employing a solution comprising 0.1 M copper(II) acetate ($Cu(CH_3COO)_2 \cdot H_2O$) and 0.01 Al deposited under optimized condition. 0.1 M copper(II) acetate was stirred in 100 ml of absolute ethanol for 18 h at temperature of 300 K. 0.01 M Al was stirred in 20 ml of ethanol for the same condition. After this, a certain amount of Al was slowly embedded into the solution of copper(II) acetate to give dissimilar doping and finally, the gained Al:CuO solutions were stirrer on magnetic stirring at room temperature for around 8 h until a homogenous solution was gained. Before the deposition procedure, the all SLG substrates were cleaned by boiling in enough quantities of a mixture of H_2O, NH_3, and H_2O_2 at 120 °C and then in sufficient quantities of a mixture of H_2O, H_2O_2, and HCl at 120 °C to eliminate any remaining waste. Then, the substrates were stirrer in deionized water for 5 min on magnetic stirring and later dried under N_2 atmosphere. After gaining the final Al:CuO solutions and washing the SLG substrates, the samples were grown via spin coated at 1800 rpm for 60 s in air conditions. The obtained solutions were grown onto the substrate of SLG sheet by sheet, and all sheets were heated to

around 220 °C for 8 min. After this process, obtained samples were annealed at around 500 °C for 1h in air. The influence of different Al doping on the CuO's structural and optical properties are studied in this work.

The crystal parameters of obtained Al:CuO thin films were determined with the help of Rigaku Smart Lab X-ray diffractometer (XRD: Cu Kα radiation, λ=1.540056 Å). Surface topology of Al doped CuO samples were investigated using Park System XE 100 Atomic Force Microscope (AFM) at room temperature. A Shimadzu UV-3600 system was used to record the energy gap, absorbance and transmittance value of the samples.

3. Results and Discussion

3.1. X-Ray Diffraction Analysis

Fig. 1. demonstrations the typical XRD patterns for Al: CuO films grown onto SLG annealed at 500 °C in furnace. As seen as this figure, the strong peaks at 35.5° and 39.0° were appeared for all films in XRD patterns and correspond to (-111) and (200), respectively and there are phases of oxide associated to the phase of impurity due to the compound formation containing Al and Cu_2O. The XRD patterns show that Al:CuO samples are a single-phase monoclinic crystal structure. Peak positions (*hkl*), values of crystallite size (D) in nanometers, full width at half maximum (FWHM) value which is known as β, and inter planar spacing (d) are given in table 1. Furthermore, there are differences in the peak positions while the intensity of the (-111) and (200) orientations peaks changed which correspond to a preferred orientation of obtained polycrystalline structure. Al addition changed the crystal structure of the films, which may be attributed to the significant difference ionic radii of the Al^{+3} ion (0.5 Å) and Cu^{+2} ion (0.73 Å), thus, Cu and Al can be changed the crystal structure of CuO. These results (the intensity of peaks, peak broadening and shift in the peak position) indicate that Al^{3+} ions were effectively inserted into the CuO lattice.

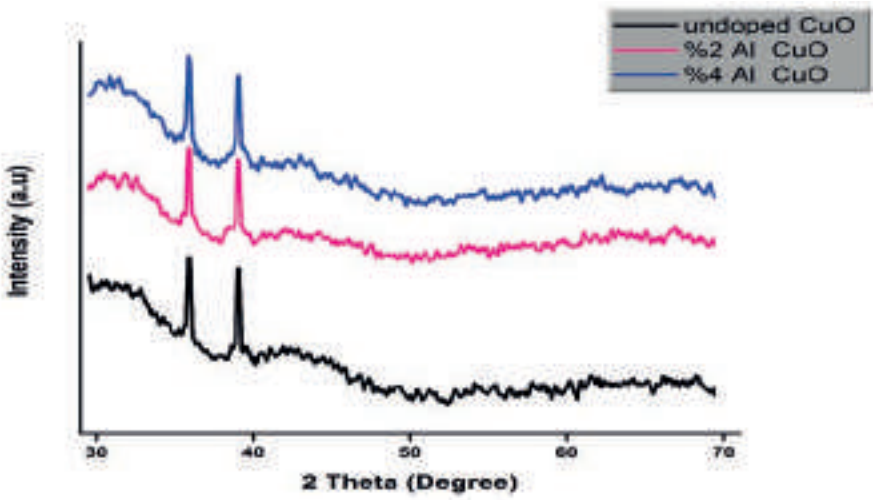

Fig. 1. XRD patterns of Al doped CuO thin film

We used Scherer's equation to calculate D value of Al doped CuO samples from data of XRD. Scherer's equation is as follows;

$$D = \frac{k\lambda}{\beta \cos\theta} \tag{1}$$

where $\lambda = 1.540056$ Å is the wavelength of Cu Kα, θ is Bragg's diffraction angle. Calculated crystallite size for (111) peak decrease from 52 to 14 nm by increasing Al doping ratio. Devi et al. (Devi et al., 2018) point out that the crystallinity of the La:CuO film increases as increasing the temperature value. La doping in CuO solution decreases the crystallinity because of the difference of ionic radii and also mains to peak shift. This is owing to strong ionic mobility and minor radius of Al ions in CuO solution. d values of the Al:CuO samples is theoretically calculated using the Bragg's equation (Cullity, 1978):

$$2d\sin\theta = n\lambda \tag{2}$$

where n is the order of diffraction. d values of the sample of (-111) and (200) peaks are found to be around 2.50 and 2.30 Å.

Table I. Crystallite parameters of the Al:CuO films obtained by XRD data

Sample	2 Theta Peak (Degree)	Grain Size (nm)	d-spacing (Å) (calculated)	d-spacing (Å) (standart)	Orientation	Dislocation Density ($x10^{15} m^{-2}$)	Strain ($x10^{-4}$)
Undoped	35.96	51.87	2.538	2.493	(-111)	0.37	0.23
	39.87	10.93	2.261	2.305	(200)	8.37	0.97
2 % Al:CuO	35.53	13.09	2.527	2.525	(-111)	5.83	0.91
	38.19	14.06	2.356	2.355	(200)	5.06	0.79
4 % Al:CuO	35.82	16.13	2.507	2.501	(-111)	3.84	0.73
	39.10	13.90	2.304	2.323	(200)	5.18	0.78

The dislocation density value (δ), which indicates the amount of defects in films, is calculated using the following equation [26]:

$$\delta = \frac{1}{D^2} \tag{3}$$

The change in the strain value of the samples is found by following formula:

$$\varepsilon = \frac{\beta}{4tan\theta} \tag{4}$$

The dislocation density value of (-111) plane is changed between 3.7 x 10^{14} and 5.83 x 10^{14} m^{-2} and 83.7 x 10^{14} and 50.6 x 10^{14} m^{-2} for (200) owing to the expansion of structural parameters with Al dopant content in solution. The strain value of (-111) and (200) planes is radically changed related to increase Al dopant content. Thus, it was seen that the main effect of change in crystallite size is related to difference in strain and dislocation value. Mageshwari and Sathyamoorthy (2013) demonstrated that value of the film decreases with the increase in fabrication cycles.

3.2. Morphological Properties

The surface morphologies of the deposited Al doped CuO films are very important to analyze the surface properties of the obtained samples. Al affects the surface morphology of CuO films for different doping concentrations: Fig. 2 indicates the 3-D images of AFM of Al doped CuO thin films grown by the spin-coating method at different scales. The figures indicate that the thin films with rod-like particles and a grain structure. The obtained results revealed that samples are comparatively smooth in the valley area while many crystals-like structures are seen in the hill area which indicates definite

orientations. It could be seen in the figure that the thin film surface is not uniform. It can be seen that the all thin films are comparatively smooth and well adhered to the SLG substrate. The coverage rate of the nanoparticles on surface changed as Al doping ratio rise, which change the mobility and resistivity value of CuO thin film. Abed et al. (2021) showed the same morphological properties and they analyzed the surface properties of thin films of carbon doped CuO:NiO to modify the physical properties of carbon.

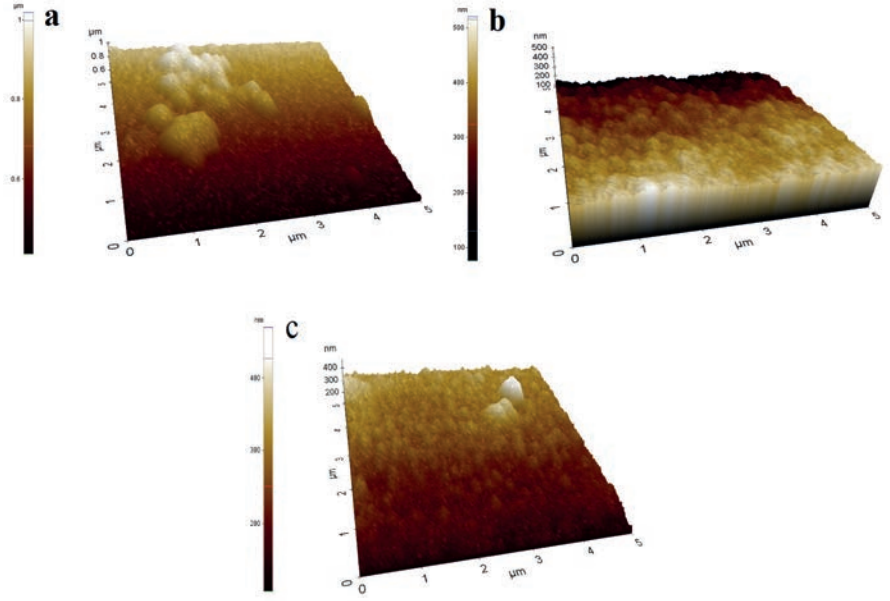

Fig. 2. 3-D AFM images of Al: CuO thin film

3.3. Optical Properties

The absorbance and transmittance of used nanostructured materials effect with many variables like the deposition technique, surface topology, and some deposition conditions (temperature, film thickness, annealed time), related to their interaction with the ambient. To investigate the effect of different metal doping concentrations on the absorbance and transmittance value of each film were carried out in 300-1100 nm spectrum range. The analysis of the value of absorption coefficient for any nanostructured gives extra knowledge concerning the levels of electrons in the high-energy range of the spectral absorption spectra, while the low-energy range of the spectral absorption spectrum related to the atoms' vibration (El-Hagary et al., 2012; Urbach, 1953). Dissimilar applications are dependent on the

spectral absorption spectrum of the Al:CuO film, and the coefficient of absorption can be calculated from the measurement of absorbance data with the wavelength in nm and calculated from the Beer–Lambert law (Abdul Nabi et al., 2014).

$$!nI / I_0 = e^{-\alpha t}, \alpha = 2.303^{*} A / t \quad (5)$$

where α is a constant which shows the value of absorbance coefficient, A is the value of absorbance, and t is the value of film thickness.

α value of the Al doped CuO thin film is dependent on the wavelength value in UV-Vis region, as shown in Fig 3. The obtained consequences in this Figure indicates that the optical absorption coefficient upsurge with the change in wavelength for Al:CuO samples until a certain wavelength.

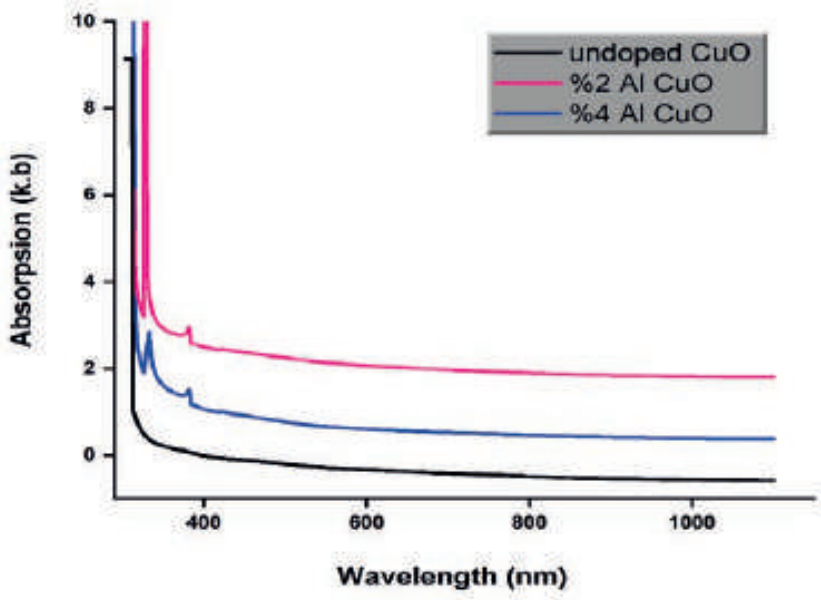

Fig. 3. Absorbance of Al: CuO thin film

The obtained samples have high absorption in the region of UV-Vis and have a high affinity for UV light. It can be said that the change in the absorption value is a result of the different crystal nature of the films and the Moss-Burstein effect (Manjunatha et al., 2018). The obtained results show that the optical properties of the samples change depending on Al doping. The change in the absorption value of the films shows that the obtained films can be applied in various optical applications.

Transmittance changes of Al:CuO samples annealed at 500 ˚C are indicated in Fig. 4. While pure sample indicated an average transparency value of ~42 % in the visible range of UV-Vis region, together with the Al doping average transmittance value decreased to ~30% for 4% Al doped sample.

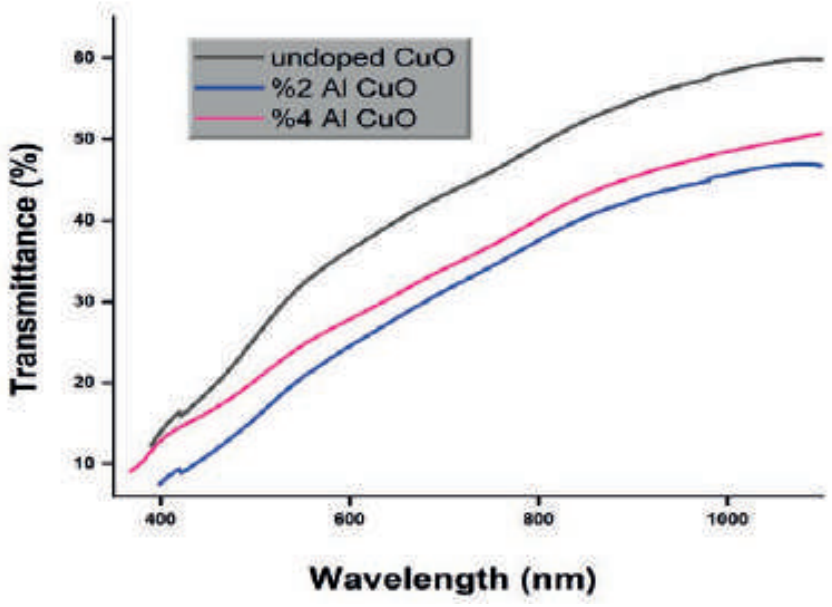

Fig. 4. Transmittance of Al doped CuO thin film

Optical properties of nanostructured CuO samples can be improved by Al doping in the UV-Vis spectra. The change in the optical transmittance value suggests that Al:CuO samples may be used as some applications like optical windows (Muiva et al., 2011).

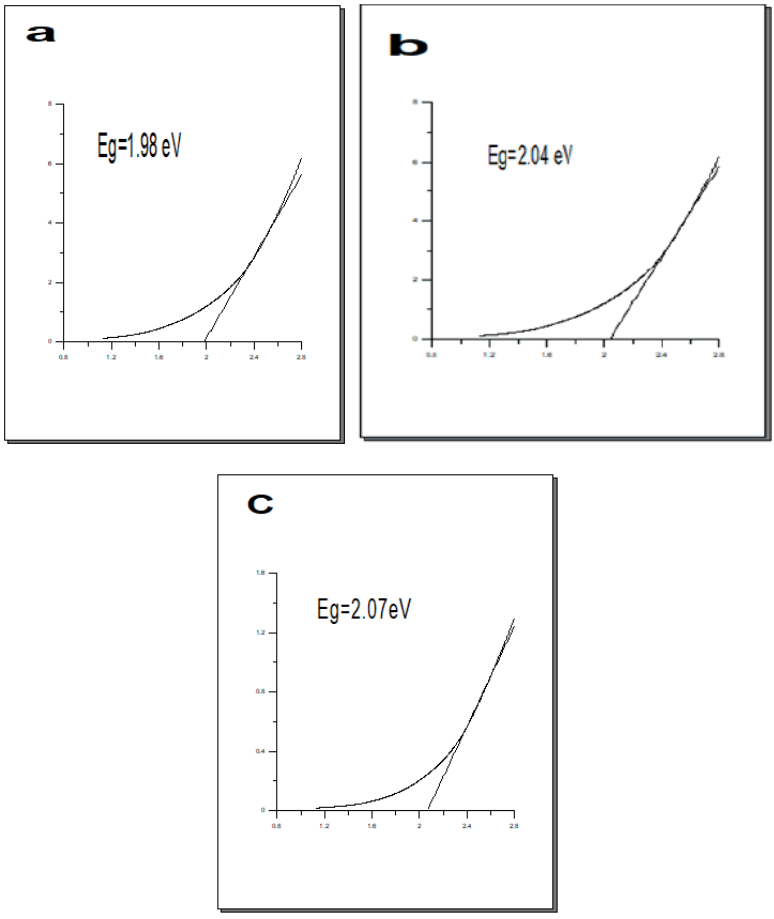

Fig. 5. Energy band gap of a) 0% Al:CuO, b) 2% Al:CuO , c) 4% Al:CuO thin film

The optical band gap energies are determined using the following equation

$$(\alpha h\nu)^2 = \beta\left(h\nu - E_g\right) \tag{6}$$

where β is an energy-independent constant, $h\nu$ is incident photon energy. The band gap energy values for all the films increased from 1.98 (no doping) to 2.04, 2.07 eV (2%, 4%, respectively) because of the basis of Moss-Burstein- (M-B) shift (Zhao et al., 2002). Jan et al. (2019) indicated that the presence of Al ions in CuO lattice has been seen to significantly affect the optical properties including transmittance and energy band gap because of difference in electro negativities, which may be associated with particle size and oxygen vacancies and formation of defects of used ions. They are

also said that the optical energy band gap of CuO has been increased with the metal doping ratio which may be attribute to oxygen vacancies and particle size.

4. Conclusions

p-type nanostructured Al: CuO samples were grown onto glass substrate using spin coating method and the crystal and optical properties of all films were studied related to Al doping ratio. The XRD spectra shown that all the Al:CuO samples had polycrystalline nature with preferential (-111), (200) orientations. The grain sizes of all the films for different concentrations at 500 ^{0}C determined from the value of FWHM by Scherer 's equation. Calculated crystallite size for (111) peak decrease from 52 to 14 nm by increasing Al doping ratio. *d* values of the sample of (-111) and (200) peaks are found to be around 2.50 and 2.30 Å. AFM images indicate that the thin films with rod-like particles and a grain structure. The spectral absorption coefficient for Al:CuO film increase with the increase in wavelength for Al:CuO thin film until a certain wavelength (about ~ 1100 nm). While pure sample indicated an optical transparency of ~42 % in the visible range, together with optical transmittance value decreased to ~30% for 4% Al doped sample. The band gap energy values for all the films changed from 1.98 (no doping) to 2.04, 2.07 eV (2%, 4%, respectively).

References

Abdul Nabi, M., Yusop, R. M., Yousif, E., Abdullah, B. M., Salimon, J., Salih, N., & Zubairi, S. I. (2014). Effect of nano ZnO on the optical properties of poly (vinyl chloride) films. *International journal of polymer science*, *2014*.

Abed, R. N., Abdallh, M., Rashad, A. A., Hadawey, A., & Yousif, E. (2021). New coating synthesis comprising CuO: NiO/C to obtain highly selective surface for enhancing solar energy absorption. *Polymer Bulletin*, *78*(1), 433-455.

Bae, H. Y., & Choi, G. M. (1999). Electrical and reducing gas sensing properties of ZnO and ZnO–CuO thin films fabricated by spin coating method. *Sensors and Actuators B: Chemical*, *55*(1), 47-54.

Cava, R. J., Santoro, A., Johnson Jr, D., & Rhodes, W. (1987). Crystal structure of the high-temperature superconductor La 1.85 Sr 0.15 CuO 4 above and below T c. *Physical Review B*, *35*(13), 6716.

Chaudhary, Y. S., Agrawal, A., Shrivastav, R., Satsangi, V. R., & Dass, S. (2004). A study on the photoelectrochemical properties of copper oxide thin films. *International journal of hydrogen energy*, *29*(2), 131-134.

Chen, J., Huang, N., Deng, S., She, J., Xu, N., Zhang, W., Wen, X., & Yang, S. (2005). Effects of light illumination on field emission from CuO nanobelt arrays. *Applied Physics Letters*, *86*(15), 151107.

Cullity, B. (1978). Elements of X-ray Diffraction, 2nd edn Addison-Wesley. *Reading*, *102*.

Devi, L. V., Sellaiyan, S., Sankar, S., & Sivaji, K. (2018). Structural and optical investigation of combustion derived La doped copper oxide nanocrystallites. *Materials Research Express*, *5*(2), 024002.

Dolai, S., Dey, R., Das, S., Hussain, S., Bhar, R., & Pal, A. (2017). Cupric oxide (CuO) thin films prepared by reactive dc magnetron sputtering technique for photovoltaic application. *Journal of Alloys and Compounds*, *724*, 456-464.

El-Hagary, M., Emam-Ismail, M., Shaaban, E., & El-Taher, A. (2012). Effect of γ-irradiation exposure on optical properties of chalcogenide glasses Se70S30− xSbx thin films. *Radiation Physics and Chemistry*, *81*(10), 1572-1577.

Hassan, S. E.-D., Fouda, A., Radwan, A. A., Salem, S. S., Barghoth, M. G., Awad, M. A., Abdo, A. M., & El-Gamal, M. S. (2019). Endophytic actinomycetes Streptomyces spp mediated biosynthesis of copper oxide nanoparticles as a promising tool for biotechnological applications. *JBIC Journal of Biological Inorganic Chemistry*, *24*(3), 377-393.

Huang, J., Wu, H., Cao, D., & Wang, G. (2012). Influence of Ag doped CuO nanosheet arrays on electrochemical behaviors for supercapacitors. *Electrochimica Acta*, *75*, 208-212. https://doi.org/https://doi.org/10.1016/j.electacta.2012.04.134

Jan, T., Azmat, S., Mansoor, Q., Ilyas, S., Ahmad, I., Khan, H., & Ismail, M. (2019). Structural, Raman, optical and novel antibacterial characteristics of Al doped CuO nanostructures. *Materials Research Express*, *6*(10), 1050a1053.

Ko, S., Lee, J. I., Yang, H. S., Park, S., & Jeong, U. (2012). Mesoporous CuO particles threaded with CNTs for high-performance lithium-ion battery anodes. *Advanced materials*, *24*(32), 4451-4456.

Mageshwari, K., & Sathyamoorthy, R. (2013). Physical properties of nanocrystalline CuO thin films prepared by the SILAR method. *Materials Science in Semiconductor Processing*, *16*(2), 337-343.

Masudy-Panah, S., Moakhar, R. S., Chua, C. S., Kushwaha, A., Wong, T. I., & Dalapati, G. K. (2016). Rapid thermal annealing assisted stability and efficiency enhancement in a sputter deposited CuO photocathode. *RSC advances*, *6*(35), 29383-29390.

Morales, J., Sanchez, L., Martin, F., Ramos-Barrado, J., & Sanchez, M. (2005). Use of low-temperature nanostructured CuO thin films deposited by spray-pyrolysis in lithium cells. *Thin Solid Films*, *474*(1-2), 133-140.

Muiva, C., Sathiaraj, T., & Maabong, K. (2011). Effect of doping concentration on the properties of aluminium doped zinc oxide thin films prepared by spray pyrolysis for transparent electrode applications. *Ceramics International*, *37*(2), 555-560.

Nandhini, R. S., Mubeen, G., Kumar, U. K., & Nithya, R. N. (2019). Synthesis and characterization of CuO/NiO and CuO/Fe3O4 nanocomposite for super capacitor application. *Int J Eng Tech*, *8*(9), 211-217.

Prasad, R., & Rattan, G. (2010). Preparation methods and applications of Cu-O-CeO2 catalysts: A short review. *Bulletin of Chemical Reaction Engineering & Catalysis*, *5*(1), 7.

Ramya, S., Viruthagiri, G., Gobi, R., Shanmugam, N., & Kannadasan, N. (2016). Synthesis and characterization of Ni2+ ions incorporated CuO nanoparticles and its application in antibacterial activity. *Journal of Materials Science: Materials in Electronics*, *27*(3), 2701-2711.

Shaikh, J. S., Pawar, R. C., Devan, R. S., Ma, Y. R., Salvi, P. P., Kolekar, S. S., & Patil, P. S. (2011). Synthesis and characterization of Ru doped CuO thin films for supercapacitor based on Bronsted acidic ionic liquid. *Electrochimica Acta*, *56*(5), 2127-2134. https://doi.org/https://doi.org/10.1016/j.electacta.2010.11.046

Suda, S., Fujitsu, S., Koumoto, K., & Yanagida, H. (1992). The effect of atmosphere and doping on electrical conductivity of CuO. *Japanese journal of applied physics*, *31*(8R), 2488.

Sultana, J., Paul, S., Karmakar, A., Yi, R., Dalapati, G. K., & Chattopadhyay, S. (2017). Chemical bath deposited (CBD) CuO thin films on n-silicon substrate for electronic and optical applications: Impact of growth time. *Applied Surface Science*, *418*, 380-387.

Tamaki, J., Shimanoe, K., Yamada, Y., Yamamoto, Y., Miura, N., & Yamazoe, N. (1998). Dilute hydrogen sulfide sensing properties of CuO–SnO2 thin film prepared by low-pressure evaporation method. *Sensors and Actuators B: Chemical*, *49*(1-2), 121-125.

Urbach, F. (1953). The long-wavelength edge of photographic sensitivity and of the electronic absorption of solids. *Physical Review*, *92*(5), 1324.

Venkateswari, P., Thirunavukkarasu, P., Ramamurthy, M., Balaji, M., & Chandrasekaran, J. (2017). Optimization and characterization of CuO thin films for P–N junction diode application by JNSP technique. *Optik*, *140*, 476-484.

Wang, P., Zhao, X., & Li, B. (2011). ZnO-coated CuO nanowire arrays: fabrications, optoelectronic properties, and photovoltaic applications. *Optics express*, *19*(12), 11271-11279.

Zhao, S., Shen, Y., Hao, F., Kang, C., Cui, B., Wei, D., & Meng, F. (2021). Pn junctions based on CuO-decorated ZnO nanowires for ethanol sensing application. *Applied Surface Science*, *538*, 148140.

Zhao, Z., Morel, D., & Ferekides, C. (2002). Electrical and optical properties of tin-doped CdO films deposited by atmospheric metalorganic chemical vapor deposition. *Thin Solid Films*, *413*(1-2), 203-211.

Zhen, F., Zhang, L., Wang, Z., Jiang, Z., Wei, S., Fu, X., Sun, R., Wong, C., Bu, W., & Chen, H. (2018). pH-induced phase evolution and enhanced physical properties of co-precipitated WO3-CuO powders and reduced bodies for microelectronics packaging. *Ceramics International*, *44*(18), 22601-22608.

Zheng, L., & Liu, X. (2007). Solution-phase synthesis of CuO hierarchical nanosheets at near-neutral pH and near-room temperature. *Materials Letters*, *61*(11-12), 2222-2226.

CHAPTER 5

Evaluation of Natural Stones in Different Usage Areas, Samsun Example

Lecturer Dr. Arif Hikmet ÇAKOĞLU[1]

INTRODUCTION

After the quarry of materials from the Kızılırmak and Yeşilırmak deposits, which are two long rivers of our country and spill into the sea in the districts of Bafra and Çarşamba, was stopped due to low sediment transport, the orientation towards quarries for the production of crushed stone for use in concrete batching plants increased (Çakoğlu, 2011). In addition, other natural Januaryries other than limestone have been put into operation for decorative or local services. Although there are more natural Januaryries in terms of number and type throughout the province, they are open to development in terms of production capacity and diversity. According to the reports Dec by the MTA, it was determined that Samsun has a limestone-dominated rock structure between Kızılırmak and Yeşilırmak and towards the south (Hakyemez et al., 1989). In addition, there are other volcanic rock structures in different districts (Öztürk, 1979). The region known as Mahmurdağı consists of basalt, andesite, tuff, agglomerate and basaltic batholith, dykes and sills. It is observed in the form of scattered surfaces (Yoldaş, 1985). Basalts in Mahmurdağ are typically surfacing. Basalts are porphyric in texture, dark black and cream-white in color. Currently, there

1 Department of Real Estate Development and Management Boyabat Faculty of Economics and Administrative, Sinop University ORCID : 0000 0002 8055 7858

are Januaryries operating here, and the extracted material is used for stone laying, ballast purposes, except for the production of concrete. However, aggregates taken from the basalt quarry in Ayvacık district are mixed with limestone sand and used in concrete plants due to the lack of sufficient January for the production of concrete. It is known that the high water absorption rate of basalt stone here is an obstacle to obtaining the desired result in concrete strength. Andesite, on the other hand, is a natural stone that is mostly used for visual purposes in building facade coatings and pedestrian sidewalks, and it is understood from the results of the experiment that it does not have the appropriate properties for the manufacture of concrete. Granite is a class of heavy natural stones with a high specific gravity. It can be used to create a weight in the manholes in the construction of ports and fishing shelters, as well as processed in workshops to obtain a decorative building material. Here, the possibility of introducing new production to the economy through the operation and installation of natural stones located within the borders of Samsun province was investigated.

MATERIAL AND METHODS

Basalt, granite and other natural rocks are mostly found in the Central Black Sea Region, especially limestone . The areas of production and use of limestone, basalt, granite and andesite types of these natural stones with volcanic properties have been mentioned. January Information about the rock structure of the city was obtained from reports prepared by the General Directorate of Mineral Exploration, production locations and numbers of natural quarries were taken from the Samsun Governorate, and Dec results of experiments on these rocks were used from analyzes conducted by authorized organizations. These analyses are experiments that give an idea of the mechanical and strength properties of the stones and show that the stones in question can also be preferred for different purposes for the purpose of use and for the future. There are January factories operated not only by private companies, but also by public organizations such as the Regional Directorate of Highways, Metropolitan Municipality, DSI Regional Directorate, Çarşamba and Ayvacık district municipalities. First, information was given about the general characteristics of natural stones, which are most often found throughout the province.

Limestone

There are rich limestone quarries especially in Kavak district. Most of them are also used for the manufacture of concrete aggregates. Even aggregate material is transported from here to concrete batching plants in neighboring

provinces and districts. In addition to the January construction sites located in the active quarries, there are also many lime manufacturing companies in the district. As is known, lime is obtained by calcining limestone containing at least 90% CaCO3 in lime kilns above 900-1000 °C and converting it into calcium oxide (MTA, 2022).

Basalt

Basalt, which is a natural stone that is a common type of volcanic rock in our country, is very dark in color and has a very solid, durable structure. It is a dense and heavy rock. In general, the suction strength is low water, wear, weather conditions, and resistance against a lot of pressure because the top and bottom being the type of natural stone as a construction material are characterised by a lot more preferred, especially as seen from the results of the experiment, located in Ayvacik, basalt rocks, unlike in the manufacture of concrete due to high availability of power, water suction, however, together with the use of a mixture of limestone, the material is considered appropriate. The results of the analysis of the basalt January located in the Çamlıyazı locality of Atakum district are positive. Main areas of use; as kırmataş, concrete aggregate, railway infrastructure material in the form of ballast, small sculptures, decorative household items with the production of baubles, paving stones, curbs, cut stone cladding, insulation material such as different purposes are produced. It is also a preferred rock of sculptors

Andesite

It is a preferred building material for both beautiful appearance and coating purposes in order to benefit the structure in terms of aesthetics and function. Paving stone, curbstone, disabled ramp, building exterior cladding, outdoor products can also be manufactured according to preference. Its surface is rough, so it is resistant to slipping. Due to the high water holding capacity of the andesite stone located in Samsun, it is not suitable for the manufacture of concrete, but rather the production of materials for decorative purposes is carried out. Its specific gravity is also low compared to other types of rocks. On the other hand, there is a study that the mechanical and physical properties of concretes can be improved by using andesite mineral wastes (Soykan O., et al.)

Figure 1. Andesite paving stone

Granite

A magmatic origin, which is tough and durable granite rock in the construction industry, paving stone, curbstone, ice, landscape arrangements can be used as easy to be deformed because it is harder than marble, and be more economical due to characteristics such as the preference in terms of visuals, especially the use of the kitchen counter has increased. In addition, with the use of granite powder in kitchen utensils, pans, pots, toasters that last longer and do not scratch can be manufactured. External factors such as humidity and high temperature resistant to rust, scratches, and breakage to avoid problems such as acid-based substances to be resistant against wind and natural appearance is important.

Figure 2. Granite chaise lounges.

Figure 3. Granite Japanese umbrella Figure 4. Granite outdoor kitchen countertops

FINDINGS

The results of the analysis of the mentioned natural stones are given in the following tables.

Table 1. Sample properties of Andesite and Granite. (TS EN 1097-2)

Sample Specifications	Unit	Andesite	Granite
Density	(gr/cm³)	2,63	3,1
Unit volume weight	(gr/cm³)	2,28	3,1
Absorption of water in boiling water (by mass)	(%)	5,5	0,1
Water absorption in boiling water (by volume)	(%)	12,2	0,4
Pressure resistance after frost	Mpa	89,3	211,4
Loss Of Frost	(%)	0	0,07
Impact Resistance	(kgf.cm/cm³)	34,3	141
Bending Resistance	MPa	9,4	25,9
Visible Porosity	(%)	9,1	0,3
Occupancy Rate	(%)	86,7	100
Degree of Porosity	(%)	13,3	0
Average Wear Resistance	(cm³/50 cm²)	15,38	10,6

See Table 1. as can be seen from the, the pressure resistance of granite is quite high, and andesite is low. Another important difference is that andesite has a fairly high water absorption rate in boiling water by volume and mass.

Table 2. Results of water absorption experiments of andesite stone

Dry weighing (g)	Sample area (m^2)	Weighing in water (g)	Time (s)	Capillary Water Absorption Coefficient ($g/m^2.s^{1/2}$), TS EN 1925
343,21	0,00283	357	345789	8,294
347,93	0,0029	363,63	345809	9,207
353,29	0,00296	367,04	345823	7,895
344,79	0,00284	358,38	345838	8,144
346,49	0,00294	360,85	345852	8,312
348,22	0,00288	361,75	345866	7,999
		Average		8,308

Table 3. Results of water absorption experiments of granite stone

Dry weighing (g)	Sample area (m^2)	Weighing in water (g)	Time (s)	Capillary Water Absorption Coefficient ($g/m^2.s^{1/2}$), TS EN 1925
484,47	0,00291	484,81	345715	0,199
487,95	0,00293	488,38	345730	0,25
488,95	0,00296	489,35	345742	0,23
483,88	0,0029	484,42	345753	0,317
480,14	0,00293	480,47	345766	0,192
483	0,00292	483,34	345778	0,198
		Average		0,231

Table 4. Test results of water absorption by mass at atmospheric pressure of andesite

Andesite Sample Sizes (mm)	By Mass of Water Absorption at Atm Pressure (%), TS EN 13755)
54*53*54	4,4
54*54*54	4,3
54*53*54	3,9
54*54*54	3,6
54*53*54	4,4
54*54*54	3,8
Average	4,1

Table 5. Test results of water absorption by mass at atmospheric pressure of granite

Granite Sample Sizes (mm)	By Mass of Water Absorption at Atm Pressure (%), TS EN 13755)
54*53*54	0,1
54*54*54	0,1
54*53*54	0,1
54*54*53	0,1
54*54*54	0,1
54*54*53	0,1
Average	0,1

From the tables above, a significant difference was found between the mass water absorption test results of andesite and granite stones with the same sample sizes. This, in turn, indicates that andesite, when exposed to water, absorbs it and increases in mass due to the fact that its specific gravity is low and hollow. The water absorption rate of aggregate is an important property that also affects the permeability of concrete and therefore affects its strength (Erdoğan, 2003).

Table 6. Pressure resistance test and fracture load of andesite stone

Andesite Sample Sizes (mm) Crushing surface (edge*height)	Fracture load (kN)	Pressure resistance (Mpa), (TS EN 1926)
53,8*54,2	271	93
54,2*54,0	302	103
54,1*54,1	305	104
54,7*54,0	288	98
54,6*53,7	261	89
53,5*53,5	268	94
54,8*53,7	267	91
51,4*54,0	203	73
54,2*54,1	227	77
53,7*54,0	291	100
Average		92

Table 7. Pressure resistance test and fracture load of granite stone

Granit Sample Sizes (mm) Crushing surface (edge*height)	Fracture load (kN)	Pressure resistance (Mpa), (TS EN 1926)
53,8*54,0	563	194
53,8*53,6	540	187
54,2*54,0	610	208
54,2*54,0	607	207
54,3*54,7	514	173
54,4*54,7	431	145
54,1*54,6	581	197
54,2*54,7	596	201
54,5*54,5	469	158
54,4*54,5	424	143
Average		181

Again, according to the test results, it was found that the pressure resistance of granite is about twice as high as andesite of the same dimensions. Granite stone can be processed almost like wood in the atelier belonging to the Metropolitan Municipality and different materials can be produced on order. The high pressure resistance of granite is evaluated in this aspect.

The analysis results of limestone and basalt stones in the districts in accordance with TS EN 933-3 and TS EN 1097-2 standards are also given in the following tables.

Table 8. Mechanical and chemical analysis values of Bafra limestone aggregate

	0-4 mm	4-11,2 mm	11,2-22,4 mm
Very fine material content (%)	13,8 f_{16}	-	-
The flatness index of large aggregates	-	7,6	7,6
Loose bulk density (Mg/m3)	1,64	1,48	1,45
Methylene blue (g dye/kg sample)	0,5	-	-
Specific gravity (Mg/m3)	2,69	2,71	2,72
Water Absorption (%)	1,2	0,7	0,4
Alkaline silica reactivity, %	0,06	-	-
The breakdown resistance of coarse aggregates	-	18 LA_{20}	18 LA_{20}
Modulus of fineness (%)	3,2	6,87	7,5
Water content	1,7	-	-
Total sulfur content	%0,07	-	-
Determination of acid-soluble sulfate	%0,10	-	-
Light rganic pollutants	< % 0,001	-	-
An experiment on the determination of water-soluble chlorine salts	%0,001	-	-
Magnesia sulfate test report		%5 MS_{18}	%5 MS_{18}

Table 9. Mechanical and chemical analysis values of Kavak limestone aggregate

	0-4 mm	4-11,2 mm	11,2-22,4 mm
Very fine material content	%10,8 f_{16}	-	-
The flatness index of coarse aggregates (%)	-	17	7
Loose bulk density (Mg/m3)	1,54	1,42	1,39
Methylene blue, g dye/kg sample	0,7		
Specific gravity (Mg/m3)	2,67	2,69	2,70
Water absorption (%)	1,0	0,5	0,2
Alkaline silica reactivity (%)	0,01	-	-
The breakdown resistance of coarse aggregates	-	22 LA_{25}	22 LA_{25}
Modulus of fineness (%)	3,20	6,48	7,90
Determination of acid-soluble sulfate	%0,17	-	-
Light Organic Pollutants	<%0,01	-	-
An experiment on the determination of water-soluble chlorine salts	%0,001	-	-
Magnesia sulfate test report	-	%2 MS_{18}	%2 MS_{18}
Total sulfur content (%S)	%0,06		

Table 10. Mechanical and chemical analysis values of Atakum basalt aggregate

	0-4 mm	4-11,2 mm	11,2-22,4 mm
Very fine material content	% 11,2 f_{10}	0,6 f_4	0,4 $f_{1,5}$
The flatness index of large aggregates	-	8(Fl_{15})	6(Fl_{15})
Resistance to freezing dissolution effect	-	4(MS_{18})	4(MS_{18})
Chlorides	%0,0023	%0,0023	%0,0022
Loose bulk density (Mg/m3)	1,62	1,40	1,40
Methylene blue	0,75	-	-
Specific gravity (Mg/m3)	2,67	2,69	2,70
Water absorption (%)	0,90	0,50	0,40
Alkaline silica reactivity	%0,031	-	-
The breakdown resistance of coarse aggregates	-	20 LA_{25}	20 LA_{25}
Modulus of fineness (%)	3,13	6,43	7,82
Water content	2,6		
Resistance of coarse aggregates to the effect of freezing thawing	-	Percentage loss by mass 4	-

Water absorption rates are especially different basalt stones in Ayvacık and Atakum districts. In addition, there was a significant difference between the results of the breakdown resistances of coarse aggregates, flatness index and methylene blue (Table 10 and 11).

Table 11. Mechanical and chemical analysis values of Ayvacık basalt aggregate

	0-4 mm	4-11,2 mm	11,2-22,4 mm
Very fine material content	2,1	0,4	0,1
The flatness index of large aggregates	16	17, Fi_{20}	16, Fi_{20}
Resistance of coarse aggregates to the effect of freezing dissolution, %	-	16	16
Chlorides	%0,0029	-	-
Methylene blue, g dye/kg sample	1,7	-	-
Specific gravity (Mg/m3)	2,62	2,66	2,67
Water absorption (%)	2,9	2,24	2,15
Alkaline silica reactivity	0,033	-	-
The breakdown resistance of coarse aggregates	-	15 LA_{20}	15 LA_{20}
Modulus of fineness (%)	3,46	6,82	7,81
The shape index experiment	-	22 Si_{40}	22 Si_{40}
Total sulfur content	0,330, %1	-	-
Determination of acid-soluble sulfate	0,099	-	-
An experiment on the determination of water-soluble chlorine salts	%0,01	-	-
Magnesium sulfate test report	-	16 MS_{16}	16 MS_{16}

RESULTS

Basalt, especially because it is a hard rock, can be used as a paving stone by municipalities or can be used as a crushed stone in the manufacture of concrete. It is also used as a ballast material under the tracks on railway lines. In addition, due to the density of the mineral structure, it can contribute to the economy in the production of ceramics and the manufacture of thermal insulation material known as rock wool. Although the mechanical properties of basalt in Ayvacık January have a negative appearance, especially due to

the high water absorption rate, the properties of basalt rock taken from the quarry located in Çamlıyazı in Atakum district are in good condition and its uses other than crushed stone, pavement, ornaments should be investigated. During the periods when energy saving is becoming important in the world, work should be done on the manufacture of products for thermal insulation.

Granite, especially in Samsun, belongs to the Metropolitan Municipality of natural stone processing plant, different shapes are given and optional materials are produced. An example is a chaise longue, an outdoor kitchen, a seesaw for children. As is known, products such as granite-coated pans and pots are causing an increase in demand due to their high temperature resistance and long service life. Granite powder or sand processed in Samsun, where one of the largest capacity facilities in Turkey is located, can also be used in the manufacture of kitchen utensils and brought to the economy.

Limestone is located throughout Samsun, as well as in other provinces of the Black Sea Region. It is used in concrete aggregate and lime factories, especially in Kavak District. Although these limestone quarries, which are more numerous, are important for construction January, as a result of the new studies to be carried out, the production capacity of the region can be increased in the field of building chemicals and economic value can be obtained.

Although andesite is not available much in Samsun, it is not suitable as a concrete aggregate due to its low specific gravity and high water absorption rate. It is preferred for pavement coatings where a slippery surface is undesirable, and for building facades. Especially the detached building is in demand by those who want to get a beautiful appearance by considering it as an exterior cladding in their summer cottage construction. Andesite Decking is not much known among the population. But in recent years, its use has become widespread in the construction of detached buildings, and it is expected that it will be more preferred in obtaining a different outdoor image. In this case, it will be able to cause the emergence of new opportunities in the sector.

REFERENCES

Çakoğlu A.H., "Samsun İli Kum Çakıl ve Kırma Taş Rezervleri", Samsun Sempozyumu, OMÜ Samsun, 2011.

Erdoğan, Y. T. (2003). *Beton*. Ankara, ODTÜ Basımevi, 741

Hakyemez, H. Y., Tekin, F., Erkal, T., Karabıyıkoğlu, M. & Mengi, H. (1989). *Çarşamba (Samsun) dolayının jeolojisi* (MTA Rapor No.8895). Maden Tetkik ve Arama Genel Müdürlüğü

https://www.mta.gov.tr/v3.0/bilgi-merkezi/kirec (erişim tarihi: 01.08.2022)

Öztürk A., (1979). *Ladik, Destek dolayının stratigrafisi. Ankara*, Türkiye Jeolojisi Kurumu Bülteni, 22/1.

Samsun Valiliği İl Planlama ve Koordinasyon Müdürlüğü (2021) Yatırım İzleme Malzeme Ocakları, 2021

Soykan O., Özel C. ve Öcal C. *Arduvaz ve Andezit'in Beton Agregası Olarak Kullanılabilirliğinin Araştırılması,* Süleyman Demirel Üniversitesi Fen Bilimleri Enstitüsü Dergisi, 2015

TS EN 933-3 Nisan 2012 Agregaların Geometrik Özellikleri için Deneyler

TS EN 1097-2 Nisan 2000 Agregaların mekanik ve fiziksel özellikleri için deneyler

TS EN 1926 Doğal taşlar- Deney metotları- Basınç dayanımı tayini

TS EN 13755 Ocak 2003 Doğal taşlar-Deney metotları-Atmosfer basıncında su emme tayini

Yoldaş, R.,(1985). *Samsun ve dolayının (Kızılırmak-Yeşilırmak arasındaki bölge) jeolojisi ve petrol olanakları*, Ankara, MTA Derleme Raporu No:8130

CHAPTER 6

Cohesive Zone Impact Analysis of Structural Adhesive Joints

Luís M.C. PERES[1]

Raul D.S.G. CAMPILHO[2]

Ricardo J.B. ROCHA[3]

Isidro J. SÁNCHEZ-ARCE[4]

Raul D.F. MOREIRA[5]

INTRODUCTION

Understand the response of a joint subjected to a dynamic load is currently a hot topic. On the one hand it is known that by using adhesive joints it is likely to obtain an significant benefits on the effect of damping vibrations (Pazand and Nobari 2016). In addition, Chowdhury et al. (2016) reported a decrease of the developed fatigue cracks when using adhesively bonded structures. In this point of view, it is clear the emerge of a strategic

1 Departamento de Engenharia Mecânica, Instituto Superior de Engenharia do Porto, Instituto Politécnico do Porto, R. Dr. António Bernardino de Almeida, 431, 4200-072 Porto, Portugal.

2 Departamento de Engenharia Mecânica, Instituto Superior de Engenharia do Porto, Instituto Politécnico do Porto, R. Dr. António Bernardino de Almeida, 431, 4200-072 Porto, Portugal. INEGI – Pólo FEUP, Rua Dr. Roberto Frias, 400, 4200-465 Porto, Portugal.

3 INEGI – Pólo FEUP, Rua Dr. Roberto Frias, 400, 4200-465 Porto, Portugal.

4 INEGI – Pólo FEUP, Rua Dr. Roberto Frias, 400, 4200-465 Porto, Portugal.

5 INEGI – Pólo FEUP, Rua Dr. Roberto Frias, 400, 4200-465 Porto, Portugal.

opportunity for the transportation industry to enhance their products by applying adhesive joints processes. Actually, the automotive industry already count on adhesive joints to enhance the collision performance (Dlugosch et al. 2017). In fact, adhesives permit the structures to deform, therefore absorbing the impact energy. Single Lap Joint (SLJ) is the most studied adhesive bonded joint due to its geometrical and manufacturing simplicity (Petrie 2007). One of the major drawbacks of this joining process, is the non-collinearity phenomena, leading to a significant peeling stress (σ_y) and therefore causing the premature failure of the bonded joint. This issue can be overcome by using a double lap joint (DLJ) which presents a slighter increase in complexity of the SLJ (Petrie 2007). Nowadays it is a common knowledge the joining area is the most important factor influencing the joints' strength, but with the introduction of geometric changes it is still possible to increase its strength.

Geometric variations can be introduced in the joint design either in terms of material or design modifications, that is as the introduction of thicker adherends to promote a more uniform stress distribution. The design of a joint, considering the area close to the adherends' edges, also affects the peak σ_y and shear (τ_{xy}) stresses and consequently it highly affects the strength of the joint strength. The effect of the local geometry variations at the edges of the overlap of a SLJ was evaluated numerically by Adams and Harris (1987) considering stress distribution and failure prediction. It was concluded that allowing to determine that it is possible to significantly increase the joint strength by inducing a fillet on the adhesive in the edges of the overlap, and also rounding the ends of the adherends. In addition, several studies can be found in the literature, which presents numerical models skilled to predict the strength of adhesively bonded joints, stress distribution and failure, when affected by the variation of geometrical design (Dean et al. 2004, Lavalette et al. 2020, Marchione 2021).

Understanding the behaviour of the joints under impact loads using numerical techniques is of great interest among the academic and industry community. Dynamic models need to take in consideration the inertial effects, that are insignificant when dealing with static analyses. To accurately perform a dynamic numerical simulation, the knowledge of material properties of the adherends and adhesive at the tested strain-rate are required. Zgoul and Crocombe (2004) and Dean et al. (1999) studied two models, a model using an adaptation to the von Mises criterion, and another applying Drucker-Prager model. The former demonstrated to be not effective with hardened adhesives. Cohesive Zone Modelling (CZM) has been implemented with great success for the design of bonded joints. Commercial software solvers

demonstrated to have enough accuracy to predict impact failure, as stated by several authors such as May et al. (2014) and Clarke et al. (2013). Araújo et al. (2017) presented an industrial study focused on the impact of adhesively bonded joints in the automotive industry. The research included experimental and numerical comparisons of a novel crash resistant epoxy adhesive used to bond CFRP adherends in a SLJ design. The numerical model was validated with experimental data. The authors noticed an increase in the P_m while increasing the L_O during impact loads. For all tested setups, the proposed numerical models were skilled to accurately capture and predict the behaviour of the SLJ tested under impact loads.

This work studies the effect of L_O and adhesive type on the strength of composite SLJ, under impact load, by performing experimental tests and CZM analysis. Two adhesives with different ductility degrees were tested (Araldite® AV138 and Sikaforce® 7752), by bonding composite adherends with unidirectional lay-up. The joints were subjected to a drop test and validated through the numerical model.

MATERIALS AND METHODS

Materials

Unidirectional carbon pre-preg adherends and two adhesives were used to manufacture SLJs to evaluate the adhesive type effect on the impact response of bonded joints. The adherends were made of unidirectional lay-ups of twenty pre-preg plies of 0.15 mm each from SEAL® (Texipreg HS 160 RM; Legnano, Italy). The stacking sequence was made by hand lay-up. Subsequently cured in a hot-plates press using the manufacturer's curing cycle (temperature of 130 ºC and pressure of 2 bar for one hour, in-between the recommended heating and cooling slopes). The applied adhesives were the Araldite® AV138 (strong but brittle epoxy adhesive with low temperature curing characteristics) and the Sikaforce® 7752 (less strong, however with a high ductility degree polyurethane, Mechanical and fracture properties of the adhesives were determined by performing different tests at 1 and 100 mm/min. On the one hand, tensile tests to the bulk adhesive allowed to obtain the tensile strength (σ_f) and the Young´s Modulus (E). On the other hand, thick-adherend shear tests (TAST) were performed to obtain the shear modulus (G) and shear strength (τ_f). In order to obtain the required fracture properties, the Double-Cantilever Beam (DCB) and End-Notched Flexure (ENF), were used to determine the tensile fracture toughness (G_{IC}) and shear fracture toughness (G_{IIC}), respectively. The outcome of the aforementioned tests at these two test speeds (static and dynamic) is shown in Table 1.

Table 1. Adhesives' mechanical and fracture properties as a function of the test velocity.

Adhesive	Test velocity [mm/min]	t_n^0 [MPa]	t_s^0 [MPa]	G_{IC} [N/mm]	G_{IIC} [N/mm]
AV138	1	41.0	30.2	0.35	0.6
	100	49.1	36.2	-	-
	105000	70.2	51.7	0.35	0.6
7752	1	11.5	10.2	2.36	5.41
	100	18.4	15.7	-	-
	105000	29.9	26.4	2.36	5.41

Geometries and tests

The SLJ design, respective dimensions and boundary conditions are depicted in Fig. 1. General dimensions are: joint length (L_T=200 mm) and joint width (b=15 mm; not shown in the figure), overlap length (L_O=12.5, 25 and 50 mm), adhesive thickness (t_A=0.2 mm), adherend thickness (t_P=3 mm). With respect to the boundary conditions used during numerical analysis, the joint was clamped on the left side and an artificial mass is considered on the right side.

A total of 4 specimens were manufactured and tested for each joint configuration. In order to prepare the specimens for the test setup and since they are fixed on pins, it is necessary to perform a drilling operation at the end of each specimen to create a hole for an M8 pin. Furthermore, it is necessary to glue steel tabs with a 2 mm thickness to reinforce the gripping points, since when subject to impact, the CFRP adherends do not have the appropriate strength and the hole can be teared in the fibres' direction, therefore invalidating the test.

A typical drop test machine was used for the experimental testing. The setup consisted in releasing a 30 kg anvil (from a pre-determined height), which falls freely on the joint, creating the impact load. The test setup is configured so that the weight hits the joint with the desired energy (40 J). Accordingly, the machine drops the weight at a height (h) of approximately 136 mm (determined from the potential energy: $E_P=m.g.h$) which, considering the anvil mass (m) of 30 kg and gravitational acceleration, induces an impact on the joint with a release of kinetic energy (E_c) equivalent to 40 J. $E_c=½mv^2$, where m is the mass and v is the velocity.

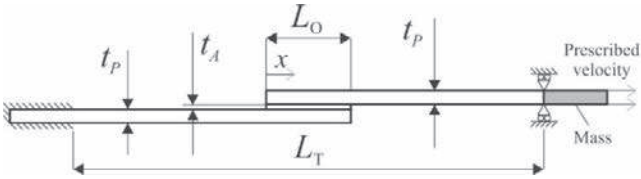

Fig. 1. SLJ architecture and boundary conditions.

Numerical modelling

The numerical work within this study was performed using the commercially available Abaqus® software with explicit solver, capable to perform the necessary dynamic simulations. A triangular CZM law shape was applied to accurately predict the impact response of the experimentally tested joints. A geometrically non-linear two-dimensional (2D) analysis type was applied. COH2D4 cohesive elements were used to capture the behaviour of the adhesive layer and CPE4 solid elements for the adherends. The numerical models were created taking into account a layer of CZM elements with a height identical to the adhesive layer (t_A). Concerning the mesh design, a minimum element size of 0.2 mm was selected, in accordance with the value of t_A, being applied at the overlap edges. Consequently, a mesh roughening was obtained with size grading to achieve a bias effect. Fig. 2 presents the mesh implemented to model the SLJ (overlap details).

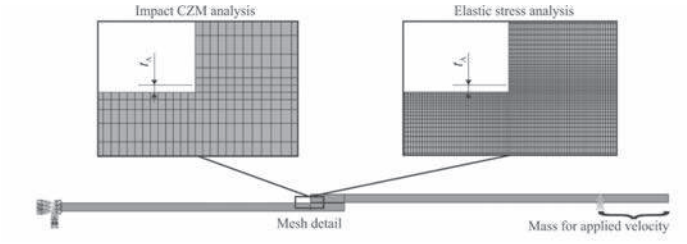

Fig. 2. Detail of the applied mesh in the impact CZM and stress analyses.

In what concerns to the boundaries conditions and impact load to simulate the experimental tests, it is possible to see the clamping of the leftmost edge of the SLJ and the transversely restraining of the right most edge (Fig. 1 and Fig. 2).

The applied impact load involved the application of an impact energy of 40 J to a mass which was artificially placed at the rightmost edge of the joint. By the equation $E_c=½mv^2$, it is possible to adjust the mass volume

and density, together with the given velocity, to attain a maximum impact energy of 40 J.

CZM theory

CZM method relies on the linking among stresses and relative displacements linking similar nodes of cohesive elements. Furthermore, those relations (known as CZM laws) may be created in pure and mixed mode and make possible to capture the material's behaviour up to failure. The present study considers triangular pure and mixed-mode laws to model the adhesive layer (Abaqus® 2013).

Under pure-mode loading, damage onset occurs when the cohesive strength in tension or shear (t_n^0 or t_s^0, respectively) is attained, i.e., the material's elastic ceases to exist and degradation begin (Sane et al. 2018). Moreover, the crack proliferates up to the adjacent pair of nodes when the values of current tensile or shear cohesive stresses (t_n or t_s, respectively) become null. Under mixed-mode loading, stress and/or energetic criteria are often used to combine the pure-mode laws, and damage begins when the mixed mode cohesive strength (t_m^0) is reached (Dimitri et al. 2015). Several criteria are suitable for damage initiation and propagation when the analyses involve mixed-mode loadings. This study focused on the quadratic nominal stress criterion and a linear power law form for the damage initiation and growth, in the same order. This approach is described in detail in the work of Rocha and Campilho (2017). The adhesives' properties used in Abaqus® are depicted in Table 1, considering t_n^0 and t_s^0 as the values of σ_f and τ_f, in the same order.

RESULTS

Test data

P-δ curves for the SLJ bonded with the AV138 and L_O=50 mm (a) and bonded with the 7752 and L_O=25 mm (b), are presented in Fig. 3. The oscillatory behaviour that can be noticed before reaching P_m is typical of an impact event and it is caused by the inertial effect induced by the dynamic loading and time-dependent propagation of stress waves, as presented in the work of (Valente et al. 2020). Fig. 4 shoes the average P_m and respective standard deviation for all evaluated joint configurations (including geometry/adhesive). the P_m values of all valid tests for each configuration (type of adhesive and L_O), average P_m, standard deviation (SD), percentile coefficient of variation (CV) and percentile P_m improvement considering the baseline geometry (L_O=12.5 mm), defined as ΔP_m are presented in Table 2. On the

one hand, it is possible to observe that for the AV138, the *P*m improvement is not proportional to L_O, even though it can be considered as nearly linear, since the slope between consecutive data points is approximately identical. On the other hand, regarding the 7752, the P_m evolution is considerable different. The P_m-L_O relation is close to proportionality, especially for lower L_O. In addition, the P_m/L_O ratio highly worsens between L_O=25 and 50 mm. It can thus be concluded that the L_O effect on the strength of a SLJ under impact load is more relevant for ductile than with brittle adhesives.

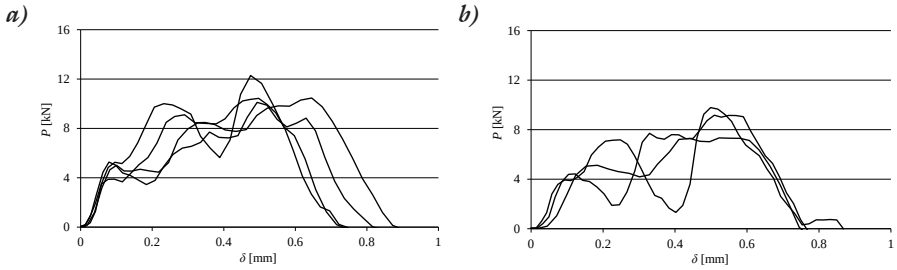

Fig. 3. P-δ curves extracted from impact load on SLJ bonded with the AV138 and L_O=50 mm (a) and bonded with the 7752 and L_O=25 mm (b).

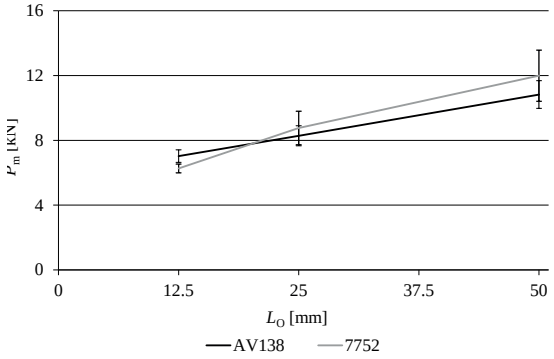

Fig. 4. P_m vs. L_O graph of the impact loaded SLJ bonded with AV138 and 7752.

Table 2. Summary of the experimental results for both adhesives.

		Araldite® AV138			Sikaforce® 7752		
L_O [mm]		12.5	25	50	12.5	25	50
Specimen	1	6.73	-	10.47	6.10	-	-
	2	6.77	8.06	-	-	9.17	10.12
	3	-	-	10.11	-	7.34	13.98
	4	7.58	7.65	12.28	6.65	9.78	11.88
	5	-	9.12	10.43	6.04	-	-
Average P_m [kN]		7.03	8.28	10.82	6.26	8.76	11.99
SD [kN]		0.39	0.62	0.85	0.27	1.04	1.58
CV [%]		5.5	7.5	7.9	4.4	11.9	13.2
ΔP_m [%]		-	17.8	53.9	-	39.9	91.5

Numerical predictions

Experimental and numerical data (P-δ curves) are now compared to validate the proposed impact CZM model in terms of P_m, failure displacement (δ_f) and the shape of the curves. Fig. 5 compares the P-δ curves for the SLJ bonded with the AV138 and an L_O=50 mm (a) and SLJ bonded with the 7752 and an L_O=25 mm (b). One can notice a good correlation between both experimental and numerical data considering the elastic part of the curve (stiffness) until P_m is attained. Nonetheless, the numerical failure displacement is slightly lower than the experimental values.

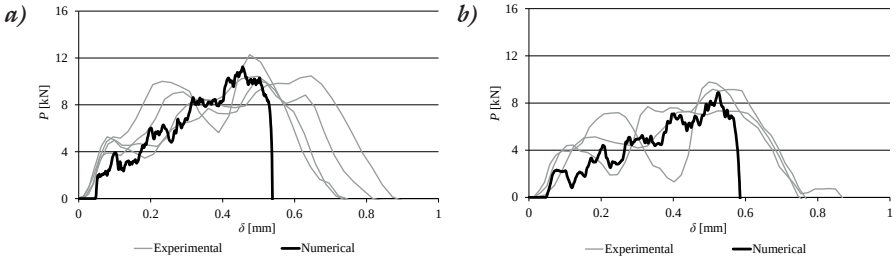

Fig. 5. Experimental and numerical P-δ curves extracted from impact event on SLJ with bonded with the AV138 and L_O=50 mm (a) and SLJ bonded with the 7752 and L_O=25 mm (b).

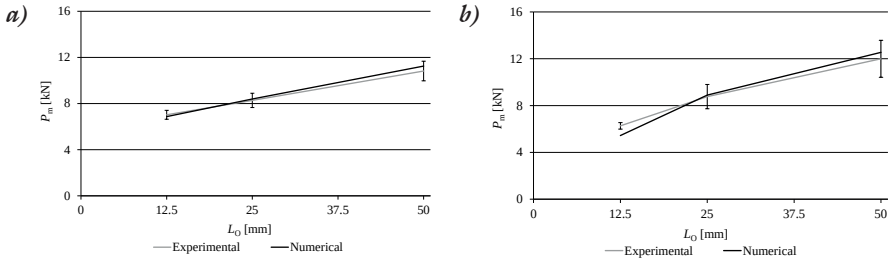

Fig. 6. Experimental and numerical P_m comparison for SLJs with bonded with the AV138 (a) and 7752 (b).

Fig. 6 presents a comparison between P_m data from testing and CZM impact simulations for the joints bonded with the AV138 (a) and 7752 (b) and all tested L_O values. It is clear the excellent correlation depicted in the plot of the AV138 adhesive. Actually, the relative P_m deviations, between tested and simulation data, were between -1.5 and 3.9% for L_O=25 and 50 mm, respectively. Nonetheless, slightly different results were found for the 7752, where relative PM deviations between -13.1 and +1.5% were found for L_O=12.5 and 50 mm, in the same order. The reported deviations occur due the applied CZM law shape (triangular) presents some issues in capturing the high degree of plasticization inherent of this adhesive. Supported by the reported data, the applied CZM impact model can be considered as valid. This methodology revealed to be accurate to model impact behaviour in adhesive joints, allowing the select the best performing design and type of adhesive for under the studied conditions.

CONCLUSION

CZM approach was used to predict the strength of a SLJ subjected to impact loads. To accomplish this objective, two adhesives with distinct ductility were used to bond unidirectional carbon composites adherends in a SLJ architecture. Geometrical effects were considered to evaluate the impact behaviour under different conditions and make available design considerations for this narrowly addressed load. In order to accurately capture the impact event and joint response, the adhesive was characterized at high velocities. Subsequently, the proposed and implemented design was validated with experimental drop weight tests. The experimental outcomes showed that the brittle AV138 was the best perfume solution for the lowest L_O, nonetheless the P_m-L_O evolution was extremely non-proportional. Despite the ductile 7752 presents as the less performing for L_O=12.5 mm, the noticeable P_m improvement for higher L_O, supported by the allowable ductility, allowed it to overcome the performance of

the brittle AV138 for the other tested L_O. The coefficients of variations, although acceptable, were higher than usual for static analyses. The CZM approach successfully captured the joint behaviour during impact tests, both on the P-δ curves' shape and P_m, even though failure was sudden soon after reaching P_m, contradictory to the experimental data. The impact adapted CZM technique can be viewed as a suitable and valuable tool for this significant loading case.

REFERENCES

Abaqus® (2013). Documentation of the software Abaqus®. Dassault Systèmes. Vélizy-Villacoublay

Adams, R. and Harris, J., 1987. The influence of local geometry on the strength of adhesive joints. International Journal of Adhesion and Adhesives 7(2), 69-80.

Araújo, H. A. M., Machado, J. J. M., Marques, E. A. S. and da Silva, L. F. M., 2017. Dynamic behaviour of composite adhesive joints for the automotive industry. Composite Structures 171, 549-561.

Chowdhury, N. M., Wang, J., Chiu, W. K. and Chang, P., 2016. Experimental and finite element studies of thin bonded and hybrid carbon fibre double lap joints used in aircraft structures. Composites Part B: Engineering 85, 233-242.

Clarke, M. I., Broughton, J. G., Hutchinson, A. R. and Buckley, M., 2013. Application of the design of experiments procedure to the behaviour of adhesively bonded joints with plastically deformable adherends to enable further understanding of strain rate sensitivity. International Journal of Adhesion and Adhesives 44, 226-231.

Dean, G., Lord, G. and Duncan, B. (1999). Comparison of the measured and predicted performance of adhesive joints under impact. NPL Report Cmmt (A) 206 Appendix 1 Finite Element Analysis Perforated Single-Lap Joint NPL Report Cmmt (A) 206, Citeseer.

Dimitri, R., Trullo, M., De Lorenzis, L. and Zavarise, G., 2015. Coupled cohesive zone models for mixed-mode fracture: A comparative study. Engineering Fracture Mechanics 148, 145-179.

Dlugosch, M., Fritsch, J., Lukaszewicz, D. and Hiermaier, S., 2017. Experimental investigation and evaluation of numerical modeling approaches for hybrid-FRP-steel sections under impact loading for the application in automotive crash-structures. Composite Structures 174, 338-347.

May, M., Voß, H. and Hiermaier, S., 2014. Predictive modeling of damage and failure in adhesively bonded metallic joints using cohesive interface elements. International Journal of Adhesion and Adhesives 49, 7-17.

Pazand, K. and Nobari, A. S., 2016. Identification of the effect of debonding on the linear and nonlinear effective damping of an adhesive joint. Journal of Sound and Vibration 380, 267-278.

Petrie, E. (2007). Handbook of Adhesives and Sealants, McGraw-Hill Education.

Rocha, R. J. B. and Campilho, R. D. S. G., 2017. Evaluation of different modelling conditions in the cohesive zone analysis of single-lap bonded joints. The Journal of Adhesion, in press.

Sane, A. U., Padole, P. M., Manjunatha, C. M., Uddanwadiker, R. V. and Jhunjhunwala, P., 2018. Mixed mode cohesive zone modelling and analysis of adhesively bonded composite T-joint under pull-out load. Journal of the Brazilian Society of Mechanical Sciences and Engineering 40(3), 167.

Valente, J. P. A., Campilho, R. D. S. G., Marques, E. A. S., Machado, J. J. M. and da Silva, L. F. M., 2020. Geometrical optimization of adhesive joints under tensile impact loads using cohesive zone modelling. International Journal of Adhesion and Adhesives 97, 102492.

Zgoul, M. and Crocombe, A. D., 2004. Numerical modelling of lap joints bonded with a rate-dependent adhesive. International journal of adhesion and adhesives 24(4), 355-366.

CHAPTER 7

Evaluation of the Optimal Tubular Adhesive Joint Geometry for Structural Applications

Marcelo M.F.O. ROSAS[1]

Raul D.S.G. CAMPILHO[2]

Raul D.F. MOREIRA[3]

Isidro J. SÁNCHEZ-ARCE[4]

Ricardo J.B. ROCHA[5]

1. INTRODUCTION

Nowadays adhesive bonding technology is present in various industries, such as aeronautics, automotive, marine, wind energy, among others, and can be employed under varied joint geometries and configurations, depending on its application (Ebnesajjad and Landrock 2014). The most frequently used configuration is the single-lap joint due to its simplicity to be manufactured and because the adhesive layer is mainly loaded in shear (O'Mahoney et al.

1 Departamento de Engenharia Mecânica, Instituto Superior de Engenharia do Porto, Instituto Politécnico do Porto, R. Dr. António Bernardino de Almeida, 431, 4200-072 Porto, Portugal.

2 Departamento de Engenharia Mecânica, Instituto Superior de Engenharia do Porto, Instituto Politécnico do Porto, R. Dr. António Bernardino de Almeida, 431, 4200-072 Porto, Portugal. INEGI – Pólo FEUP, Rua Dr. Roberto Frias, 400, 4200-465 Porto, Portugal.

3 INEGI – Pólo FEUP, Rua Dr. Roberto Frias, 400, 4200-465 Porto, Portugal.

4 INEGI – Pólo FEUP, Rua Dr. Roberto Frias, 400, 4200-465 Porto, Portugal.

5 INEGI – Pólo FEUP, Rua Dr. Roberto Frias, 400, 4200-465 Porto, Portugal.

2013). Other joint configurations such as double-lap, stepped-lap or joggle-lap can also be used (Petrie 2000, Machado et al. 2019). In particular cases, it is also feasible to employ butt joints, T-joints, corner joints and tubular adhesive joints (TAJ) configurations (Petrie 2000). In the specific case of the TJA, this type of geometry presents several advantages like larger bonded areas and higher flexural strength due to its overall stiffness (Petrie 2000). Presently, adhesive bonding is widely used in the pipeline industry to perform the connection between pipes (Kaiser and Tan 2020). The earlier methods that were developed in order to predicict the strength of adhesive joints relied on analytical stress analysis (Quispe Rodríguez et al. 2012, de Sousa et al. 2017) and evolved to numerical methods like Finite Element (FE). Currently, the method that is most applied and well-accepted is the Chohesive Zone Models (CZM) (Campilho et al. 2009, Woelke et al. 2013), and with it is possible to accurately simulate bonded joints. The CZM requires previous determination of the adhesive fracture properties. The exactness of the CZM depends on the precise determination of the cohesive strengths, in tension (t_n^0) and shear (t_s^0), and on the fracture toughness, in tension (G_{IC}) and shear (G_{IIC}) (Campilho et al. 2012, Campilho et al. 2013). Athough there are not many studies dedicated to TAJs in the literature, some important works are available (Choi and Lee 1996, Ferreira et al. 2019, Ferreira et al. 2019). In (Albiez et al. 2019) the authors studied experimentally, steel TAJ bonded with two different adhesives (polyurethane and epoxy) and also analyzed the influence of geometrical variations on the joints strength. They settled that the joint strength increases with the increase of the overlap length (L_O), and that no difference is observed between the adhesives. Another remark is that the increase of the adhesive layer thickness (t_A) is prejudical to the joint strength. Nguyen and Kedward (2001) developed an analytical formulation aiming to obtain the shear stress (τ_{xy}) distribution in a TAJ subjet to tension loads. Their analytical formulation was applied to TAJ with aluminium adherends and the results were compared to a FE study with the objective of validating the analytical formulation. The analytical formulation and FE results revealed a good agreement which indicates soundess of the proposed formulation. The authors also concluded that TAJ with a 10° chamfer in the adherends, presented a more uniform stress distribution and a lower value of stress when comparying to joints without chamfering.

In this work it was performed a FE study in combination with CZM to numerically asses the performance of aluminium TAJ loaded under tension and bonded with Araldite® 2015 adhesive. Several geometrical alterations were proposed and analysed to evaluate the strength performance of the joints. In previous works, the numerical model based on CZM considering

axisymmetric elements was compared to experimental results and the model was validated. The selected geometrical alterations analysed in this work were outer chamfer, inner chamfer (both in the adherends), and adding an adhesive fillet at the overlap extremities.

2. MATERIALS AND METHODS

2.1. Materials

The material selected for the tubular adherends was the high strength aluminium alloy AW6082 T651, which was previously characterized (Moreira and Campilho 2015) in bulk tension, which allowed the determination of the following properties: Young's modulus (E) of 70.07±0.83 GPa, tensile yield stress (σ_y) of 261.67±7.65 MPa, tensile failure strength (σ_f) of 324.00±0.16 MPa and tensile failure strain (ε_f) of 21.70±4.24%. For the adhesive it was chosen the moderate ductile adhesive Araldite® 2015 and from the bulk testing (Campilho et al. 2011, Campilho et al. 2013), it was possible to determine E, σ_y, σ_f and ε_f. The shear mechanical properties were determined with Thick Adherend Shear Tests (TAST). For the fracture properties it was used Double-Cantilever Beam (DCB) to determine pure mode I (G_{IC}) and End-Notched Flexure (ENF) tests to determine pure mode II (G_{IIC}) (Campilho et al. 2011, Campilho et al. 2013). The Araldite® 2015 properties are listed in Table1.

Table 1. Mechanical and fracture properties of the adhesive Araldite® 2015 (Campilho et al. 2011, Campilho et al. 2013).

Property	**Araldite® 2015**
Young's modulus, E [GPa]	1.85±0.21
Poisson's ratio, ν	0.33 [a]
Tensile yield stress, σ_y [MPa]	12.63±0.61
Tensile strength, σ_f [MPa]	21.63±1.61
Tensile failure strain, ε_f [%]	4.77±0.15
Shear modulus, G [GPa]	0.70 [b]
Shear yield stress, τ_y [MPa]	14.6±1.3
Shear strength, τ_f [MPa]	17.9±1.8
Shear failure strain, γ_f [%]	43.9±3.4
Toughness in tension, G_{IC} [N/mm]	0.43±0.02
Toughness in shear, G_{IIC} [N/mm]	4.70±0.34

[a] manufacturer's data

[b] estimated from the Hooke's law using E and ν

2.2. Geometry and testing

A schematic representation of the TAJ is shown in Figure 1 and the main dimensions are listed in Table 2. The experimental tests were performed at room temperature in universal testing machine, Shimadzu-Autograph AG-X tester (Shimadzu, Kyoto, Japan) equipped with a 100 kN load cell, and with displacement control of 1 mm/min. Five specimens were tested for each joint configuration and the load-displacement (P-δ) curves were registered for posteriors comparison with the numerical results.

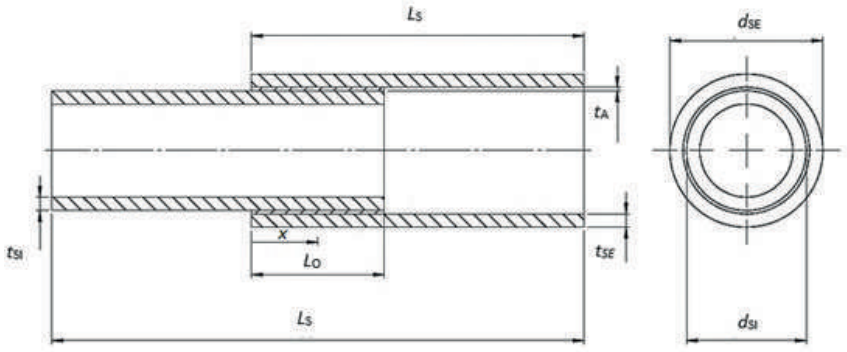

Figure 1. Geometry and characteristic dimensions of the tubular joints.

Table 2. Designation of the dimensions of the specimens and their values (mm)

Designation	**Values [mm]**	
Overlap length, L_O	20	40
Adherends' free length, L_S	50	60
Joint free length, L_T	80	80
Outer diameter of the inner tube, d_{SI}	20,0	20,0
Outer diameter of the outer tube, d_{SE}	22.4	22.4
Thickness of the inner tube, t_{SI}	2	2
Thickness of the outer tube, t_{SE}	2	2
Adhesive thickness, t_A	0.2	0.2

2.3. Numerical modelling

The numerical simulations were perfomed in the FE software Abaqus® and a two-dimensional (2D) axisemetric analysis was considered. Two

models were developed, one for the stress analysis and another for the strength prediction. The aluminium tube adherends were modellled with solid elasto-plastic axisymmetric (CAX4 4-node) elements and the stress-strain (σ-ε) curves were determined (Nunes et al. 2016). For the stress distribution study the adhesive was also modelled with the same solid elements. In the other hand, for the strenght prediciton study the adhesive layer was modelled with one row of axisymmetric cohesive elements that bond the two tubes (COHAX4 4-node). The behaviour of the adheisve layer is mimicked by a contiuunm approcah employing CZM and with mixed-mode softening triangular law shape elements. Only one through-thickness element is consiedered for the adhesive layer that bonds both tubes. More details about this procedure is given in a previous work (Campilho et al. 2011). In order to properly capture the stress profile distribution, it was used models with more refined meshes than the ones for the strength prediction. The element size for the adhesive layer in the models of the stress study (solid elements) was 0.02 mm×0.02 mm and for the strength prediction study (CZM elements) was 0.2 mm×0.2 mm. In Figure 2 is shown a mesh refinement exemple of the TAJ with an overlpap length (L_O) of 20 mm that was used in the strength prediticon study. In terms of boundary condition it was considered that the specimens were clamped at one of the extremeties, and for the loading is applied a longitudinal displacement at the other extremety with transversal restriction.

Figure 2. FE mesh detail and boundary conditions of the axisymmetric model for a tubular joint with L_O=20 mm.

3. RESULTS

3.1. Validation with experimental results

With the goal of validating the numerical maximum load (P_m) results attained by the CZM triangular cohesive softening law, they were compared to experimental ones with two different L_O. The experimental versus numerical results comparison of the strength prediction (P_m) values in function of the L_O for the TAJ bonded with the adhesive Araldite® 2015 are shown in Figure 3. It is possible to observe that the numerical P_m values are in close agreement with the experimental ones. The maximum observed difference between the comparison is 6.1% for the L_O=20 mm and 2.9%

for L_O=40 mm. Since an excellent convergence between the numerical and experimental results was observed, the proposed methodology is considered valid, which will grant soundness to the development of the parametric study carried out in this work.

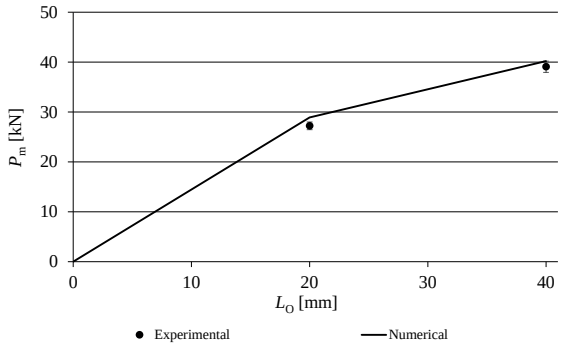

Figure 3. Experimental and numerical values of P_m vs. L_O for the tubular joints with the adhesive Araldite® 2015.

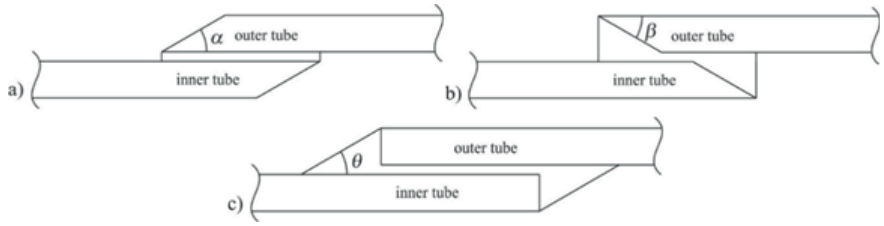

Figure 4. Schematic representation of the outer (a), inner chamfer (b) and adhesive fillet (c) modifications and respective definition of the angles.

3.3. Stress distribution analysis

In this section it will be presented the stress distribution analysis and τ_{avg} is the average value of τ_{xy} for the respective joint.

The first geoemtrical variation analyzed is the outer chamfer angle (α) and the srudied values were: 7,5°, 15°, 30°, 45°, 60° and 90°. It shoulb be emphazised that an angle equal to 90° corresponds to the base case, i.e., adherends without chamfering. In Figure 5 (a) is presented the σ_y/τ_{avg} stress distribution curves, and it is possible to observe peak stresses located at the overlap extremities. The greatest observed decrease on the maximum σ_y/τ_{avg} was 45.6% for α=7.5°, when comparying to the base case(α=90°). The τ_{xy}/τ_{avg} stress distribution is ilustrated in Figure 5 (b) and shows a reduction of

the peak τ_{xy}/τ_{avg} with the decrease of α. It was also observed a 42.7% decrease of the maximum τ_{xy}/τ_{avg} for α=7.5º.

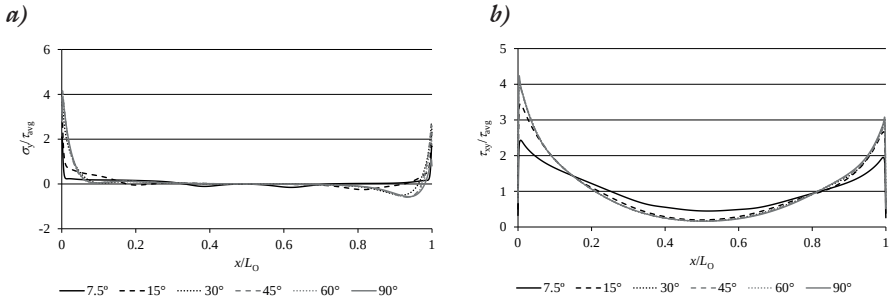

Figure 5. *σ_y (a) and τ_{xy} (b) stress distributions in the adhesive as a function of* α*.*

The stress distribution for the inner chamfer angle (β) is presented in Figure 6. The values assumed for β were 7.5°, 15°, 30°, 45°, 60° and 90°. The σ_y/τ_{avg} stress distribution curves as a function of inner chamfer angle (β) are ilustrated in With the use of inner chamfers at the overlap extremities it can be observed, on the stress profiles, two additional peak stress concentrations, that are added to the already existing ones located at the overlap extremities. The cross section of the chamfered regions was reduced, by the machining process, which gave rise to an increase of the longitudinal strains and consequently led to an increase of the local σ_y/τ_{avg} stress. In contrast the peak stresses located at the overlap extremities were reduced due to the chamfering of the adherends. The inner chamfer results show a reduction of 14.9% for β=30° in the maximum σ_y/τ_{avg} when compared to the base case without chamfer (β=90°). The τ_{xy}/τ_{avg} stress distribution curves are shown in Figure 6 (b). It is also observed two supplementary peak stresses, added to the already existing stress peaks of the overlap extremities. Nevertheless, the difference in this case is more significant, because the intermediate peaks show higher τ_{xy}/τ_{avg} stress values. This indicates that the beginning of the inner chamfer of the TAJ is the most critical zone. In similar way, as the previous analysis, also in this case is observed a reduction of the peak stress τ_{xy}/τ_{avg} with the decrease of β. The maximum obtained reduction was 59.7% for β=7.5º when comparying to β=90º.

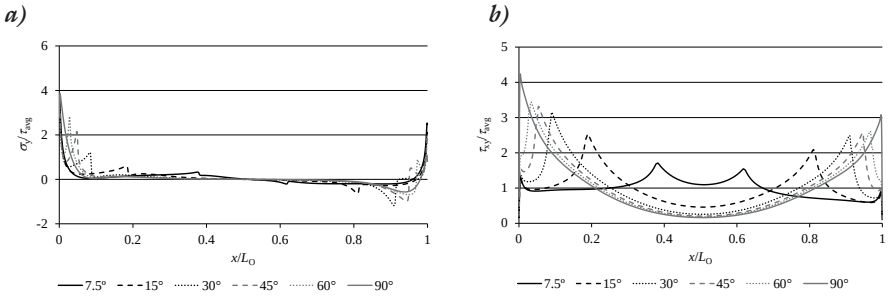

Figure 6. σ_y ***(a) and*** τ_{xy} ***(b) stress distributions in the adhesive as a function of*** β.

Figure 8 shows the stress distribution for the adhesive fillet angle (θ). This geometric varitation causes an increase of L_O and the values of θ analyzed for this case were 7.5°, 15°, 30°, 45°, 60° and 90°. The σ_y/τ_{avg} stress distribution curves depending on θ are presented in Figure 8 (a). The use of adhesive fillet creates additional peak stresses, that appear at $x/L_O<0$ and $x/L_O>1$ in addition to the ones located at $x/L_O=0$ and $x/L_O=1$. Again it is observed an decrease in the the σ_y/τ_{avg} peak stresses with the decrease of θ. The maximum reduction of the peak value (16.7%) is verified for θ=7.5°, when compared to the base case without adhesive fillets (θ=90°). The τ_{xy}/τ_{avg} stress distributions as a function of θ is illustrated in Figure 8 (b) The supplementary peak stresses reveal lower magnitude, when comparying to the ones at the overlap extremities ($x/L_O=0$ and $x/L_O=1$). It was observed a reduction of the peak stresses in the order of 11.7% for θ=7.5°, in comparisson tho the base case (θ=90°), and also a stabilization of peak τ_{xy}/τ_{avg} for the angles ranging between θ=7.5° to θ=60°.

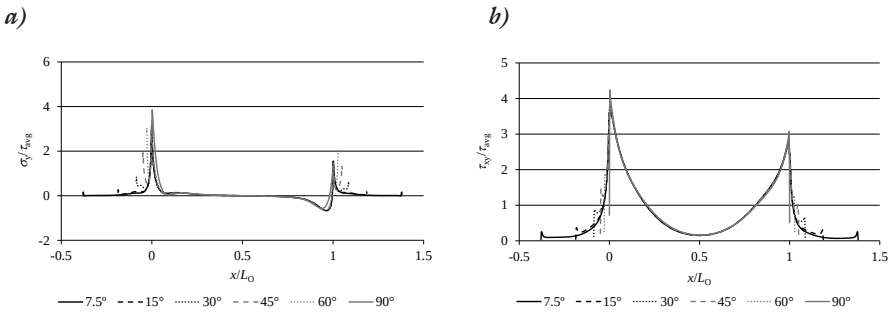

Figure 7. σ_y ***(a) and*** τ_{xy} ***(b) stress distributions in the adhesive as a function of*** θ.

3.4. Strength prediction analysis

The numerical *P*-δ curves for the TAJ bonded with Araldite® 2015 analysed in this work is presented in Figure 8. The strength prediciton for the inner chamfer (Figure 8 (a)) revealed that there is no significant variation of the P_m among the different angles of the outer chamfer. Owing to the overall excellent mechanical properties of this adhesive, plasticitication of the inner tube adherends takes place giving rise to failure dominated by this phenomenon. All numerical P_m values are similar independently of the inner chamfer angle α.

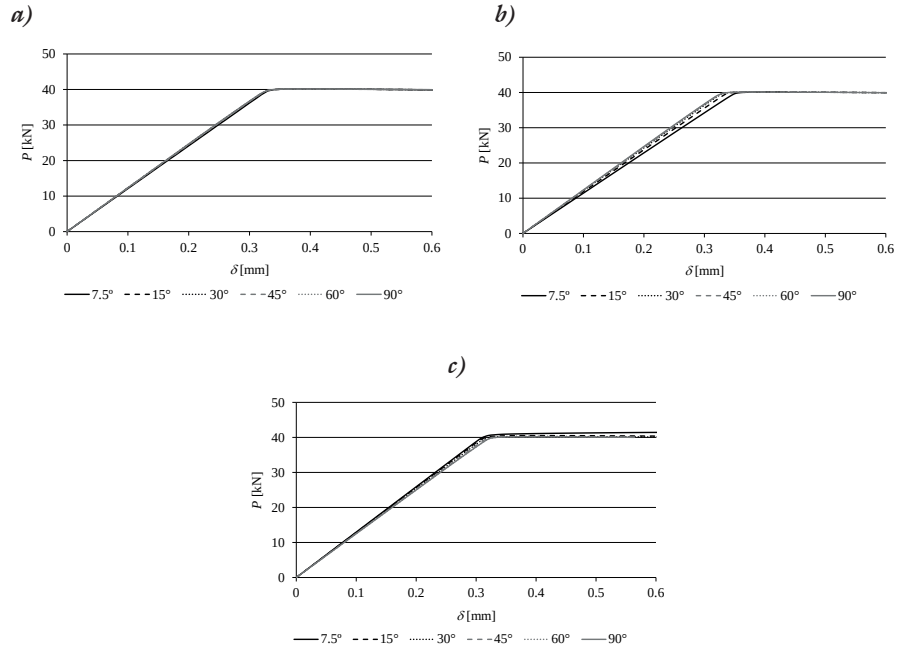

Figure 8. Numerical** P-δ **curves as a function of outer chamfer angle** α **(a), as a function of inner chamfer angle** β **(b), and as a function of ahdeisve fillet angle** θ **(c).

Figure 8 (b) shows the numerical *P*-δ curves for the outter chamfer angle β and is possible to observe that the aluminium tubes undergo plastic deformation in all cases. As a consequence there is a marginal alteration (0.02% for β=30º in comparisson to β=90º) in the P_m with the variation of β. Furthermore, there is a variation in the elastic stiffness of the TAJ with outer chamfers.

The numerical *P*-δ curves for the geometric variation of adhesive fillet θ are given in Figure 8 (c) and in all the cases is possible to detect plasticization of the aluminum adherends. In terms of P_m, it increases while decreasing θ.

The maximum increase obtained is 3.5% for $\theta=7.5^{o}$ in comparisson to the base case without adhesive fillet ($\theta=90^{o}$).

4. CONCLUSION

The tubular adhesive joints strength prediction based on Cohesive Zone Modelling was validated, owing to the numerical maximum strength values being in close agreement to the averaged experimental results. Therefore, the geometrical variations analysed in this work give rise to the following results:

- Outer chamfer (α): for $\alpha=7.5^{o}$ there was a marked σ_y/τ_{avg} and τ_{xy}/τ_{avg} stress decrease in the order of 46%. Regarding the P_m there is no difference between the values of α, since it was observed plastic deformation in the inner aluminium tube;
- Inner chamfer (β): this geometrical variation led to additional stress concentrations peaks. Small σ_y/τ_{avg} stress reductions were obtained ($\approx$15%) and high τ_{xy}/τ_{avg} stress increase were obtained ($\approx$60%). Owing to adherends plasticization there was no marked change in the P_m values;
- Adhesive fillet (θ): The fillet generates supplementary peak stresses at its extremities. With the fillet addition, the overlap peak stresses were reduced approximately 17% for σ_y/τ_{avg} and approximately 12% for τ_{xy}/τ_{avg}. A residual improvement in the P_m (4%) was verified because the shear resistant area increased at the overlap.

In sum it can be settled that the analysed geometric variations can significantly affect the performance of the tubular adhesive joints. Owing to inner tubes plasticization, the pointed out behaviour is not reflected into maximum strength improvements.

REFERENCES

Albiez, M., Vallée, T., Fricke, H. and Ummenhofer, T., 2019. Adhesively bonded steel tubes — Part I: Experimental investigations. International Journal of Adhesion and Adhesives 90, 199-210.

Campilho, R. D. S. G., Banea, M. D., Neto, J. A. B. P. and da Silva, L. F. M., 2012. Modelling of single-lap joints using cohesive zone models: Effect of the cohesive parameters on the output of the simulations. The Journal of Adhesion 88(4-6), 513-533.

Campilho, R. D. S. G., Banea, M. D., Neto, J. A. B. P. and da Silva, L. F. M., 2013. Modelling adhesive joints with cohesive zone models: effect of the

cohesive law shape of the adhesive layer. International Journal of Adhesion and Adhesives 44, 48-56.

Campilho, R. D. S. G., Banea, M. D., Pinto, A. M. G., da Silva, L. F. M. and de Jesus, A. M. P., 2011. Strength prediction of single- and double-lap joints by standard and extended finite element modelling. International Journal of Adhesion and Adhesives 31(5), 363-372.

Campilho, R. D. S. G., de Moura, M. F. S. F., Barreto, A. M. J. P., Morais, J. J. L. and Domingues, J. J. M. S., 2009. Fracture behaviour of damaged wood beams repaired with an adhesively-bonded composite patch. Composites Part A: Applied Science and Manufacturing 40(6–7), 852-859.

Choi, J. H. and Lee, D. G., 1996. An Experimental Study of the Static Torque Capacity of the Adhesively-Bonded Tubular Single Lap Joint. The Journal of Adhesion 55(3-4), 245-260.

de Sousa, C. C. R. G., Campilho, R. D. S. G., Marques, E. A. S., Costa, M. and da Silva, L. F. M., 2017. Overview of different strength prediction techniques for single-lap bonded joints. Proceedings of the Institution of Mechanical Engineers, Part L: Journal of Materials: Design and Applications 231(1-2), 210-223.

Ebnesajjad, S. and Landrock, A. H. (2014). Adhesives technology handbook. New York, USA, William Andrew.

Ferreira, L. R. F., Campilho, R. D. S. G., Barbosa, D. R., Rocha, R. J. B. and Silva, F. J. G., 2019. Static strength improvement of tubular aluminium adhesive joints by the outer chamfering technique. Procedia Manufacturing 38, 629-636.

Ferreira, L. R. F., Campilho, R. D. S. G., Rocha, R. J. B. and Barbosa, D. R., 2019. Geometrical and material optimization of tensile loaded tubular adhesive joints using cohesive zone modelling. The Journal of Adhesion 95(5-7), 425-449.

Kaiser, I. and Tan, K. T., 2020. Damage and strength analysis of Carbon Fiber Reinforced Polymer and Titanium tubular-lap joint using hybrid adhesive design. International Journal of Adhesion and Adhesives 103, 102710.

Machado, R. M. D., Campilho, R. D. S. G. and Rocha, R. J. B., 2019. Extended finite element modelling of aluminium stepped-adhesive joints. The Journal of Adhesion 95(5-7), 450-473.

Moreira, R. D. F. and Campilho, R. D. S. G., 2015. Strength improvement of adhesively-bonded scarf repairs in aluminium structures with external reinforcements. Engineering Structures 101, 99-110.

Nguyen, V. and Kedward, K. T., 2001. Non-linear Modeling of Tubular Adhesive Scarf Joints Loaded in Tension. The Journal of Adhesion 76(3), 265-292.

Nunes, S. L. S., Campilho, R. D. S. G., da Silva, F. J. G., de Sousa, C. C. R. G., Fernandes, T. A. B., Banea, M. D. and da Silva, L. F. M., 2016. Comparative failure assessment of single and double-lap joints with varying adhesive systems. The Journal of Adhesion 92, 610-634.

O'Mahoney, D. C., Katnam, K. B., O'Dowd, N. P., McCarthy, C. T. and Young, T. M., 2013. Taguchi analysis of bonded composite single-lap joints using a combined interface–adhesive damage model. International Journal of Adhesion and Adhesives 40, 168-178.

Petrie, E. M. (2000). Handbook of adhesives and sealants. New York, USA, McGraw-Hill.

Quispe Rodríguez, R., de Paiva, W. P., Sollero, P., Bertoni Rodrigues, M. R. and de Albuquerque, É. L., 2012. Failure criteria for adhesively bonded joints. International Journal of Adhesion and Adhesives 37, 26-36.

Woelke, P. B., Shields, M. D., Abboud, N. N. and Hutchinson, J. W., 2013. Simulations of ductile fracture in an idealized ship grounding scenario using phenomenological damage and cohesive zone models. Computational Materials Science 80, 79-95.

CHAPTER 8

A Functional Food: Anzer Honey

Elif ÇİL[1]

INTRODUCTION

Functional food is not in the form of drugs, pills, or capsules like nutritional supplements, but the foods that are thought to be beneficial in preventing diseases as well as meeting the body's need for essential nutrients and that people prefer to consume for a healthier life are called functional foods.

Terms such as "functional foods" or "nutraceuticals" are widely used in the marketplace. Such foods are regulated by FDA (Food & Drug Administration) under the authority of the Federal Food, Drug, and Cosmetic Act, even though they are not explicitly defined by law.

Honey is a sweet product created by bees by collecting plant nectar and changing its content in their bodies, then taking its final form with maturation in the honeycomb (Turkish Food Codex Honey Communiqué 2020/7). Honey can be runny, viscous, partially or completely crystallized; its taste and aroma vary according to the type of plant. The color of honey can range from water white to dark brown. The quality and biochemical properties of honey, especially the nectar source, its maturation, production method, climatic conditions, and processing and storage conditions, are determined.

1 Institute of Science, Education Faculty, Department of Mathematics & Science Education, Ordu, Turkiye. ORCID Code: 0000-0003-1420-8729, elifcil@odu.edu.tr

The price of honey is above all other foods on the market. But the market price of Anzer honey is ten times higher than other kinds of honey (Gok et al., 2015). Today, the world's honey supply cannot meet the demand, leading to honey's debasement. This result usually comes in the form of diluted honey.

Anzer honey is produced by Caucasian honey bees (*Apis mellifera caucasia*, Pollmann 1889) using flower nectars from the Anzer plateau of Rize province. Anzer honey received its geographical indication registration certificate in 2021. New season Anzer honey sales start in September with pre-orders. Although it is sold at high prices due to its popularity, it is sold out in a short time.

Anzer honey is a heterofloral blossom honey containing wildflowers from the Anzer plateau near Ikizdere and Rize in the East Black Sea Region, Turkey (Tezcan et al., 2011). As a result of internet research, it was stated that Anzer honey is expensive because it is produced by more than 400 flower species and unique bee species. Still, no articles support this information. Despite so much scientific research about Turkish honey primarily produced in the Anzer plateau - Black Sea Region of Turkey, there are few scientific publications about honey produced in the Ayder plateau of Rize-Turkey (Fig 1).

Figure 1. Anzer Plateau (https://rize.tarimorman.gov.tr/FotografGalerisi/2021)

When Azer Honey is typed into the academic google search, 498 publications can be accessed. However, only thirteen of them constitute experimental studies on the biological activity and medical use of Anzer honey.

Pollen analysis is important to find the botanical and geographical origin of honey. Malkoç et al., reported that the major pollens detected in the Anzer honey samples were *Thymus, Rumex, Onobrychis, Cistus, Plantago, Ranunculus, Rhododendron, Myosotis,* and *Geranium* (Malkoç et al., 2019). In the study published by Şenyuva et al. in 2009, Anzer honey contains only *Thymus praecox* from *Thymus* spp., while *Trifolium* spp. Pollen of *Lotus corniculatus, Castanea sativa, Cynoglossum glochidiatum* and *Helianthemum nummularium* were also detected. In addition, the highest amino acid content in this study was reached in Anzer honey (Senyuva et al., 2009).

Anzer honey has greater free radical-scavenging and antioxidant activities than numerous honeys cited in the literature (Ulusoy et al., 2010; Şahin et al., 2011; Malkoç et al., 2019). Anzer honey shows high antioxidant activity compared to some flower honeys and low compared to dark-colored honeys such as chestnut and puree. According to Malkoç et al., phenolic substances found in Anzer Honey at the highest levels were pinocembrin, hesperidin, and chrysin. Pinocembrin, detected at the highest concentration in Anzer honey, is an essential flavonoid with proven pharmacological activity in neurodegenerative and cardiovascular diseases (Malkoç et al., 2019). It is known that there is a positive correlation between total phenolic and total flavonoid content and antioxidant activity.

In Saral's article in 2018, the total phenolic and antioxidant properties of eleven different honey samples collected from the Eastern Black Sea region were examined. In this study comparing chestnut and flower honeys, it was stated that chestnut honey showed higher antioxidant activity than flower honey. However, it can be said that the antioxidant effect of Anzer honey is high among flower honeys (Saral 2018).

In a study published by Korkmaz & Kolonkaya in 2009, they reported that Anzer honey protects rats from N-ethylmaleimide-induced liver damage. This in vivo study with a control group showed that Anzer honey is hepatoprotective against N-ethylmaleimide, a sulfhydryl blocker. The authors stated that this result might be due to the high antioxidant activity of Anzer honey (Korkmaz & Kolonkaya, 2009).

Ulusoy et al., in their study published in 2010, investigated antioxidant and antimicrobial activity in flower honey. Honey samples from Anzer and Kars regions reported moderate antibacterial activity on *E. fecealis* compared to standard antibiotics. In the same study, Anzer suggests that honey can be a functional food due to its high antioxidant properties (Ulusoy et al., 2010).

Cakir et al. In the study in which they investigated the chemical composition, structure types/vibrations, and palynological and antimicrobial properties of honey samples obtained from Rize-Anzer, Gümüşhane, and Sivas-Zara regions, all honey samples were effective in *Staphylococcus aureus* and *Saccharomyces cerevisae*, only honey from Anzer region was effective on *Escherichia coli* and reported that none of the honey samples showed activity on *Listeria monocytogenes* and *Candida albicans*. They stated that oleamide, one of the bioactive oil esters, may be responsible for the antibacterial property. Oleamide also adds antioxidant properties to honey (Cakir et al., 2020).

In the study published by Selçuk and Nevin in 2001, seventy-three honeys obtained from different regions of Turkey were diluted in five concentrations and tested on *E. coli*, *Klebsiella pneumoniae*, *S. aureus*, and *C. albicans*. As a result, while honey generally showed antibacterial activity at 50% dilution, Anzer honey was also able to exhibit antibacterial activity at 40% concentration. However, the same situation is not valid for *C. albicans*. (Selçuk & Nevin 2001).

Malkoç et al., published in 2019, is one of the most comprehensive studies on Anzer honey. In vitro in Anzer honey total flavonoid content (TFC), total phenolic content (TPC), antioxidant properties (DPPH, FRAP), and melissopalynological analyzes were performed, pinocembrin, hesperidin, chrysin, protocatechuic acid, p-coumaric acid, catechin, caffeic acid phenyl ester (CAPE), It was determined that p-OH benzoic acid and caffeic acid were major compounds, myricetin, luteolin, rutin, resveratrol, epicatechin, t-cinnamic acid, ferulic acid, and gallic acid were minor components. Antioxidant and anti-inflammatory properties of hesperidin, and anti-tumoral properties of Chrysin are known. The fact that these ingredients are the major components in Anzer honey reveals the medical aspect of this honey (Malkoç et al., 2019).

In Hotaman's master's thesis in 2015, the bioactive properties of Anzer honey and pollen were examined. In the study, the proline value of Anzer honey was reported to be between 808 and 1139 mg/kg. It has been stated that Anzer honey has a higher proline content than other flower honeys, and it is even close to the proline value of puree honey given in the literature. Since the amount of proline in honey is accepted as an indicator of the amount of protein in honey, it has been revealed that Anzer honey is honey with high nutritional value. In addition to the high antioxidant activity of Anzer honey, the inhibition effect on urease and hyaluronidase enzymes was also revealed in the study. This shows that Anzer honey may have medicinal,

anti-ulcerative, antibacterial, and anti-inflammatory effects (Hotaman 2015).

Hepsag et al. In his study in 2019, the physicochemical and bioactive properties of 21 Anzer honey samples were investigated. The rich total phenolic content of honey samples and, therefore, the high antioxidant properties are the first striking results. However, it has been revealed that the minerals found in Anzer honey are potassium, calcium, sodium, and magnesium. The study also mentions the importance of studying the properties of Anzer honey in detail and determining the limit values for the export of Anzer honey.

Medicinal properties of Anzer honey

In a study conducted by Kolaylı et al. in 2008, the antioxidant and antimicrobial properties of chestnut (n=15), Bayburt (n=8), and Anzer honey (n=7) were investigated. Similar to other studies, the total polyphenol content and antioxidant properties of Anzer honey were lower than chestnut honey and higher than Bayburt honey. The study also includes in vitro study results showing that Anzer honey is effective on the ulcer disease agent Helicobacter pylori. (Kolaylı et al., 2008a). In the same year, Kolaylı et al. published an article about Anzer honey being rich in iron. In this study, Na, K, Ca Fe, Cu, Zn, Mn, Cr, Pb minerals were investigated in honey produced on the Black Sea coasts of Turkey, and it was mentioned that there are intense K, Na and Ca in honeys (Kolaylı et al., 2008b).

Protection from cancer: In ethnobotanical studies, it is reported that Anzer honey is used in medicine. It has been reported that its consumption, especially mixed with *Urtica dioica* L (nettle) seed, is protective against cancer (Gürbüz et al., 2019).

Protection from X-radiation: Bagatır et al. reported that genotoxic damage in the peripheral blood lymphocytes of healthy volunteers induced by X-radiation might be prevented or alleviated by adding Anzer honey in vitro. These results encourage further research on the protective effects of honey (Bagatır et al., 2022).

CONCLUSION

As a result of the search on google academic limited publication on the antimicrobial activity of Anzer honey could be reached. Generally, antimicrobial activity studies on Anzer honey pollen and propolis are available in the literature. Studies on Anzer honey are very limited in the literature, and its bioactivity properties are still waiting to be revealed.

REFERENCES

Bagatir, G., Kaya, M., Suer, I., Cefle, K., Palanduz, A., Palanduz, S., ... & Ozturk, S. (2022). The effect of Anzer honey on X-ray induced genotoxicity in human lymphocytes: An in vitro study. *Microscopy Research and Technique*.

Bagdatli, E., Atmaca, H., & Erturk, O. (2022). Bioactive Properties and Phytochemical Screening of Mad Honey Bee Pollen. *Complementary Medicine Research*, 1-11.

Çakır, Y., Çobanoğlu, D. N., Dervişoğlu, G., Koçyiğit, S., Karahan, D., & Yelkovan, S. (2020). Determination Antimicrobial Activity, Palynological Characteristics and Chemical Composition of Some Honey Samples from Turkey. *Mellifera*, *20*(1), 41-60.

Doğan, A., & Kolankaya, D. (2005). Protective effect of Anzer honey against ethanol-induced increased vascular permeability in the rat stomach. *Experimental and Toxicologic Pathology*, *57*(2), 173-178.

Gercek, Y. C., Celik, S., & Bayram, S. (2021). Screening of Plant Pollen Sources, Polyphenolic Compounds, Fatty Acids and Antioxidant/Antimicrobial Activity from Bee Pollen. *Molecules*, *27*(1), 117.

Gok, S., Severcan, M., Goormaghtigh, E., Kandemir, I., & Severcan, F. (2015). Differentiation of Anatolian honey samples from different botanical origins by ATR-FTIR spectroscopy using multivariate analysis. *Food chemistry*, *170*, 234-240.

Gürbüz, İ., Özkan, A. M. G., Akaydin, G., Salihoğlu, E., Günbatan, T., Demirci, F., & Yeşilada, E. (2019). Folk medicine in düzce province (Turkey). *Turkish Journal of Botany*, *43*(6), 769-784.

Hepsağ, F. (2019). Determınatıon Of Total Phenolıc Compounds And Antıoxıdant Capacıty Of Anzer Honey Produced In Rıze, Turkey. *Gıda/The Journal Of Food*, *44*(4).

Hotaman, H. E. (2015). *Anzer bal ve poleninin bazı biyoaktif özelliklerinin in vitro olarak incelenmesi* (Master's thesis, Recep Tayyip Erdoğan Üniversitesi/ Sağlık Bilimleri Enstitüsü/Tıbbi Biyokimya Anabilim Dalı).

Karlıdağ, S., Keskin, M., & Keskin, Ş. (2021). At Yaralarında Balın Kullanımı. *Kadirli Uygulamalı Bilimler Fakültesi Dergisi*, *1*(1), 48-57.

Kolaylı, S., Aliyazıcıoğlu, R., Ulusoy, E., & Karaoğlu, Ş. (2008a). Antioxidant and antimicrobial activities of selected Turkish honeys. *Hacettepe Journal of Biology and Chemistry*, *36*(2), 163-172.

Kolayli, S., Kongur, N., Gündoğdu, A., Kemer, B., Duran, C., & Aliyazıcıoğlu, R. (2008b). Mineral composition of selected honeys from Turkey. *Asian Journal of Chemistry*, *20*(3).

Korkmaz, A., & Kolankaya, D. (2009). Anzer honey prevents N-ethylmaleimide-induced liver damage in rats. *Experimental and Toxicologic Pathology*, *61*(4), 333-337.

Malkoç, M., ÇAKIR, H., Yakup, K. A. R. A., Zehra, C. A. N., & KOLAYLI, S. (2019). Phenolic composition and antioxidant properties of Anzer honey from black sea region of Turkey. *Uludağ Arıcılık Dergisi*, *19*(2), 143-151.

Tezcan, F., Kolaylı, S., Sahin, H., Ulusoy, E., & Erim, F.B. (2011). Evaluation of organic acid, saccharide composition and antioxidant properties of some authentic Turkish honeys. *Journal of Food and Nutrition Research*, *50*(1), 33-40.

Selçuk, H., & Nevin, K. (2002). Investigation of antimicrobial effect of honey collected from various regions of Turkey. *Pakistan J. Biol. Sci*, *5*, 325-328.

Senyuva, H. Z., Gilbert, J., Silici, S., Charlton, A., Dal, C., Gürel, N., & Cimen, D. (2009). Profiling Turkish honeys to determine authenticity using physical and chemical characteristics. *Journal of Agricultural and Food Chemistry*, *57*(9), 3911-3919.

Ulusoy, E., Kolayli, S., & Sarikaya, A. O. (2010). Antioxidant and antimicrobial activity of different floral origin honeys from Turkiye. *Journal of food biochemistry*, *34*, 321-335.

Türk Gıda Kodeksi (2020). Bal Tebliği 2020/7.

CHAPTER 9

Achievement Measures of Batch Arrival Queuing System in Fuzzy Habitat

Ramesh. R,[1]

1. INTRODUCTION

Queueing models are effective methods for performance analysis of computer and telecommunication systems, manufacturing/production systems and inventory control (Kleinrock [11], Buzacott and Shanthikumar [1], Gross and Harris [7], Trivedi [19]). In general, these analyses consider a queueing system where requests for service arrive in units, one at a time (single-unit arrival). In many practical situations, however, requests for service usually arrive in batches. For example, in manufacturing systems of the job-shop type, each job order often requires the manufacture of more than one unit; in computer communication systems, messages which are to be transmitted could consist of a random number of packets. If the usual crisp batch-arrival queues with multiple servers can be extended to fuzzy batch-arrival queues, such queueing models would have wider applications.

For queueing models with multiple servers under various considerations, the M/M/c vacation systems with a single-unit arrival have attracted much attention from numerous researchers since Levy and Yechiali [12]. The extensions of this model can be referred to Vinod [20], Igaki [8], Tian et al. [17], Tian and Xu [18], and Zhang and Tian [23] studied the M/M/c vacation systems with a single-unit arrival and a "partial server vacation

1 Department of Mathematics, Arignar Anna Government Arts College, Musiri, Tamilnadu, India. E mail : rameshsanju123@gmail.com

policy". They proved several conditional stochastic decomposition results for the queue length and waiting time. Chao and Zhao [3] investigated the GI/M/c vacation models with a single-unit arrival and provided iterative algorithms for computing the stationary probability distributions.

In the literature described above, customer inter-arrival times and customer service times are required to follow certain probability distributions with fixed parameters. However, in many real-world applications, the parameter distributions may only be characterized subjectively; that is, the arrival and service are typically described in everyday language summaries of central tendency, such as "the mean arrival rate is around 5 per day", or "the mean service rate is about 10 per hour", rather than with complete probability distributions. In other words, these system parameters are both possibilistic and probabilistic. Thus, fuzzy queues are potentially much more useful and realistic than the commonly used crisp queues (see Li and Lee [13] and Zadeh [22]). By extending the usual crisp batch-arrival queues to fuzzy batch-arrival queues in the context of multiple servers, these queuing models become appropriate for a wider range of applications. Ramesh et.al [24-31] presented dissimilar queueing models. Seenivasan et. al [32-34] provided server breakdown with catastrophe, server breakdown with feed back and so many queueing models.

Li and Lee [13] investigated the analytical results for two typical fuzzy queues (denoted $M/F/1/\infty$ and $FM/FM/1/\infty$, where F represents fuzzy time and FM represents fuzzified exponential distributions) using a general approach based on Zadeh's extension principle (see also Prade [15] and Yager [21]), the possibility concept and fuzzy Markov chains (see Stanford [16]). Seenivasan et. al [31] illustrated about heterogeneous queueing system. A useful modeling and inferential technique would be applied their approach to general fuzzy queuing problems (see Stanford [16]). However, their approach is complicated and not suitable for computational purposes; moreover, it cannot easily be used to derive analytic results for other complicated queuing systems (see Negi and Lee [14]). In particular, it is very difficult to apply this approach to fuzzy queues with more fuzzy variables or multiple servers. Negi and Lee [14] proposed a procedure using α-cuts and two-variable simulation to analyze fuzzy queues (see also Chanas and Nowakowski [2]). Unfortunately, their approach provides only crisp solutions; *i.e.*, it does not fully describe the membership functions of the system characteristics. Using parametric programming, Kao et al. [9] constructed the membership functions of the system characteristics for fuzzy queues and successfully applied them to four simple fuzzy queue models: $M/F/1/\infty$, $F/M/1/\infty$, $F/F/1/\infty$ and $FM/FM/1/\infty$. Recently, Chen

[4,5] developed $FM/FM/1/L$ and $FM/FM^{[K]}/1/\infty$ fuzzy systems using the same approach. All previous researches on fuzzy queuing models are focused on ordinary queues with a single server. In this paper, we develop an approach that provides system characteristics for batch-arrival queues with multiple servers and fuzzy parameters: fuzzified exponential batch-arrival and service rates. Through α-cuts and Zadeh's extension principle, we transform the fuzzy queues to a family of crisp queues. As α varies, the family of crisp queues is described and solved using parametric nonlinear programming (NLP). The NLP solutions completely and successfully yield the membership functions of the system characteristics, including the expected number of customers in the system and the expected waiting time in the queue.

The remainder of this paper is organized as follows. Section 2 presents the system characteristics of standard and fuzzy batch-arrival queuing models with multiple servers. In Section 3, a mathematical programming approach is developed to derive the membership functions of these system characteristics. To demonstrate the validity of the proposed approach, one realistic numerical example is described and solved. Discussion is provided in Section 4, and conclusions are drawn in Section 5. For notational convenience, our model in this paper is hereafter denoted $FM^{[x]}/FM/c$.

2. FUZZY BATCH QUEUE WITH MULTIPLE SERVERS

Think about a batch arrival queuing system with c servers where the customers arrive in batches to occur according to a compound Poisson process with batch-arrival rate λ. Let A_k denote the number of customers belonging to the k^{th} arrival batch, where A_k, $k =$ $\cdots$ are with a common distribution $\Pr[A_k = n] = a_n, n = 1, 2, 3, \cdots$, and $E[A] = \sum_{n=1}^{\infty} n a_n$. Customers arriving at the service facility (servers) form a single-file queue and are served in order. The service time for each of all c servers is exponentially distributed with rate μ and each server can serve only one customer at a time. Customers who upon entry the service facility find that all servers are busy have to wait in the queue until any one server is available. Let N_s and W_q represents the expected number of customers in the system and the expected waiting time in the queue, respectively. Through a Markov process, we can easily obtain N_s and W_q in terms of system parameters

$$N_s = \frac{\lambda(2E[A] + E[A(A-1)]) + 2\mu \cdot \sum_{n=0}^{c-1} n(c-n) P_n(\lambda, \mu)}{2(c\mu - \lambda E[A])}, \qquad (1)$$

$$W_q = \frac{\lambda(2E[A] + E[A(A-1)]) + 2\mu \cdot \sum_{n=0}^{c-1} n(c-n)P_n(\lambda,\mu)}{2\lambda E[A](c\mu - \lambda E[A])} - \frac{1}{\mu}, \tag{2}$$

where $P_n(\lambda,\mu)$ represents the probability that there are *n* customers in the system. And the probability depends on λ and μ. In steady-state, it is necessary that we have $0 < \frac{\lambda E[A]}{c\mu} < 1$.

To extend the applicability of the batch-arrival queuing model with multiple servers, we allow for fuzzy specification of system parameters. Suppose the batch-arrival rate λ for customers and service rate μ for each server are approximately known and can be represented by the fuzzy sets $\tilde{\lambda}$ and $\tilde{\mu}$. Let $\phi_{\tilde{\lambda}}(x)$ and $\phi_{\tilde{\mu}}(y)$ denote the membership functions of $\tilde{\lambda}$ and $\tilde{\mu}$. We then have the following fuzzy sets:

$$\tilde{\lambda} = \left\{ (x, \phi_{\tilde{\lambda}}(x)) \;\middle|\; x \in X \right\}, \tag{3a}$$

$$\tilde{\mu} = \left\{ (y, \phi_{\tilde{\mu}}(y)) \;\middle|\; y \in Y \right\}, \tag{3b}$$

where X and Y are the crisp universal sets of the batch-arrival and service rates.

Let $f(x,y)$ denote the system characteristic of interest. Since $\tilde{\lambda}$ and $\tilde{\mu}$ are fuzzy numbers, $f(\tilde{\lambda},\tilde{\mu})$ is also a fuzzy number. Following Zadeh's extension principle (see Yager [21] and Zadeh [22]), the membership function of the system characteristic $f(\tilde{\lambda},\tilde{\mu})$ is defined as:

$$\phi_{f(\tilde{\lambda},\tilde{\mu})}(z) = \sup_{x \in X, y \in Y, 0 < xE[A]/cy < 1} \min\left\{ \phi_{\tilde{\lambda}}(x), \phi_{\tilde{\mu}}(y) \;\middle|\; z = f(x,y) \right\}, \tag{4}$$

Assume that the system characteristic of interest is the expected number of customers in the system. It follows from (1) that the expected number of customers in the system is:

$$f(x,y) = \frac{x(2E[A] + E[A(A-1)]) + 2y \cdot \sum_{n=0}^{c-1} n(c-n)P_n(x,y)}{2(cy - xE[A])}. \tag{5}$$

The membership function for the expected number of customers in the system is:

$$\phi_{\tilde{N}_s}(z) = \sup_{x \in X, y \in Y, 0 < xE[A]/cy < 1} \min\left\{ \phi_{\tilde{\lambda}}(x), \phi_{\tilde{\mu}}(y) \;\middle|\; z = \frac{x(2E[A] + E[A(A-1)]) + 2y \cdot \sum_{n=0}^{c-1} n(c-n)P_n(x,y)}{2(cy - xE[A])} \right\}. \tag{6}$$

Unfortunately, the membership function is not expressed in the usual form, making it very difficult to imagine its shape. In this paper we approach

the representation problem using a mathematical programming technique. Parametric NLPs are developed to find the α -cuts of $f(\tilde{\lambda}, \tilde{\mu})$ based on the extension principle.

3. PARAMETRIC NONLINEAR PROGRAMMING

To re-express the membership function $\phi_{\tilde{N}_s}(z)$ of $\tilde{N}_s$ in an understandable and usable form, we adopt Zadeh's approach, which relies on α -cuts of $\tilde{N}_s$. Definitions for the α -cuts of $\tilde{\lambda}$ and $\tilde{\mu}$ as crisp intervals are as follows:

$$\lambda(\alpha) = \left[x_\alpha^L, x_\alpha^U\right] = \left[\min_{x \in X}\left\{x \mid \phi_{\tilde{\lambda}}(x) \geq \alpha\right\}, \max_{x \in X}\left\{x \mid \phi_{\tilde{\lambda}}(x) \geq \alpha\right\}\right], \quad (7a)$$

$$\mu(\alpha) = \left[y_\alpha^L, y_\alpha^U\right] = \left[\inf_{y \in Y}\left\{y \mid \phi_{\tilde{\mu}}(y) \geq \alpha\right\}, \inf_{y \in Y}\left\{y \mid \phi_{\tilde{\mu}}(y) \geq \alpha\right\}\right], \quad (7b)$$

The constant batch-arrival and service rates are shown as intervals when the membership functions are no less than a given possibility level for α . As a result, the bounds of these intervals can be described as functions of α and can be obtained as: $x_\alpha^L = \min \phi_{\tilde{\lambda}}^{-1}(\alpha)$, $x_\alpha^U = \max \phi_{\tilde{\lambda}}^{-1}(\alpha)$, $y_\alpha^L = \min \phi_{\tilde{\mu}}^{-1}(\alpha)$, and $y_\alpha^U = \max \phi_{\tilde{\mu}}^{-1}(\alpha)$. Therefore, we can use the α -cuts of $\tilde{N}_s$ to construct its membership function since the membership function defined in (6) is parameterized by α .

Using Zadeh's extension principle, $\phi_{\tilde{N}_s}(z)$ is the minimum of $\phi_{\tilde{\lambda}}(x)$ and $\phi_{\tilde{\mu}}(y)$. To derive the membership function $\phi_{\tilde{N}_s}(z)$, we need at least one of the following cases to hold such that

$$z = \frac{x(2E[A] + E[A(A-1)]) + 2y \cdot \sum_{n=0}^{c-1} n(c-n)P_n(x,y)}{2(cy - xE[A])} \text{ satisfies } \phi_{\tilde{N}_s}(z) = \alpha :$$

Case (i): ($\phi_{\tilde{\lambda}}(x) = \alpha$, $\phi_{\tilde{\mu}}(y) \geq \alpha$),

Case (ii): ($\phi_{\tilde{\lambda}}(x) \geq \alpha$, $\phi_{\tilde{\mu}}(y) = \alpha$),

This can be accomplished using parametric NLP techniques. The NLP to find the lower and upper bounds of the α -cut of $\phi_{\tilde{N}_s}(z)$ for Case (i) are:

$$(N_s)_\alpha^{L_1} = \min \frac{x(2E[A] + E[A(A-1)]) + 2y \cdot \sum_{n=0}^{c-1} n(c-n)P_n(x,y)}{2(cy - xE[A])}, \quad (8a)$$

$$(N_s)_\alpha^{U_1} = \max \frac{x(2E[A] + E[A(A-1)]) + 2y \cdot \sum_{n=0}^{c-1} n(c-n)P_n(x,y)}{2(cy - xE[A])}, \quad (8b)$$

and for Case (ii) are:

$$(N_s)_\alpha^{L_2} = \min \frac{x(2E[A] + E[A(A-1)]) + 2y \cdot \sum_{n=0}^{c-1} n(c-n)P_n(x,y)}{2(cy - xE[A])}, \quad (8c)$$

$$(N_s)_\alpha^{U_2} = \max \frac{x(2E[A] + E[A(A-1)]) + 2y \cdot \sum_{n=0}^{c-1} n(c-n)P_n(x,y)}{2(cy - xE[A])}. \quad (8d)$$

From the definitions of $\lambda(\alpha)$ and $\mu(\alpha)$ in (7), $x \in \lambda(\alpha)$ and $y \in \mu(\alpha)$ can be replaced by $x \in [x_\alpha^L, x_\alpha^U]$ and $y \in [y_\alpha^L, y_\alpha^U]$. The α-cuts form a nested structure with respect to α (see Kaufmann [10] and Zimmermann [25]); *i.e.*, given $0 < \alpha_2 < \alpha_1 \leq 1$, we have $[x_{\alpha_1}^L, x_{\alpha_1}^U] \subseteq [x_{\alpha_2}^L, x_{\alpha_2}^U]$ and $[y_{\alpha_1}^L, y_{\alpha_1}^U] \subseteq [y_{\alpha_2}^L, y_{\alpha_2}^U]$. Therefore, (8a) and (8c) have the same smallest element and (8b) and (8d) have the same largest element. To find the membership function $\phi_{\tilde{N}_s}(z)$, it suffices to find the left and right shape functions of $\phi_{\tilde{N}_s}(z)$, which is equivalent to finding the lower bound $(N_s)_\alpha^L$ and upper bound $(N_s)_\alpha^U$ of the α-cuts of $\tilde{N}_s$, which can be rewritten as:

$$(N_s)_\alpha^L = \min \frac{x(2E[A] + E[A(A-1)]) + 2y \cdot \sum_{n=0}^{c-1} n(c-n)P_n(x,y)}{2(cy - xE[A])} \quad (9a)$$

s.t. $x_\alpha^L \leq x \leq x_\alpha^U$ and $y_\alpha^L \leq y \leq y_\alpha^U$,

$$(N_s)_\alpha^U = \max \frac{x(2E[A] + E[A(A-1)]) + 2y \cdot \sum_{n=0}^{c-1} n(c-n)P_n(x,y)}{2(cy - xE[A])} \quad (9b)$$

s.t. $x_\alpha^L \leq x \leq x_\alpha^U$ and $y_\alpha^L \leq y \leq y_\alpha^U$,

At least one of x and y must hit the boundaries of their α-cuts to satisfy $\phi_{\tilde{N}_s}(z) = \alpha$. This model is a set of mathematical programs with boundary constraints and lends itself to the systematic study of how the optimal solutions change with x_α^L, x_α^U, y_α^L, and y_α^U as α varies over $(0,1]$. The model is a special case of parametric NLPs (see Gal [6]).

The crisp interval $[(N_s)_\alpha^L, (N_s)_\alpha^U]$ obtained from (9) represents the α-cuts of $\tilde{N}_s$. Again, by applying the results of Kaufmann [10] and Zimmermann [25] and convexity properties to $\tilde{N}_s$, we have $(N_s)_{\alpha_1}^L \geq (N_s)_{\alpha_2}^L$ and $(N_s)_{\alpha_1}^U \leq (N_s)_{\alpha_2}^U$, where $0 < \alpha_2 < \alpha_1 \leq 1$. In other words, $(N_s)_\alpha^L$ increases and $(N_s)_\alpha^U$ decreases as α increases. Consequently, the membership function $\phi_{\tilde{N}_s}(z)$ can be found from (9).

If both $(N_s)_\alpha^L$ and $(N_s)_\alpha^U$ in (9) are invertible with respect to α, then a left shape function $L(z) = [(N_s)_\alpha^L]^{-1}$ and a right shape function $R(z) = [(N_s)_\alpha^U]^{-1}$ can be derived, from which the membership function $\phi_{\tilde{N}_s}(z)$ is constructed:

$$\phi_{\tilde{N}_s}(z) = \begin{cases} L(z), & (N_s)_{\alpha=0}^L \le z \le (N_s)_{\alpha=1}^L, \\ 1, & (N_s)_{\alpha=1}^L \le z \le (N_s)_{\alpha=1}^U, \\ R(z), & (N_s)_{\alpha=1}^U \le z \le (N_s)_{\alpha=0}^U. \end{cases} \quad (10)$$

In most cases, the values of $(N_s)_\alpha^L$ and $(N_s)_\alpha^U$ cannot be solved analytically. Consequently, a closed-form membership function for $\phi_{\tilde{N}_s}(z)$ cannot be obtained. However, the numerical solutions for $(N_s)_\alpha^L$ and $(N_s)_\alpha^U$ at different possibility levels can be collected to approximate the shapes of $L(z)$ and $R(z)$. That is, the set of intervals $\{[(N_s)_\alpha^L, (N_s)_\alpha^U] \mid \alpha \in [0,1]\}$ shows the shape of $\phi_{\tilde{N}_s}(z)$, although the exact function is not known explicitly.

Note that the membership functions for the expected waiting time in the queue can be expressed in a similar manner.

4. NUMERICAL EXAMPLE

This section we present one example motivated by real-life systems to demonstrate the practical use of the proposed approach, which is based on http://www.macaudata.com/macauweb/book175/html/19301.htm

Example: Considering one sewerage treatment system collects sewage from the urban areas and sends them to the sewerage treatment plant. The sewerage treatment plant has three supply pipes (referred to 3-servers). Each pipe can settle the larger solids and put the settled into the chemical process tank. After the chemical process, the treated water is discharged to the sea. We assume that the number of arriving sewage solids each time follows a geometric distribution with parameter $p = 0.5$; *i.e.*, the size of arriving sewage solids A is $\Pr(A = k) = 0.5(1-0.5)^{k-1}, k = 1, 2, \cdots$. Clearly, this problem can be described by FM[x]/FM/3 system. For efficiency, the management wants to get the system characteristics such as the expected waiting time in the queue.

Suppose the batch-arrival rate and service rate are trapezoidal fuzzy numbers represented by $\tilde{\lambda} = [1, 2, 3, 4]$ and $\tilde{\mu} = [11, 12, 13, 14]$. First, it is easy to find that $[x_\alpha^L, x_\alpha^U] = [1+\alpha, 4-\alpha]$ and $[y_\alpha^L, y_\alpha^U] = [1+\alpha, 14-\alpha]$. Next, it is obvious that when $x = x_\alpha^U$ and $y = y_\alpha^L$, the expected number of sewage solids in the system attains its maximum value, and when $x = x_\alpha^L$

, and $y = y_{\alpha}^{U}$ the expected number of sewage solids in the system attains its minimum value.

According to (2),

The membership function for the fuzzy expected waiting time in the queue ($\tilde{W}_q$) is obtained as shown in Fig. 1. Crisp intervals for the fuzzy expected waiting time in the queue at different possibilistic α levels are given in Table 1. For the fuzzy expected waiting time $\tilde{W}_q$, the range of $\tilde{W}_q$ at $\alpha = 1$ is [0.0714, 0.0790], indicating that expected waiting time for any sewage solids definitely falls between 0.0714 and 0.0790. Moreover, the range of $\tilde{W}_q$ at $\alpha = 0$ is [0.0657, 0.0896], indicating that the expected waiting time in the queue will never exceed 0.0896 or fall below 0.0657.

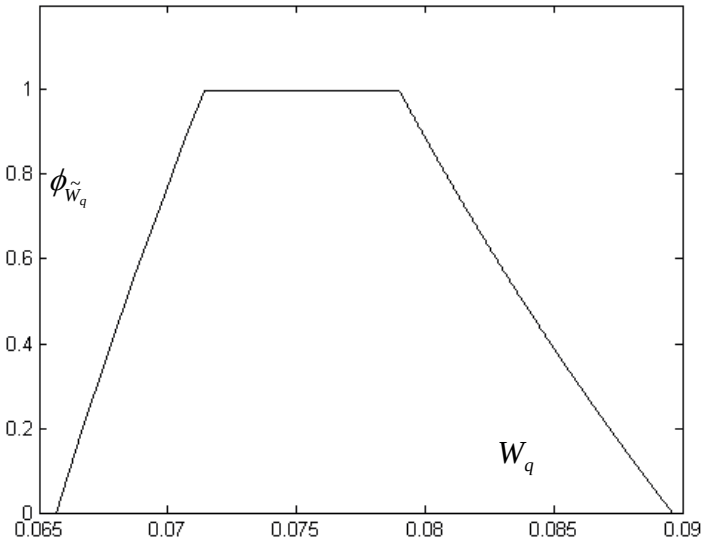

Fig. 1. The membership function for fuzzy expected waiting time in the queue

Table 1. α ***-cuts of batch-arrival and service rates and expected waiting time***

α	x_α^L	x_α^U	y_α^L	y_α^U	$(W_q)_\alpha^L$	$(W_q)_\alpha^U$
0.00	1.00	4.00	11.00	14.00	0.0657	0.0896
0.10	1.10	3.90	11.10	13.90	0.0662	0.0884
0.20	1.20	3.80	11.20	13.80	0.0667	0.0872
0.30	1.30	3.70	11.30	13.70	0.0672	0.0860
0.40	1.40	3.60	11.40	13.60	0.0678	0.0849
0.50	1.50	3.50	11.50	13.50	0.0684	0.0838
0.60	1.60	3.40	11.60	13.40	0.0689	0.0828
0.70	1.70	3.30	11.70	13.30	0.0695	0.0818
0.80	1.80	3.20	11.80	13.20	0.0701	0.0808
0.90	1.90	3.10	11.90	13.10	0.0708	0.0799
1.00	2.00	3.00	12.00	13.00	0.0714	0.0790

5. CONCLUSIONS

This paper applies the concepts of α-cuts and Zadeh's extension principle to a batch-arrival queuing system with multiple servers and constructs membership functions of the expected waiting time using paired NLP models. Following the proposed approach, α -cuts of the membership functions are found and their interval limits inverted to attain explicit closed-form expressions for the system characteristics. Even when the membership function intervals cannot be inverted, system designers or managers can specify the system characteristics of interest, perform numerical experiments to examine the corresponding α-cuts and then use this information to develop or improve system processes.

REFERENCES

[1] J. Buzacott and J. Shanthikumar, *Stochastic Models of Manufacturing Systems*, Englewood Cliffs, NJ: Prentice-Hall, 1993 .

[2] S. Chanas and M. Nowakowski, Single value simulation of fuzzy variable, *Fuzzy Sets and Systems,* 21, 43–57, 1988.

[3] X. Chao and Y. Zhao, Analysis of multiple-server queue with station and server vacation, *European Journal of Operational Research*, 110, 392-406,1998.

[4] S. P. Chen, Parametric nonlinear programming for analyzing fuzzy queues with finite capacity, *European Journal of Operational Research*, 157, 429-438, 2004.

[5] S. P. Chen, Parametric nonlinear programming approach to fuzzy queues with bulk service. *European Journal of Operational Research*, 163, 434-444, 2005.

[6] T. Gal, *Postoptimal Analysis*, *Parametric Programming*, and *Related Topics*, New York: McGraw-Hill, 1979.

[7] D. Gross, and C. M. Harris, *Fundamentals of Queueing Theory*, 3rd Ed, New-York: JohnWiley, 1998.

[8] N. Igaki, Exponential two server queue with N-policy and multiple vacations, *Queueing systems*, 10, 279-294,1992.

[9] C. Kao, C. C. Li and S. P. Chen, Parametric programming to the analysis of fuzzy queues, *Fuzzy Sets and Systems*, 107, 93–100, 1999.

[10] A. Kaufmann, *Introduction to the Theory of Fuzzy Subsets*, Volume 1, New York: Academic Press, 1975.

[11] L. Kleinrock, *Queueing Systems*, Vol. I. Theory, New York: Wiley, 1975.

[12] Y. Levy and U. Yechiali, A M/M/c queue with servers vacations, *INFOR*, 14, 153-163, 1976.

[13] R. J. Li and E. S. Lee, Analysis of fuzzy queues, *Computers and Mathematics with Applications*, 17, 1143–1147, 1989.

[14] D. S. Negi and E. S. Lee, Analysis and simulation of fuzzy queue, *Fuzzy Sets and Systems*, 46, 321–330, 1992.

[15] H. M. Prade, *An Outline of Fuzzy or Possibilistic Models for Queueing Systems*, Fuzzy Sets, Ed. P. P. Wang and S. K. Chang, New York: Plenum Press, (1980)

[16] R.E. Stanford, The set of limiting distributions for a Markov chain with fuzzy transition probabilities, *Fuzzy Sets and Systems*, 7, 71–78,1982.

[17] N. Tian, Q. Li and J. Cao, Conditional stochastic decompositions in the M/M/c queue with server vacations, *Stochastic Models*, 14(2), 367-377, 1999.

[18] N. Tian and X. Xu, M/M/c queue with synchronous multiple vacation of partial servers, *OR Transactions*, 5(3), 85-94, 2001.

[19] K. S. Trivedi, Probability and Statistics with Reliability, Queueing and Computer Science Applications. New York: John Wiley & Sons Inc, 2002.

[20] B. Vinod, Exponential queue with server vacation, *Journal of Operational Research Society*, 37, 1007-1014, 1986.

[21] R. R. Yager, A characterization of the extension principle, *Fuzzy Sets and Systems*, 18, 205–217, 1986.

[22] L. A. Zadeh, Fuzzy sets as a basis for a theory of possibility, *Fuzzy Sets and Systems*, 1, 3–28, 1978.

[23] G. Zhang and N. Tian, Analysis of queueing systems with synchronous single vacation for some servers, *Queueing systems*, 45, 161-175, 2003.

[24]. Ramesh . R and Kumaraghuru . S, Analysis of performance measures of fuzzy queuing model with an unreliable server using ranking function method, International Journal of Advances in Computer Science and Technology, (2014), October 2014, vol. 3(10), 441-445.

[25]. Ramesh . R and Kumaraghuru .S , Analysis ofPerformance in Four Non-Preemptive Priority Fuzzy Queues by Centroid of Centroids Ranking Method, International Journal of Computer Techniques, 2017 Jan – Feb, Volume 4 Issue 1, 12-20.

[26]. Ramesh .R, Hari Ganesh .A, M/M/m/m Fuzzy Loss System under Expansion Center Fuzzy Ranking Method, Journal of Applied Science and Computations, Volume VI, Issue III, March/2019, 2188-2195.

[27]. Ramesh .R, Hari Ganesh .A, M/M/1/N Fuzzy Queueing Models with Discouraged Arrivals under Wingspans Fuzzy Ranking Method, International Journal of Applied Engineering Research, Volume 14, Number 4, 2019, 1-12.

[28]. Ramesh. R, Srinivasan. R, Performance measures of two heterogeneous servers queueing models under trisectional fuzzy trapezoidal approach, Malaya Journal of Mathematik, Vol. S, No. 1, 392-396, 2020.

[29]. Ramesh. R, Seenivasan. M, Performance calibrations of a single server Glycolic acid based beauty parlour by fuzzy retrial queuing models, Materials Today: Proceedings, Vol. 51(8) Pp. 2422 – 2426 (2022).

[30]. Ramesh. R, Seenivasan. M, Achievement Expedients of Fuzzy Queuing Models with an Unreliable Electrical Transformer, IEEE EXPLORE, (ICEEICT 2022) vol. 22 pp. 978-1-6654-3647-2, **February 2022**

[31]. Ramesh. R, Seenivasan. M, Markovian Queueing System with Discouraged Arrivals by Fuzzy Ordering Approach, Mathematical Statistician and Engineering Applications, Vol 71, no: 4, 3787 – 3800(2022).

[32]. Seenivasan. M, Ramesh. R , Abinayac. R and Chandiraleka. S, Markovian Queueing Model with Multiple Working Vacation and Catastrophe, Neuroquantology June 2022 Volume 20, issue 6 Page 6302-6310(2022).

[33]. Seenivasan. M, Ramesh. R, And Particia. F, A Markovian Queueing Model With Catastrophe, Unreliable And Backup Server, Intrenational Journal of Health Sciences, Issue V(2022), Pp. 9136-9150, **2022.**

[34]. Seenivasan. M, Ramesh. R, And Particia. F, Single Server Finite Queueing Model with Catastrophe, Restoration and Partial Breakdown, Mathematical Statistician and Engineering Applications, Vol 71, no: 4, 3661 – 3685(2022).

CHAPTER 10

Analysis of Performances of Fuzzy Batch Arrival Queuing System

Seenivasan. M[1]

1. INTRODUCTION

Queueing theory takes part in an important role in real life problems. Now-a- days , we face a lot of congesting problems in the queueing habitat such as ATM points, Medical shops, Reservation centers, Ration shops, Hospitals, Making calls in Telecommunications, etc…, . Emphasize the importance of time management is the ultimate aim of the researcher. At this juncture, queueing models take a very prominent role. Queueing models are effective methods for performance analysis of computer and telecommunication systems, manufacturing/production systems and inventory control (Kleinrock [11], Buzacott and Shanthikumar [1], Gross and Harris [7], Trivedi [19]). In general, these analyses consider a queueing system where requests for service arrive in units, one at a time (single-unit arrival). In many practical situations, however, requests for service usually arrive in batches. For example, in manufacturing systems of the job-shop type, each job order often requires the manufacture of more than one unit; in computer communication systems, messages which are to be transmitted could consist of a random number of packets. If the usual crisp batch-arrival

1 Mathematics Wing - DDE, Annamalai University, Annamalai nagar, Tamilnadu, India. email: emseeni@yahoo.com

queues with multiple servers can be extended to fuzzy batch-arrival queues, such queueing models would have wider applications.

For queueing models with multiple servers under various considerations, the M/M/c vacation systems with a single-unit arrival have attracted much attention from numerous researchers since Levy and Yechiali [12]. The extensions of this model can be referred to Vinod [20], Igaki [8], Tian et al. [17], Tian and Xu [18], and Zhang and Tian [23] studied the M/M/c vacation systems with a single-unit arrival and a "partial server vacation policy". They proved several conditional stochastic decomposition results for the queue length and waiting time. Chao and Zhao [3] investigated the GI/M/c vacation models with a single-unit arrival and provided iterative algorithms for computing the stationary probability distributions.

In the literature described above, customer inter-arrival times and customer service times are required to follow certain probability distributions with fixed parameters. However, in many real-world applications, the parameter distributions may only be characterized subjectively; that is, the arrival and service are typically described in everyday language summaries of central tendency, such as "the mean arrival rate is around 5 per day", or "the mean service rate is about 10 per hour", rather than with complete probability distributions. In other words, these system parameters are both possibilistic and probabilistic. Thus, fuzzy queues are potentially much more useful and realistic than the commonly used crisp queues (see Li and Lee [13] and Zadeh [22]). By extending the usual crisp batch-arrival queues to fuzzy batch-arrival queues in the context of multiple servers, these queuing models become appropriate for a wider range of applications. Ramesh et.al [24-31] presented dissimilar queueing models. Seenivasan et. al [32-34] provided server breakdown with catastrophe, server breakdown with feed back and so many queueing models.

Li and Lee [13] investigated the analytical results for two typical fuzzy queues (denoted $M/F/1/\infty$ and $FM/FM/1/\infty$, where F represents fuzzy time and FM represents fuzzified exponential distributions) using a general approach based on Zadeh's extension principle (see also Prade [15] and Yager [21]), the possibility concept and fuzzy Markov chains (see Stanford [16]). Seenivasan et. al [31] illustrated about heterogeneous queueing system. A useful modeling and inferential technique would be applied their approach to general fuzzy queuing problems (see Stanford [16]). However, their approach is complicated and not suitable for computational purposes; moreover, it cannot easily be used to derive analytic results for other complicated queuing systems (see Negi and Lee [14]). In particular,

it is very difficult to apply this approach to fuzzy queues with more fuzzy variables or multiple servers. Negi and Lee [14] proposed a procedure using α-cuts and two-variable simulation to analyze fuzzy queues (see also Chanas and Nowakowski [2]). Unfortunately, their approach provides only crisp solutions; *i.e.*, it does not fully describe the membership functions of the system characteristics. Using parametric programming, Kao et al. [9] constructed the membership functions of the system characteristics for fuzzy queues and successfully applied them to four simple fuzzy queue models: $M/F/1/\infty$, $F/M/1/\infty$, $F/F/1/\infty$ and $FM/FM/1/\infty$. Recently, Chen [4,5] developed $FM/FM/1/L$ and $FM/FM^{[K]}/1/\infty$ fuzzy systems using the same approach. All previous researches on fuzzy queuing models are focused on ordinary queues with a single server. In this paper, we develop an approach that provides system characteristics for batch-arrival queues with multiple servers and fuzzy parameters: fuzzified exponential batch-arrival and service rates. Through α-cuts and Zadeh's extension principle, we transform the fuzzy queues to a family of crisp queues. As α varies, the family of crisp queues is described and solved using parametric nonlinear programming (NLP). The NLP solutions completely and successfully yield the membership functions of the system characteristics, including the expected number of customers in the system and the expected waiting time in the queue.

The remainder of this paper is organized as follows. Section 2 presents the system characteristics of standard and fuzzy batch-arrival queuing models with multiple servers. In Section 3, a mathematical programming approach is developed to derive the membership functions of these system characteristics. To demonstrate the validity of the proposed approach, one realistic numerical example is described and solved. Discussion is provided in Section 4, and conclusions are drawn in Section 5. For notational convenience, our model in this paper is hereafter denoted $FM^{[x]}/FM/c$.

2. FUZZY BATCH QUEUE WITH MULTIPLE SERVERS

Think about a batch arrival queuing system with c servers where the customers arrive in batches to occur according to a compound Poisson process with batch-arrival rate λ. Let A_k denote the number of customers belonging to the k^{th} arrival batch, where A_k, $k = 1, 2, 3, \cdots$, are with a common distribution $\Pr[A_k = n] = a_n, n = 1,\ 2,\ 3, \cdots$, and $E[A] = \sum_{n=1}^{\infty} n a_n$. Customers arriving at the service facility (servers) form a single-file queue and are served in order. The service time for each of all c servers is exponentially distributed with rate μ and each server can serve only one customer at a time. Customers who upon entry the service facility find that all servers are busy have to wait in the queue until any one server is available.

Let N_s and W_q represents the expected number of customers in the system and the expected waiting time in the queue, respectively. Through a Markov process, we can easily obtain N_s and W_q in terms of system parameters

$$N_s = \frac{\lambda(2E[A] + E[A(A-1)]) + 2\mu \cdot \sum_{n=0}^{c-1} n(c-n)P_n(\lambda,\mu)}{2(c\mu - \lambda E[A])}, \tag{1}$$

$$W_q = \frac{\lambda(2E[A] + E[A(A-1)]) + 2\mu \cdot \sum_{n=0}^{c-1} n(c-n)P_n(\lambda,\mu)}{2\lambda E[A](c\mu - \lambda E[A])} - \frac{1}{\mu}, \tag{2}$$

where $P_n(\lambda,\mu)$ represents the probability that there are *n* customers in the system. And the probability depends on λ and μ. In steady-state, it is necessary that we have $0 < \frac{\lambda E[A]}{c\mu} < 1$.

To extend the applicability of the batch-arrival queuing model with multiple servers, we allow for fuzzy specification of system parameters. Suppose the batch-arrival rate λ for customers and service rate μ for each server are approximately known and can be represented by the fuzzy sets $\tilde{\lambda}$ and $\tilde{\mu}$. Let $\phi_{\tilde{\lambda}}(\ )$ and $\phi_{\tilde{\mu}}(y)$ denote the membership functions of $\tilde{\lambda}$ and $\tilde{\mu}$ Then we have the following fuzzy sets:

$$\tilde{\lambda} = \left\{ (x, \phi_{\tilde{\lambda}}(x)) \ \middle| \ x \in X \right\}, \tag{3a}$$

$$\tilde{\mu} = \left\{ (y, \phi_{\tilde{\mu}}(y)) \ \middle| \ y \in Y \right\}, \tag{3b}$$

where X and Y are the crisp universal sets of the batch-arrival and service rates.

Let $f(x,y)$ denote the system characteristic of interest. Since $\tilde{\lambda}$ and $\tilde{\mu}$ are fuzzy numbers, $f(\tilde{\lambda},\tilde{\mu})$ is also a fuzzy number. Following Zadeh's extension principle (see Yager [21] and Zadeh [22]), the membership function of the system characteristic $f(\tilde{\lambda},\tilde{\mu})$ is defined as:

$$\phi_{f(\tilde{\lambda},\tilde{\mu})}(z) = \sup_{x\in X, y\in Y, 0<xE[A]/cy<1} \min\left\{ \phi_{\tilde{\lambda}}(x), \phi_{\tilde{\mu}}(y) \ \middle| \ z = f(x,y) \right\}, \tag{4}$$

Assume that the system characteristic of interest is the expected number of customers in the system. It follows from (1) that the expected number of customers in the system is:

$$f(x,y) = \frac{x(2E[A] + E[A(A-1)]) + 2y \cdot \sum_{n=0}^{c-1} n(c-n)P_n(x,y)}{2(cy - xE[A])}. \tag{5}$$

The membership function for the expected number of customers in the system is:

$$\phi_{\tilde{N}_s}(z) = \sup_{x\in X, y\in Y, 0<xE[A]/cy<1} \min\left\{\phi_{\tilde{\lambda}}(x), \phi_{\tilde{\mu}}(y) \,\middle|\, z = \frac{x(2E[A]+E[A(A-1)])+2y\cdot\sum_{n=0}^{c-1} n(c-n)P_n(x,y)}{2(cy-xE[A])}\right\}. \quad (6)$$

Unfortunately, the membership function is not expressed in the usual form, making it very difficult to imagine its shape. In this paper we approach the representation problem using a mathematical programming technique. Parametric NLPs are developed to find the α -cuts of $f(\tilde{\lambda}, \tilde{\mu})$ based on the extension principle.

3. PARAMETRIC NONLINEAR PROGRAMMING

To re-express the membership function $\phi_{\tilde{N}_s}(z)$ of $\tilde{N}_s$ in an understandable and usable form, we adopt Zadeh's approach, which relies on α -cuts of $\tilde{N}_s$. Definitions for the α -cuts of $\tilde{\lambda}$ and $\tilde{\mu}$ as crisp intervals are as follows:

$$\lambda(\alpha) = \left[x_\alpha^L, x_\alpha^U\right] = \left[\min_{x\in X}\left\{x \,\middle|\, \phi_{\tilde{\lambda}}(x) \ge \alpha\right\}, \max_{x\in X}\left\{x \,\middle|\, \phi_{\tilde{\lambda}}(x) \ge \alpha\right\}\right], \quad (7a)$$

$$\mu(\alpha) = \left[y_\alpha^L, y_\alpha^U\right] = \left[\min_{y\in Y}\left\{y \,\middle|\, \phi_{\tilde{\mu}}(y) \ge \alpha\right\}, \max_{y\in Y}\left\{y \,\middle|\, \phi_{\tilde{\mu}}(y) \ge \alpha\right\}\right], \quad (7b)$$

The constant batch-arrival and service rates are shown as intervals when the membership functions are no less than a given possibility level for α . As a result, the bounds of these intervals can be described as functions of α and can be obtained as: $x_\alpha^L = \min \phi_{\tilde{\lambda}}^{-1}\ \alpha \quad x_\alpha^U = \max \phi_{\tilde{\lambda}}^{-1}(\alpha)$, $y_\alpha^L = \min \phi_{\tilde{\mu}}^{-1}(\alpha)$, and $y_\alpha^U = \max \phi_{\tilde{\mu}}^{-1}(\alpha)$. Therefore, we can use the α -cuts of $\tilde{N}_s$ to construct its membership function since the membership function defined in (6) is parameterized by α .

Using Zadeh's extension principle, $\phi_{\tilde{N}_s}(z)$ is the minimum of $\phi_{\tilde{\lambda}}(x)$ and $\phi_{\tilde{\mu}}(y)$. To derive the membership function $\phi_{\tilde{N}_s}(z)$, we need at least one of the following cases to hold such that $z = \frac{x(2E[A]+E[A(A-1)])+2y\cdot\sum_{n=0}^{c-1} n(c-n)P_n(x,y)}{2(cy-xE[A])}$ satisfies $\phi_{\tilde{N}_s}(z) = \alpha$: Case (i): ($\phi_{\tilde{\lambda}}(x) = \alpha$, $\phi_{\tilde{\mu}}(y) \ge \alpha$),

Case (ii): ($\phi_{\tilde{\lambda}}(x) \ge \alpha$, $\phi_{\tilde{\mu}}(y) = \alpha$),

This can be accomplished using parametric NLP techniques. The NLP to find the lower and upper bounds of the α -cut of $\phi_{\tilde{N}_s}(z)$ for Case (i) are:

$$(N_s)_\alpha^{L_1} = \min \frac{x(2E[A]+E[A(A-1)])+2y\cdot\sum_{n=0}^{c-1} n(c-n)P_n(x,y)}{2(cy-xE[A])}, \quad (8a)$$

$$(N_s)_{\alpha}^{U_1} = \max \frac{x(2E[A]+E[A(A-1)])+2y\cdot\sum_{n=0}^{c-1} n(c-n)P_n(x,y)}{2(cy-xE[A])}, \tag{8b}$$

and for Case (ii) are: $(N_s)_{\alpha}^{L_2} = \min \frac{x(2E[A]+E[A(A-1)])+2y\cdot\sum_{n=0}^{c-1} n(c-n)P_n(x,y)}{2(cy-xE[A])}$, (8c)

$$(N_s)_{\alpha}^{U_2} = \max \frac{x(2E[A]+E[A(A-1)])+2y\cdot\sum_{n=0}^{c-1} n(c-n)P_n(x,y)}{2(cy-xE[A])}. \tag{8d}$$

From the definitions of $\lambda(\alpha)$ and $\mu(\alpha)$ in (7), $x \in \lambda(\alpha)$ and $y \in \mu(\alpha)$ can be replaced by $x \in [x_{\alpha}^{L}, x_{\alpha}^{U}]$ and $y \in [y_{\alpha}^{L}, y_{\alpha}^{U}]$. The α-cuts form a nested structure with respect to α (see Kaufmann [10] and Zimmermann [25]); *i.e.*, given $0 < \alpha_2 < \alpha_1 \leq 1$, we have $[x_{\alpha_1}^{L}, x_{\alpha_1}^{U}] \subseteq [x_{\alpha_2}^{L}, x_{\alpha_2}^{U}]$ and $[y_{\alpha_1}^{L}, y_{\alpha_1}^{U}] \subseteq [y_{\alpha_2}^{L}, y_{\alpha_2}^{U}]$. Therefore, (8a) and (8c) have the same smallest element and (8b) and (8d) have the same largest element. To find the membership function $\phi_{\tilde{N}_s}(z)$, it suffices to find the left and right shape functions of $\phi_{\tilde{N}_s}(z)$, which is equivalent to finding the lower bound $(N_s)_{\alpha}^{L}$ and upper bound $(N_s)_{\alpha}^{U}$ of the α-cuts of $\tilde{N}_s$, which can be rewritten as:

$$(N_s)_{\alpha}^{L} = \min \frac{x(2E[A]+E[A(A-1)])+2y\cdot\sum_{n=0}^{c-1} n(c-n)P_n(x,y)}{2(cy-xE[A])} \tag{9a}$$

s.t. $x_{\alpha}^{L} \leq x \leq x_{\alpha}^{U}$ and $y_{\alpha}^{L} \leq y \leq y_{\alpha}^{U}$,

$$(N_s)_{\alpha}^{U} = \max \frac{x(2E[A]+E[A(A-1)])+2y\cdot\sum_{n=0}^{c-1} n(c-n)P_n(x,y)}{2(cy-xE[A])} \tag{9b}$$

s.t. $x_{\alpha}^{L} \leq x \leq x_{\alpha}^{U}$ and $y_{\alpha}^{L} \leq y \leq y_{\alpha}^{U}$,

At least one of x and y must hit the boundaries of their α-cuts to satisfy $\phi_{\tilde{N}_s}(z) = \alpha$. This model is a set of mathematical programs with boundary constraints and lends itself to the systematic study of how the optimal solutions change with x_{α}^{L}, x_{α}^{U}, y_{α}^{L}, and y_{α}^{U} as α varies over $(0,1]$. The model is a special case of parametric NLPs (see Gal [6]).

The crisp interval $[(N_s)_\alpha^L, (N_s)_\alpha^U]$ obtained from (9) represents the α -cuts of $\tilde{N}_s$. Again, by applying the results of Kaufmann [10] and Zimmermann [25] and convexity properties to $\tilde{N}_s$, we have $(N_s)_{\alpha_1}^L \geq (N_s)_{\alpha_2}^L$ and $(N_s)_{\alpha_1}^U \leq (N_s)_{\alpha_2}^U$, where $0 < \alpha_2 < \alpha_1 \leq 1$. In other words, $(N_s)_\alpha^L$ increases and $(N_s)_\alpha^U$ decreases as α increases. Consequently, the membership function $\phi_{\tilde{N}_s}(z)$ can be found from (9).

If both $(N_s)_\alpha^L$ and $(N_s)_\alpha^U$ in (9) are invertible with respect to α, then a left shape function $L(z) = [(N_s)_\alpha^L]^{-1}$ and a right shape function $R(z) = [(N_s)_\alpha^U]^{-1}$ can be derived, from which the membership function $\phi_{\tilde{N}_s}(z)$ is constructed:

$$\phi_{\tilde{N}_s}(z) = \begin{cases} L(z), & (N_s)_{\alpha=0}^L \leq z \leq (N_s)_{\alpha=1}^L, \\ 1, & (N_s)_{\alpha=1}^L \leq z \leq (N_s)_{\alpha=1}^U, \\ R(z), & (N_s)_{\alpha=1}^U \leq z \leq (N_s)_{\alpha=0}^U. \end{cases} \tag{10}$$

In most cases, the values of $(N_s)_\alpha^L$ and $(N_s)_\alpha^U$ cannot be solved analytically. Consequently, a closed-form membership function for $\phi_{\tilde{N}_s}(z)$ cannot be obtained. However, the numerical solutions for $(N_s)_\alpha^L$ and $(N_s)_\alpha^U$ at different possibility levels can be collected to approximate the shapes of $L(z)$ and $R(z)$. That is, the set of intervals $\{[(N_s)_\alpha^L, (N_s)_\alpha^U] \mid \alpha \in [0,1]\}$ shows the shape of $\phi_{\tilde{N}_s}(z)$, although the exact function is not known explicitly.

Note that the membership functions for the expected waiting time in the queue can be expressed in a similar manner.

4. NUMERICAL EXAMPLE

Considering one sewerage treatment system collects sewage from the urban areas and sends them to the sewerage treatment plant. The sewerage treatment plant has three supply pipes (referred to 3-servers). Each pipe can settle the larger solids and put the settled into the chemical process tank. After the chemical process, the treated water is discharged to the sea. We assume that the number of arriving sewage solids each time follows a geometric distribution with parameter $p = 0.5$; *i.e.*, the size of arriving sewage solids A is $\Pr(A = k = \quad - \quad^{k-1} k = \quad \cdots$. Clearly, this problem can be described by FM[x]/FM/3 system. For efficiency, the management wants to get the system characteristics such as the expected number of sewage solids in the system and the expected waiting time in the queue.

Suppose the batch-arrival rate and service rate are trapezoidal fuzzy numbers represented by $\tilde{\lambda} = [1, 2, 3, 4]$ and $\tilde{\mu} = [11, 12, 13, 14]$. First, it is easy to find that $[x_\alpha^L, x_\alpha^U] = [1 + \alpha, 4 - \alpha]$ and $[y_\alpha^L, y_\alpha^U] = [1 + \alpha, 14 - \alpha]$. Next, it is obvious that when $x = x_\alpha^U$ and $y = y_\alpha^L$, the expected number of sewage solids in the system attains its maximum value, and when $x = x_\alpha^L$, and $y = y_\alpha^U$, the expected number of sewage solids in the system attains its minimum value. According to (9), the α-cuts of $\tilde{N}_s$ are:

$$(N_s)_\alpha^L = \frac{27200 + 23460\alpha - 3630\alpha^2 + 110\alpha^3}{99200 - 21000\alpha + 1275\alpha^2 - 25\alpha^3},$$

$$(N_s)_\alpha^U = \frac{67880 - 4650\alpha - 2640\alpha^2 - 110\alpha^3}{47000 + 14025\alpha + 1050\alpha^2 + 25\alpha^3}.$$

With the help of MATLAB® 7.0.4, the membership function is:

$$\phi_{\tilde{N}_s}(z) = \begin{cases} L(z), & \frac{17}{62} \le z \le \frac{4714}{7945} \\ 1, & \frac{4714}{7945} \le z \le \frac{112}{115} \\ R(z), & \frac{112}{115} \le z \le \frac{1697}{1175} \end{cases}$$

where:

$$L(z) = \frac{3(-1+\sqrt{3}i)P^{\frac{2}{3}} + 2(85z+242)P^{\frac{1}{3}} - 3(1+\sqrt{3}i)(25z^2+280z+2684)}{2(5z+22)P^{\frac{1}{3}}},$$

$$R(z) = \frac{3Q^{\frac{2}{3}} - 2(35z+88)Q^{\frac{1}{3}} + 3(25z^2+280z+2684)}{(5z+22)Q^{\frac{1}{3}}},$$

with:

$$P = -1125z^3 - 3900z^2 + 27060z + 13552 + (50z+220)\sqrt{500z^4 - 1100z^3 - 22635z^2 + 69988z - 395692},$$

$$P = -1125z^3 - 3900z^2 + 27060z + 13552 + (50z+220)\sqrt{500z^4 - 1100z^3 - 22635z^2 + 69988z - 395692},$$

as shown in Fig. 1. The overall shape turns out as expected. The membership functions $L(z)$ and $R(z)$ have complex values with their imaginary parts approaching zero when $\frac{17}{62} \le z \le \frac{4714}{7945}$ for $L(z)$ and $\frac{112}{115} \le z \le \frac{1697}{1175}$ for $R(z)$. Hence, the imaginary parts of these two functions have no influence on the computational results and can be disregarded.

Next, we perform α-cuts of batch-arrival and service rates and fuzzy expected number of sewage solids in the system at eleven distinct α values: 0, 0.1, …, 1. Crisp intervals for fuzzy expected number of sewage solids in the system at different possibilistic α levels are presented in Table 1. The fuzzy expected number of sewage solids in the system $\tilde{N}_s$ has two characteristics to be noted. First, the support of $\tilde{N}_s$ ranges from 0.2742 to 1.4443; this indicates that, though the expected number of sewage solids in the system is fuzzy, it is impossible for its values to fall below 0.2742 or exceed 1.4443. Second, the α-cut at $\alpha = 1$ contains the values from 0.5933 to 0.9739, which are the most possible values for the fuzzy expected number of sewage solids in the system.

Table 1. α ***-cuts of batch-arrival and service rates and expected number of sewage solids in the system.***

α	x_α^L	x_α^U	y_α^L	y_α^U	$(N_s)_\alpha^L$	$(N_s)_\alpha^U$
0.00	1.00	4.00	11.00	14.00	0.2742	1.4443
0.10	1.10	3.90	11.10	13.90	0.3039	1.3919
0.20	1.20	3.80	11.20	13.80	0.3340	1.3410
0.30	1.30	3.70	11.30	13.70	0.3646	1.2912
0.40	1.40	3.60	11.40	13.60	0.3957	1.2427
0.50	1.50	3.50	11.50	13.50	0.4273	1.1953
0.60	1.60	3.40	11.60	13.40	0.4594	1.1491
0.70	1.70	3.30	11.70	13.30	0.4920	1.1038
0.80	1.80	3.20	11.80	13.20	0.5252	1.0596
0.90	1.90	3.10	11.90	13.10	0.5590	1.0163
1.00	2.00	3.00	12.00	13.00	0.5933	0.9739

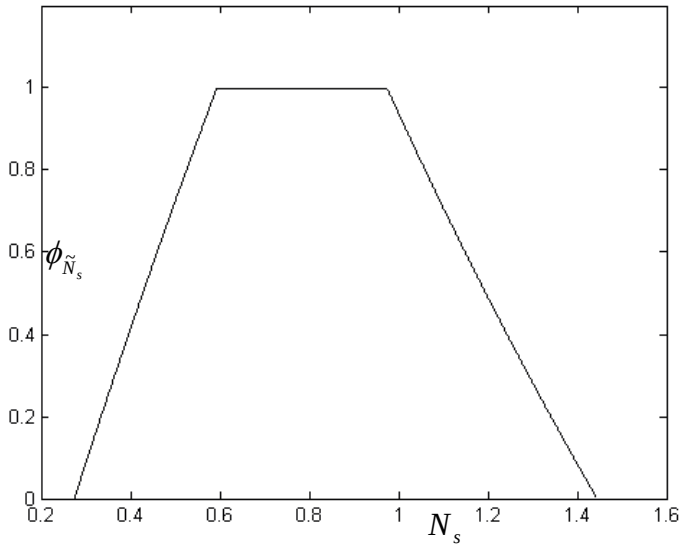

Fig. 1. The membership function for fuzzy expected number of sewage solids in the system.

5. CONCLUSIONS

We applied the concepts of α -cuts and Zadeh's extension principle to a fuzzy batch-arrival queuing system and constructs membership functions of the expected number of customers using paired NLP models. Following the proposed approach, α -cuts of the membership functions are found and their interval limits inverted to attain explicit closed-form expressions for the system characteristics. Even when the membership function intervals cannot be inverted, system designers or managers can specify the system characteristics of interest perform numerical example to examine the corresponding α -cuts.

REFERENCES

[1] J. Buzacott and J. Shanthikumar, *Stochastic Models of Manufacturing Systems*, Englewood Cliffs, NJ: Prentice-Hall, 1993 .

[2] S. Chanas and M. Nowakowski, Single value simulation of fuzzy variable, *Fuzzy Sets and Systems,* 21, 43–57, 1988.

[3] X. Chao and Y. Zhao, Analysis of multiple-server queue with station and server vacation, *European Journal of Operational Research*, 110, 392-406,1998.

[4] S. P. Chen, Parametric nonlinear programming for analyzing fuzzy queues with finite capacity, *European Journal of Operational Research*, 157, 429-438, 2004.

[5] S. P. Chen, Parametric nonlinear programming approach to fuzzy queues with bulk service. *European Journal of Operational Research*, 163, 434-444, 2005.

[6] T. Gal, *Postoptimal Analysis*, *Parametric Programming*, and *Related Topics*, New York: McGraw-Hill, 1979.

[7] D. Gross, and C. M. Harris, *Fundamentals of Queueing Theory*, 3rd Ed, New-York: JohnWiley, 1998.

[8] N. Igaki, Exponential two server queue with N-policy and multiple vacations, *Queueing systems*, 10, 279-294,1992.

[9] C. Kao, C. C. Li and S. P. Chen, Parametric programming to the analysis of fuzzy queues, *Fuzzy Sets and Systems*, 107, 93–100, 1999.

[10] A. Kaufmann, *Introduction to the Theory of Fuzzy Subsets*, Volume 1, New York: Academic Press, 1975.

[11] L. Kleinrock, *Queueing Systems*, Vol. I. Theory, New York: Wiley, 1975.

[12] Y. Levy and U. Yechiali, A M/M/c queue with servers vacations, *INFOR*, 14, 153-163, 1976.

[13] R. J. Li and E. S. Lee, Analysis of fuzzy queues, *Computers and Mathematics with Applications*, 17, 1143–1147, 1989.

[14] D. S. Negi and E. S. Lee, Analysis and simulation of fuzzy queue, *Fuzzy Sets and Systems*, 46, 321–330, 1992.

[15] H. M. Prade, *An Outline of Fuzzy or Possibilistic Models for Queueing Systems*, Fuzzy Sets, Ed. P. P. Wang and S. K. Chang, New York: Plenum Press, (1980)

[16] R.E. Stanford, The set of limiting distributions for a Markov chain with fuzzy transition probabilities, *Fuzzy Sets and Systems*, 7, 71–78,1982.

[17] N. Tian, Q. Li and J. Cao, Conditional stochastic decompositions in the M/M/c queue with server vacations, *Stochastic Models*, 14(2), 367-377, 1999.

[18] N. Tian and X. Xu, M/M/c queue with synchronous multiple vacation of partial servers, *OR Transactions*, 5(3), 85-94, 2001.

[19] K. S. Trivedi, Probability and Statistics with Reliability, Queueing and Computer Science Applications. New York: John Wiley & Sons Inc, 2002.

[20] B. Vinod, Exponential queue with server vacation, *Journal of Operational Research Society*, 37, 1007-1014, 1986.

[21] R. R. Yager, A characterization of the extension principle, *Fuzzy Sets and Systems*, 18, 205–217, 1986.

[22] L. A. Zadeh, Fuzzy sets as a basis for a theory of possibility, *Fuzzy Sets and Systems*, 1, 3–28, 1978.

[23] G. Zhang and N. Tian, Analysis of queueing systems with synchronous single vacation for some servers, *Queueing systems*, 45, 161-175, 2003.

[24]. Ramesh . R and Kumaraghuru . S, Analysis of performance measures of fuzzy queuing model with an unreliable server using ranking function method, International Journal of Advances in Computer Science and Technology, (2014), October 2014, vol. 3(10), 441-445.

[25]. Ramesh . R and Kumaraghuru .S , Analysis ofPerformance in Four Non-Preemptive Priority Fuzzy Queues by Centroid of Centroids Ranking Method, International Journal of Computer Techniques, 2017 Jan – Feb, Volume 4 Issue 1, 12-20.

[26]. Ramesh .R, Hari Ganesh .A, M/M/m/m Fuzzy Loss System under Expansion Center Fuzzy Ranking Method, Journal of Applied Science and Computations, Volume VI, Issue III, March/2019, 2188-2195.

[27]. Ramesh .R, Hari Ganesh .A, M/M/1/N Fuzzy Queueing Models with Discouraged Arrivals under Wingspans Fuzzy Ranking Method, International Journal of Applied Engineering Research, Volume 14, Number 4, 2019, 1-12.

[28]. Ramesh. R, Srinivasan. R, Performance measures of two heterogeneous servers queueing models under trisectional fuzzy trapezoidal approach, Malaya Journal of Mathematik, Vol. S, No. 1, 392-396, 2020.

[29]. Ramesh. R, Seenivasan. M, Performance calibrations of a single server Glycolic acid based beauty parlour by fuzzy retrial queuing models, Materials Today: Proceedings, Vol. 51(8) Pp. 2422 – 2426 (2022).

[30]. Ramesh. R, Seenivasan. M, Achievement Expedients of Fuzzy Queuing Models with an Unreliable Electrical Transformer, IEEE EXPLORE, (ICEEICT 2022) vol. 22 pp. 978-1-6654-3647-2, February 2022

[31]. Ramesh. R, Seenivasan. M, Markovian Queueing System with Discouraged Arrivals by Fuzzy Ordering Approach, Mathematical Statistician and Engineering Applications, Vol 71, no: 4, 3787 – 3800(2022).

[32]. Seenivasan. M, Ramesh. R , Abinayac. R and Chandiraleka. S, Markovian Queueing Model with Multiple Working Vacation and Catastrophe, Neuroquantology June 2022 Volume 20, issue 6 Page 6302-6310(2022).

[33]. Seenivasan. M, Ramesh. R, And Particia. F, A Markovian Queueing Model With Catastrophe, Unreliable And Backup Server, Intrenational Journal of Health Sciences, Issue V(2022), Pp. 9136-9150, 2022.

[34]. Seenivasan. M, Ramesh. R, And Particia. F, Single Server Finite Queueing Model with Catastrophe, Restoration and Partial Breakdown, Mathematical Statistician and Engineering Applications, Vol 71, no: 4, 3661 – 3685(2022).

CHAPTER 11

Renewable Energy Sources and Energy Storage

Muhammet Raşit SANCAR[1]

INTRODUCTION

The energy sector in the world is undergoing great changes and energy transformation is the key point of the technical, economic and political agenda of all countries of the world. One of the first talks globally to overcome the problems at this key point started with the acceptance of the Paris climate agreement in 2015. 195 countries around the world have made a commitment to prevent the increase in global average temperature levels. In accordance with this treaty, all countries have turned to new energy sources to reduce CO2 emissions. The reason for this is the rapid increase in the world's energy demand and this demand is primarily provided by fossil energy sources. Due to the limited availability of fossil fuels and their negative effects on the environment, a significant change in energy systems and new approaches are needed to meet the increasing global energy demand without harming the environment, society, economy and the welfare of the future population. In order to reduce and eliminate these negative effects, the use of renewable energy sources should be increased and the available energy should be used efficiently.

1 Isparta University of Applied Sciences, Institute of Postgraduate Education, Energy Systems Engineering, Isparta, Turkiye, ORCID Code: (0000-0002-4488-8393), d1840640001@isparta.edu.tr. Muhammet Raşit SANCAR is a priority field researcher of YÖK 100/2000.

RENEWABLE ENERGY SOURCES

Hydroelectic Energy

Hydroelectric energy is among the most widely used renewable energy sources. In hydroelectric power plants, electricity is produced by utilizing the power of flowing water. Hydroelectric energy is divided into two as dam and river. Water is accumulated in the dams and then the kinetic energy of the water is utilized as a result of transferring the water from the high position to the low position. On the other hand, the kinetic energy of the water is used directly in the stream type ones. The capacity of this energy changes according to climatic conditions.

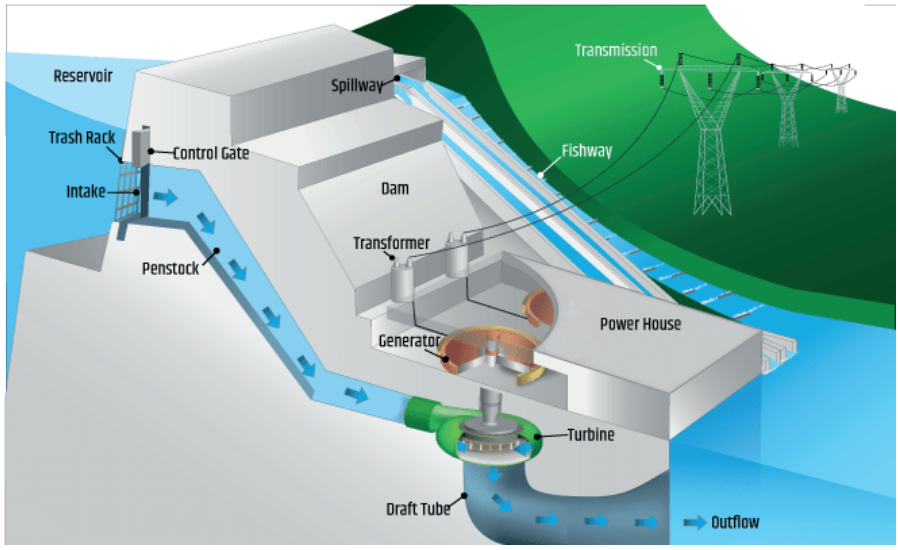

Figure 1. Hydroelectric Power Plant

Wind Energy

Wind is the movement of air caused by temperature and pressure differences in the air. Wind energy is the energy of the air flow. Mechanical systems are needed to use wind energy in electrical power generation. These systems are called wind turbines. These systems first convert wind energy into mechanical energy and then into electrical energy. A wind turbine has more than 1000 components (Olabi, 2021). These components are examined under five main headings. These are the blades, the foundation, the engine compartment, the tower and the generator (Wind Turbine, 2022). The kinetic energy of the wind is converted into mechanical energy in the rotor.

The rotational movement of the rotor shaft is accelerated and transferred to the generator in the body. The electrical energy obtained from the generator is stored by batteries or delivered directly to the buyers (Elibüyük, 2014). Wind turbines are classified in 3 main groups as horizontal axis, vertical axis and inclined axis. Horizontal axis wind turbine is most commonly used.

Figure 2. Horizontal axis and vertical axis wind turbines (Wind Power, 2022)

Solar energy

Solar energy is the source of life, unlimited and one of the best energy solutions that does not cause environmental pollution. Solar energy usage technology is increasing, progressing and becoming economical day by day. Solar energy comes to the world in the form of electromagnetic waves consisting of photons. The amount of solar radiation coming to the earth's surface depends on the region where it comes from, temporal and meteorological, etc. It reaches different amounts depending on many factors (Redweik, 2013).

An accurate estimation of the hourly, daily, weekly, monthly or annual amount of global solar radiation reaching the Earth's surface is of great importance while developing solar energy sources and technology and determining the appropriate locations where this technology will be used. It is predicted that determining suitable places for solar panel placement will provide benefits not only environmentally, but also economically by analyzing the energy production potential, existing transmission system and solar energy market, considering environmentally sensitive areas and land accessibility (Gastli, 2010).

One of the most important usage areas of solar energy is to generate electrical energy from this energy. Solar cells are used to convert this energy into electrical energy. Solar cells work on the principle of photovoltaic operation. This principle is based on semiconductor technology. These cells enable the direct conversion of solar energy into electricity using crystalline silicon or semiconductors made of different materials. Solar panels are formed by connecting solar cells in parallel and in series. Solar panels are mono and poly crystalline silicon, CdTe, bifacial, halfcut etc. It is produced and used according to its material, structure and technology. Concentrated Solar Energy (CSP) Technology is based on concentrating solar radiation into a small area using lenses and mirrors. Solar energy can also be used as a heat source in a conventional power plant (Muneer, 2011). In this field, 4 common technologies are used as parabolic chute, bowl mixers, concentrated linear Fresnel reflector and solar tower. This classification is based on different techniques used to track and focus solar radiation; however, they are close to each other in basic principle (Muneer, 2011).

Figure 3. Solar panels (Solar Energy, 2022).

Biomass Energy

Biomass refers to the mass of living organisms, including animals, microorganisms and plants, or, in biochemical terms, protein, cellulose, sugar and fats. It also includes above-ground and underground parts of plants such as branches, trunks and tree roots. Many plants such as sugarcane, corn, flaxseed, soybean can be grown to obtain biomass. Biomass is a comprehensive term for all substances of biological origin.

All natural substances of vegetable or animal origin, the main components of which are carbohydrates, are biomass energy sources, and the energy obtained from these sources is called biomass energy. Biomass energy has been used by human beings for many years. It continues to be used on a small scale as a fuel in stoves and stoves, primarily used for domestic purposes, in developing countries. In modern countries with advanced technology, it is known that in larger scale cogeneration systems, electricity generation and the waste heat generated are used for heating purposes. In transportation, biofuels are used as an alternative to fossil fuels such as gasoline, diesel and LPG. The share of biomass energy in renewable energy sources continues to increase day by day. It is foreseen that the development and regular management of biomass use and conversion technology will provide many advantages. Some of these are given below.

Potential to replace fossil fuels

To be able to meet the deficit in energy supply to a large extent,

Causes a significant reduction in greenhouse gas emissions

Being easily accessible as a local resource and reducing energy security problems during importation like fossil fuels

It has many advantages such as contributing to the economy of the rural area and social effects.

Figure 4. Biomass power plant (Energy Power Plant, 2022).

Geothermal energy

Geothermal energy is called steam or hot water energy, which is formed by the effect of heat in the core of the earth at certain depths of the earth's crust. This type of energy will not lose its feature of being a renewable energy source and its sustainability as long as the geological conditions are not deteriorated due to the fact that the sources that provide the formation of geothermal energy are the fluids on the earth and they constantly feed the underground reservoirs. This thermal energy is stored in rocks and fluids at the center of the earth. Due to the high temperature difference between the earth's core and the earth's crust, there is a continuous flow of thermal energy from the core to the earth. Geothermal energy is classified in three ways as low (20-70 °C), medium (70-150 °C) and high temperature (>150 °C). It is used in different areas according to temperature values. While it is generally used in areas such as heating, cooling and industrial sectors in areas where low and medium temperature geothermal energy is present, it is used in electricity power generation plants in high temperature energy regions. It has many advantages because it is a renewable, sustainable, clean, cheap and natural resource.

Figure 5. Geothermal power plant (Renewable Energy, 2022).

Wave energy

Wave energy is actually an intense form of solar energy produced by the action of the wind blowing on the ocean surface. When the sun's rays

warm the earth's atmosphere, a temperature difference occurs between the air masses and the air moves from the warmer regions to the colder regions, causing the formation of winds. Waves occur as a result of the wind transferring some of its energy to the water as it blows from the surface of the ocean or sea. In fact, it can also be seen as a large energy storage collector transferred to the oceans by the sun, along with the waves carrying the kinetic energy transferred across the surface of the oceans." Wave energy is one of the other types of renewable energy that can be used for electricity generation. Wave energy is captured by equipment placed on the surface of the oceans and this mechanical energy is converted into electrical energy. Thus, waves appear to be a form of energy, not a body of water moving across the ocean surface. One of the most important features of this type of energy is that they can travel long distances in open oceans with very little energy loss. As they approach the coastal area, their speed may slow down depending on the depth of the water, but their size increases. Therefore, waves hitting the shoreline release a very high amount of kinetic energy. Wave energy varies depending on geographical location, season, wind strength and duration.

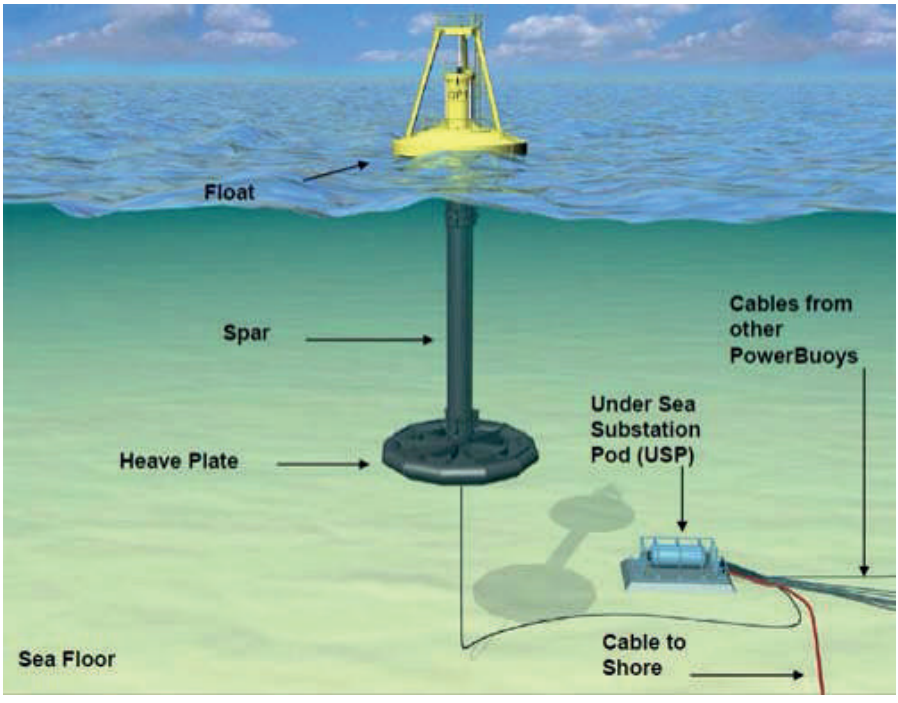

Figure 6. Wave energy converter (OPT, 2022).

Energy storage

Due to the intermittent nature of Renewable Energy systems, studies are carried out on different methods to ensure sustainability. One of the most important of these studies is the storage of energy. In order to increase the life and efficiency of power systems, there is a need for energy storage in a primary or secondary form to transfer excess demand energy to more suitable future times.

Energy storage systems can be examined under three general headings: electromagnetic, mechanical and electrochemical storage. Mechanical energy storage technologies include compressed air energy storage, Flywheels and hydro pump energy storage. Electrochemical energy storage technologies include battery and hydrogen-based energy storage systems. Electromagnetic energy storage technologies consist of super capacitors and superconducting magnetic energy storage systems. Energy storage systems can meet energy needs in a wide range of time, ranging from a few seconds to a few days. A schematic representation of energy storage systems is given in Figure 7.

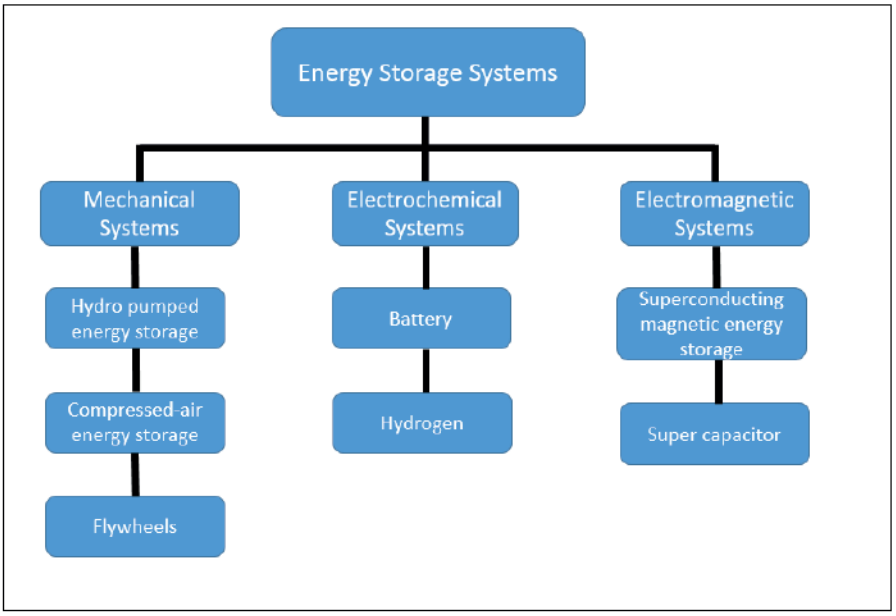

Figure 7. Schematic representation of energy storage systems

There have been many different energy storage systems on the market for many years, and technological improvement studies continue. There are many reasons why energy storage technologies are unique and used in smart

renewable energy systems. The prominence of this technology is its synergy with new processes in energy planning, its use for specific purposes and its combinations with energy resources.

Despite the positive effects of the integration of storage systems into renewable energy systems, its problems reduce its economic viability in current market conditions due to its high cost and increasing the cost of switching to renewable energy sources.

CONCLUSION

The interest in renewable energy has increased in recent years due to the fact that the reserves of fossil fuels are about to run out and the damage it causes to the environment. Studies on energy production technology from renewable sources continue. In this study, the definitions of renewable energy and storage systems are made and their technologies are mentioned. It is aimed to be a short and concise source of information for those who want to study and research in this field.

REFERENCES

Elibüyük U., Üçgül, İ., 2014. Rüzgar Türbinleri, Çeşitleri Ve Rüzgar Enerjisi Depolama Yöntemleri, SDÜ Yekarum e-Dergi, 2, 3, 1–14.

Energy Power Plant, Available at: https://www.tpc.com.tr/otomasyon/ [05.12.2022].

Gastli, A., Charabi, Y., 2010. Solar electricity prospects in Oman using GIS-based solar radiation maps, Renewable Sustainable Energy Review, 14, 2, 790–797.

Hydropower Plants, Available at: https://www.energy.gov/eere/water/types-hydropower-plants [01.12.2022]

Muneer, W., 2011. Large-Scale Solar PV Investment Planning Studies, Energy, no. January 2011.

Olabi A. G. et al., 2021. A review on failure modes of wind turbine components, Energies, 14, 17.

OPT WEC, Available at: http://nenmore.blogspot.ca/2010/04/doe-grant-for-wave-energy-project.html [01.12.2022]

Redweik, P., Catita, C., Brito, M., 2013. Solar energy potential on roofs and facades in an urban landscape, Solar Energy, 97, 332–341.

Renewable Energy, Available at: https://www.risingenerji.com.tr/projeler [12.12.2022].

Solar Energy, Available at: https://list.solar/news/hungary-opens/ [10.12.2022].

Wind Power, Available at: https://ca.audubon.org/conservation/wind-power [08.07.2022].

Wind Turbine, Available at: https://www.airpes.com/wind-turbine-parts [12.12.2022].

CHAPTER 12

Green Synthesis of Nanoparticles and Their Applications

Ebru KARATAŞ[1]

Fehiman ÇİNER[2]

INTRODUCTION

Nanotechnology is an emerging technology that can revolutionize different scientific fields (Fakhari et al., 2019). The subject of nanotechnology was mentioned for the first time in 1959 at the annual meeting of the American Physical Society (APS) by Richard Feynman with his speech "There is Plenty of Room at the Bottom" and this speech became a source of inspiration for nanotechnology (Güven, 2022). Professor Norio Taniguchi of Tokyo University of Science has very well defined the term "nanotechnology" with the phrase "Nanotechnology deals with the processing of separation, assembly and deformation of materials by an atom or a molecule". In his words, nanotechnology deals with the branch of science of manipulating matter on an atomic or molecular scale.

1 Niğde Ömer Halisdemir University, Ulukışla Vocational School, Department of Environmental Cleaning Services, NİĞDE, TÜRKİYE, ORCID ID: 0000-0002-5780-20993, ek252725@gmail.com

2 Niğde Ömer Halisdemir University, Faculty of Engineering, Department of Environmental Engineering, NİĞDE, TÜRKİYE, ORCID ID: 0000-0002-9684-4392, fciner@ohu.edu.tr, fciner51@gmail.com

Nanotechnology allows the production and manipulation of minute objects that measure as little as one billionth of a meter (the nanometer). Nanotechnology got started in the early 1980s with the appearance of a new type of microscope (atomic force microscope), that allowed not only the observation of atomic and moleculer units, but also their physical manipulation and the relative scale of comparison as shown in Figure 1 (Brar et al., 2010). Nanomaterials are structures that are smaller than 100 nm, have a large surface area, and show various physical and chemical properties (Yakut and Karataş, 2021) and they have a remarkable difference in properties compared to the same material in bulk. These differences lie in the physical and structural properties of the element's atoms, molecules and bulk materials due to the difference in physicochemical properties and surface/volume ratio. With the advancement in nanotechnology, many nanomaterials with unique properties are emerging, opening up the range of applications and research opportunities (Srikar et al., 2016).

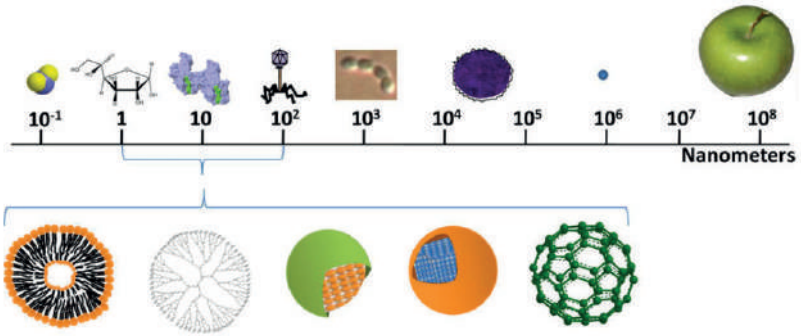

Figure 1. Comparison of nanoparticles with macroscale particles (Brar at al., 2010).

Nanotechnology is used in many fields such as optics, electronics, biomedical science, mechanics, drug-gene delivery, chemical industry, optoelectronic devices, nonlinear optical devices, catalysis, space industries, energy science and plays a critical role in many important technologies through nanoparticles (Jadoun et al., 2021). The field of nanotechnology is the most dynamic field of research in materials science and the synthesis of nanoparticles (NPs) is increasing significantly all over the world (Rafique et al., 2017).

NPs display completely new or improved properties, taking into account certain properties such as shape and structure (Rafique et al., 2017). Inorganic NPs; semiconductor NPs (such as ZnO, ZnS, CdS), metallic NPs

(such as Au, Ag, Cu, Al) and magnetic NPs (such as Co, Fe, Ni), while organic NPs contain carbon NPs (such as fullerenes) (Rafique et al., 2017). With the development of nanotechnology, interest in the synthesis and characterization of metal nanoparticles has increased in recent years.

Two methods called "top-down" and "bottom-up" are used in the synthesis of NPs. The synthesis of nanomaterials via top-down and bottom-up approaches are given in Figure 2. The top-down method is based on the principle of reducing large-size materials to nano-size by chemical or mechanical interventions. In contrast to the physical top-down method, which is based on chemical reactions, in the bottom-up method, the process of growing atoms or molecules with a number of chemical reactions takes place (Şimşek, 2015).

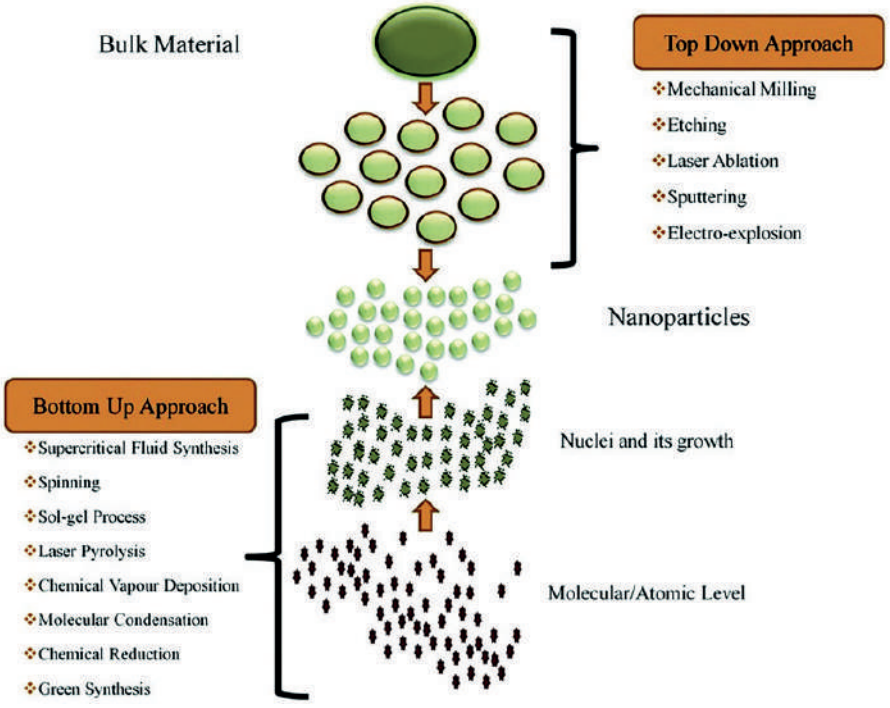

Figure 2. Approaches used in NPs production (Baig et al., 2021)

NPs can be produced by many methods such as chemical reduction, physicochemical reduction, photochemical reduction, electrochemical reduction, radiolysis and heat evaporation (Hatipoğlu, 2021). The use of NPs has increased in many areas with the increase of researches on NPs and obtaining efficient results. Especially in the field of engineering, the

use of these materials is frequently encountered (Yakut and Karataş, 2021). Nowadays, it is more preferred to produce nanoparticles with low-cost "green synthesis" procedures that do not pollute the environment, do not use toxic solvents, instead of traditional methods. In this context, scientific studies have focused on synthesizing these nanoparticles from biomaterials such as plants, bacteria, fungi, algae and viruses (Hatipoğlu, 2021).

SYNTHESIS METHODS OF NANOPARTICLES AND ITS APPLICATIONS

The synthesis of NPs is carried out by three methods. These are chemical, physical and biological methods (Umaz and Koç, 2019). Most chemical methods use toxic chemicals and often produce non-polar organic solutions and non-environmentally friendly by-products. In addition, physical and chemical methods are not preferred much because of their excessive power consumption, high cost and requiring the use of various devices (Baykal, 2022). Synthesis of NPs by biological method is superior to physical and chemical methods due to its low cost, process simplicity, less chemical use, less energy requirement and environmentally friendly (Umaz and Koç, 2019).

Recently, many approaches have been developed with the biological synthesis method to synthesize different NPs (Umaz and Koç, 2019). The synthesis of NPs is generally carried out by two different synthesis methods, the bottom-up approach and the top-down approach (Gour and Jain, 2019). In the top-down approach, synthesis methods such as suitable bulk material, grinding, sputtering, thermal/laser ablation (Gour and Jain, 2019; Jadoun et al., 2021), mechanochemical synthesis method, and electron beam lithography (Baykal, 2022) are used (Gour and Jain, 2022). 2019; Jadoun et al., 2021). It is based on the principle that larger molecules decompose into smaller units and then these units are converted into suitable NPs by physical methods. Ag, Au, PbS and fullerene nanoparticles are synthesized using this technique. Mechanical grinding is associated with the synthesis of fine particles and powders by providing pressure and friction to bulk materials. Sputtering is used for nanostructured material synthesis of the surface atoms of the evaporated material. The laser ablation method is used to synthesize NPs with narrow size distribution with laser beam pulses. The mechanochemical method is based on the synthesis of NPs using a ball mill and a reducing agent at room temperature. Electron beam lithography is a method used for synthesizing nanometer scale patterns and synthesizing 3-D micro and nano structures. These methods are simple and have the advantage of bulk synthesis of NPs. However, the biggest disadvantages of these approaches are that they are a costly and slow technique and negatively affect the surface structure due to crystallographic damage (Baykal, 2022).

In the bottom-up approach, atoms or molecules are synthesized into nanoscales by self-assembly using chemical and biological methods (Gour and Jain, 2019; Jadoun et al., 2021). Chemical and biological synthesis methods such as sol gel, green synthesis, chemical reduction and laser pyrolysis are considered bottom-up synthesis of NPs. The laser pyrolysis method is based on the synthesis of small sized nanoparticles with rapid heating and cooling using a powerful laser beam in some noble gas environment. The physical vapor deposition method focuses on synthesizing gas phase nanostructures by heating the main bulk material using an electron beam. The chemical vapor deposition method is used for the synthesis of highly pure nanostructural thin films with high performance at high temperatures, while the sol-gel method is used for the synthesis of nanomaterials with magnetic or optical properties. Synthesis by chemical reduction is an oxidation-reduction reaction. The microemulsion method is based on the use of oil-water and water-oil inorganic phases in the homogeneous and size-controlled synthesis of metal NPs. The biggest advantages of these methods are the synthesis of large amounts of homogeneous NPs in a short time and the controllable particle size and morphology. Low synthesis rate, high energy consumption, use of toxic materials and being expensive are the disadvantages of these synthesis methods (Baykal, 2022).

NPs are used in a wide variety of applications due to their physicochemical properties. These applications include medical, biomedical, environmental, agriculture, catalysis, textile, electronics, transportation and other fields. Nano-sized inorganic NPs are frequently used in the development of new nanodevices that can be used in biomedical and pharmaceutical applications thanks to their physical and chemical properties. With the help of nanomaterials, early diagnosis, prevention and appropriate treatment of diseases is possible. Carbon nanotubes (CNT) have been developed as biosensors in the medical field, in the diagnosis of cancer disease, lipid and polymer-based NPs in drug delivery systems, ironoxide NPs in applications such as magnetic resonance imaging (MRI) and drug delivery, AgNPs are used in wound healing due to their antimicrobial activities. It is increasingly used in dressings, catheters, various household products. NPs is widely used in energy production and storage, photocatalytic applications due to its large surface areas, optical behavior and catalytic structures. Carbon nanotube fuel cells are used in electric cars, semiconductor nanomaterials in the form of miniature chips in the electronics industry, nano-structured fillers are used as electrical insulators in high voltage lines, and in thermoelectricity using nano-structured layer systems. The applications of nanotechnology in the field of environment, by addressing issues such as water and soil

treatment processes, energy storage; It includes sustainable products that do not harm the environment, remediation of materials contaminated with hazardous substances, and the development of sensors for the detection of environmental pollutants. Nanotechnological devices and tools such as nanocapsules, nanoparticles and viral capsids are used in water treatment processes, CNTs, iron oxide and titanium dioxide nanomaterials are used in the removal of many pollutants from water such as heavy metals, organic compounds, pharmaceuticals, personal care products due to their high surface areas. As adsorbent material, titanium dioxide nanoparticles are used as nano membranes to prevent air pollution. Noble metal nanoparticles, magnetic nanoparticles and CNTs are also used in the detection of pollutants, thanks to their wide absorption spectra (Baykal, 2022).

With the help of smart sensors developed with biotechnology, the productivity in this process can be increased by destroying viruses and pathogens that negatively affect the growth and development of plants in agricultural studies. Nanotechnology is used in many fields as well as in the field of food. Studies in this field provide benefits in many areas such as developing and producing food products, increasing nutritional values, detecting microorganisms, measuring food quality. As a field of application, when smart packaging is observed rather than traditional methods in the packaging of food products, it can provide convenience in many criteria such as food safety, shelf life, signs of deterioration. One of the other disciplines that nanotechnology is interested in is veterinary medicine. Making animal feed more efficient, increasing its positive effects on herd health and reproduction are among the studies carried out. While nanotechnology increases the performance of products that can be used in the military field, it reduces their size and enables the production of lighter, longer-lasting and high-strength materials. With its video camera options (unmanned aerial vehicles, etc.), it provides surveillance superiority and at the same time, it can provide superiority in the field of defense by facilitating the detection of harmful and radioactive gases by nano-detectors. Developed to protect from the harmful rays of the sun, sunscreens are an indispensable cosmetic product with their zinc oxide nanoparticles up to 20 nm in size, while preventing the damage of ultraviolet rays and reflecting all other colors. Nanocapsules, which can be produced due to their nano properties, are used in the production of anti-wrinkle creams, allowing them to reach the depths of the skin, and this feature can increase the preferability of zinc oxide nanoparticles. Nanomaterials, which have a wide use in textile products, serve the field of materials that provide longer- lasting use by adding or developing new features to the products (Gençay, 2022).

GREEN SYNTHESIS AND APPLICATIONS

Conventional methods for the production of nanoparticles are not expensive, toxic and environmentally friendly. To overcome these problems, researchers have found naturally occurring sources and their products that can be used for green synthesis, that is, the synthesis of NPs (Rafique et al., 2017). The presented biological method as an alternative to chemical and physical methods provides an environmentally friendly way to synthesize NPs. Moreover, this method does not require expensive, harmful and toxic chemicals. Thanks to green synthesis, which has been actively used in recent years, metallic nanoparticles with various shapes, sizes, contents and physicochemical properties can be synthesized. Green synthesis can be done in one step using biological organisms (Nadaroğlu et al., 2017). Green synthesis of NPs is carried out using different biomaterials such as bacteria, fungi, yeast, algae, plant and virus DNA (Rafique et al., 2017). Molecules such as proteins, enzymes, phenolic compounds, amines, alkaloids and pigments found in plants and microorganisms are reduced and synthesize nanoparticles (Nadaroğlu et al., 2017).

The three most important conditions for the synthesis of NPs are the choice of a green or environmentally friendly solvent, a good reducing agent, and a harmless material for stabilization (Jadoun et al., 2021). In traditional chemical and physical methods; Reducing agents involved in the reduction of metal ions and stabilizing agents used to prevent unwanted aggregation of the produced nanoparticles carry a risk of toxicity for the environment and the cell. In addition, the contents of the produced nanoparticles are thought to be toxic in terms of shape, size and surface chemistry. In the green synthesis method, where biocompatible nanoparticles are produced, these substances are naturally present in the biological organisms used (Nadaroğlu et al., 2017). Copper (Cu) and copper oxide (CuO), zinc oxide (ZnO), cerium oxide (CeO2), cadmium sulfide (CdS), silver (Ag) and gold (Au), iron (Fe) and their oxides synthesized by green synthesis, cadmium sulfide (CdS), palladium (Pd), lead sulfide (PbS), ruthenium (Ru), and titanium dioxide TiO_2 NPs have important roles in human well-being (Gour and Jain, 2019).

Green synthesis offers areas with effective applications from traditional chemical techniques to medical and environmental technologies (Ahmad et al., 2019). The use of metal NPs in fields such as biomedical, pharmaceutical, medicine, agriculture, environment and energy is increasing day by day (Çiftçi et al., 2021). Green synthesized NPs play important roles in drugs, clinical applications, and in vitro diagnostic applications. NPs synthesized by green methods show excellent antibacterial, antifungal and antiparasitic

effects (Figure 3). NPs in the 1-100 nm size range readily bind with HIV-1 virus on gp120 glycoprotein knobs. This particular interaction of NPs prevents the virus from binding to host cells, thus helping to prevent and control HIV infection. NPs can cause cell wall damage, membrane damage, or generate free radicals, causing oxidative, DNA or electron transport chain damage, ultimately leading to bacterial death (Hussain et al., 2016).

Au-NPs have been applied for the specific release of drugs such as paclitaxel, methotrexate, and doxorubicin. Au-NPs have also been used in tumor detection, angiogenesis, genetic disease and genetic disorder diagnosis, photoimaging, and photothermal therapies. Iron oxide NPs are applied in cancer therapy, hyperthermia, drug delivery, tissue repair, cell labeling, targeting and immunological testing, detoxification of biological fluids, magnetic resonance imaging, and magnetically sensitive drug delivery.

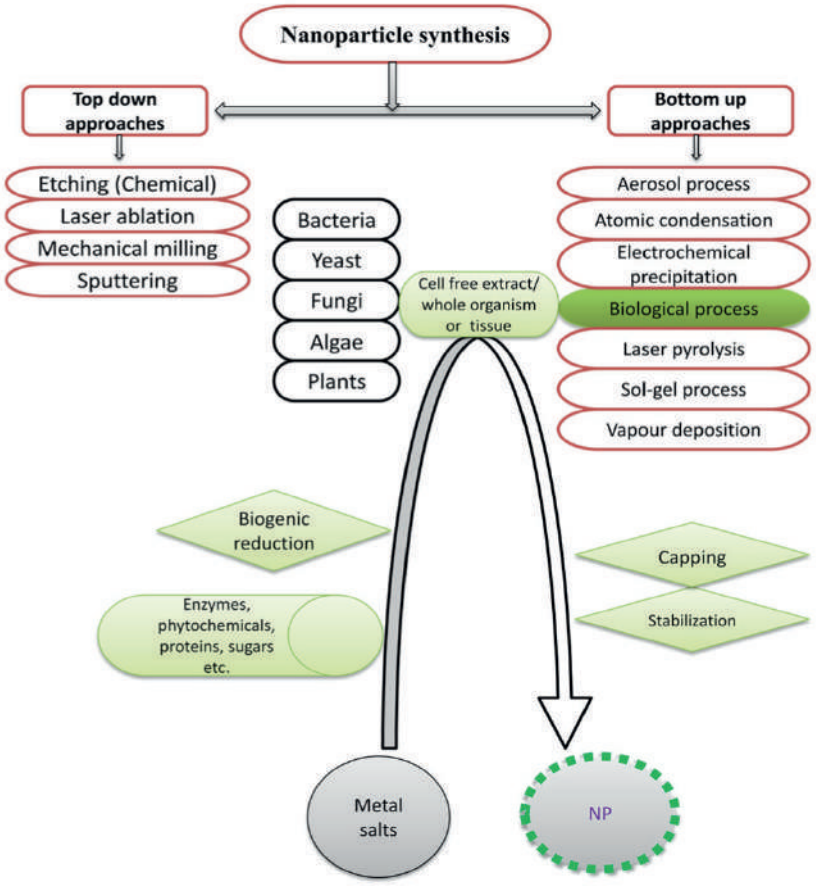

Figure 3. The flow chart of various physico– chemical approaches of nanoparticles synthesis with highlighting of biological synthesis (Hussain et al., 2016)

Ag-NPs are used for many antimicrobial purposes, as well as in anticancer, anti-inflammatory and wound treatment applications. In addition, Ag-NPs are among the most attractive nanomaterials. Ag-NPs, diagnosis, treatment, drug delivery, medical device coating, personal health care (Çiftçi et al., 2021) cardiovascular implants, wound dressings, catheters, orthopedic implants, dental composites, nano-bio-sensing and agricultural engineering (Rafique et al., 2017) have emerged with leading contributions in nanomedicine, chemical sensing, data storage, cell biology, textile, food industry. It has a great function as a disinfectant and antimicrobial agent (Ahmad et al., 2019).

Ag-NPs can increase the durability and service life of fabrics. Ag-NPs are used in self-cleaning fabrics, towels, furniture items, kitchen fabrics, bed linens or reusable surgical gloves, veils, patient gowns and antibacterial injury dressings, protective face covers, biohazard clothing, sportswear and water-repellent materials. There are potential application areas in production (Rafique et al., 2017). Thanks to nano textile applications, textile products with properties such as waterproof, dirt-proof, non-wrinkling of the fabric, antimicrobial effect, flammability or non-flammability, air permeability and holding the applied paint can be produced. While increasing the performance of products that can be used in the military field, it reduces the dimensions and enables the production of lighter, long-lasting and high-strength materials. With its video camera options (unmanned aerial vehicles, etc.), it provides surveillance superiority and at the same time, it can provide superiority in the field of defense by facilitating the detection of harmful and radioactive gases by nano-detectors (Güven, 2022).

Excellent delivery system for nanofertilizers, nanopesticides containing nanoherbicides, nanocoating and plant nutrients are widely used as part of agribusiness with numerous manufacturing industries containing 100–250 nm Ag-NPs that are more water soluble, thereby increasing their activity. Nanofertilizers have the capacity to synchronize nutrient release with the uptake of plants, avoiding nutrient losses and reducing the risks of groundwater contamination. Ag-NPs are also used in the field of expanded nanotechnology, in various consumer by-products such as water filters and sanitation system, deodorants, soaps, socks, food preservation and air fresheners, expanding the commercial sector of Ag-NPs and their composites have greater catalytic activities in dye reduction and removal (Rafique et al., 2017).

Nanoparticles can provide versatile benefits, especially in food packaging materials. They can create a gas barrier, suppress the growth of microorganisms, and improve the temperature and humidity resistance of

the packaging. Thus, food safety and shelf life can be increased (Hatipoğlu, 2022). In addition, there are applications to ensure the creation of new functional products by adding nanoparticles with different colors, flavors and nutritional content (Güven, 2022).

Zinc and titanium NPs with biocompatible, non-toxic, self-cleaning, skin compatible, antimicrobial and dermatological properties are used in biomedical, cosmetic, ultraviolet blocking agents. Dose optimization is necessary for drugs to reach the level of bioavailability, and the drug taken must have a specific target. That is, theoretically high doses of the drug should be taken to achieve proper bioavailability, but this will cause more side effects. With NPs, it is possible to distribute drugs specific to the region. Thanks to this approach, appropriate drug dosage will be used and side effects will be significantly reduced. The use of small amounts of drugs for specific targets both reduces drug costs and increases patient comfort (Çiftçi et al., 2021).

In recent years, researchers have been working on the delivery of chemotherapy drugs with nanoparticles, especially in anticancer applications. Passive and active targeting methods can be done with dendrimer, liposomes, metal nanoparticles and polymer micelles. The drug delivery system has the best distribution of therapeutic agents for cancer treatment. Especially Au and Ag NPs have enabled important studies on this subject. Nanoparticle forms of metals such as copper, iron and zinc are also used as drug delivery systems in biomedical applications (Kütük and Çetinkaya, 2019).

NPs or their products are useful in environmental remediation. On these greener routes, organisms or their products, or NPs, clean up hazardous waste sites and treat pollutants. Green NPs have a wide scope in the treatment of surface water, groundwater and wastewater contaminated with toxic metal ions, organic and inorganic solutes and microorganisms. Self-cleaning nanoscale surface coatings can eliminate many cleaning chemicals used in regular maintenance routines. NPs are used in domestic water treatment systems to remove viruses from drinking water. Fe-NPs are of great interest due to their rapidly developing applications for disinfection of water and recovery of heavy metals from soil. The use of nanoparticles, as an alternative to expensive methods such as excavation, soil washing and thermal desorption for soil pollution removal, gives successful results in the treatment of contaminated soils, removal of heavy metals, polycyclic aromatic hydrocarbons and pesticides (Wang et al., 2019). NPs are an alternative to pesticides in the control and management of plant diseases and also act as effective fertilizers that are environmentally friendly and increase crop

production. The use of green nanoparticles has increased in recent years in the removal of PAHs from air pollutants, gases such as carbon monoxide and sulfur dioxide, and in the detection of some gases (Ghandhi et al., 2014). Magnetite (Fe_3O_4)/gregite (Fe_3S_4) and siliceous materials produced using bacteria and diatoms are successfully used in optical coatings for solar energy applications and as ion placement materials for electric cell applications. Nanoscale catalysts perform chemical reactions more efficiently (Hussain et al., 2016).

NPs are popular due to their excellent catalysis and good sensor properties, large NPs surface area and high reactivity, and can be used as adsorbent. The densities of small and spherical NPs increase exponentially as their diameter gets smaller. In addition, the nanoparticle dexterity (agility) in the solution is greater and can scan the entire solution due to its small size and large surface area. NPs with these unique properties can be used to remove pollutants from water. Organic wastes are absorbed on the surface of the NPs and can then be removed by gravity or magnetic forces. For this reason, the size, shape and morphology of NPs are very important (Kütük and Çetinkaya, 2019).

CONCLUSION

Compared to traditional physical and chemical methods, green synthesis is a sustainable, safe, low-cost, easily available, environmentally friendly, easy-to-apply, low-energy biological method that does not require harsh or toxic chemicals in its synthesis. Moreover, NPs synthesized by green synthesis are more stable and effective compared to those produced by physical and chemical methods. In this method, NPs can be synthesized in one step. Waste products are non-toxic and easy to dispose of. NPs synthesized by green synthesis have applications in almost every field such as medicine, agriculture, biotechnology, imaging, optics, environment and energy. The many advantages of the green synthesis method will enable this method to be widely used in the future, and research on its potential applications will accelerate, and the field of sustainable, environmentally friendly applications will expand.

* This book chapter is the extended version of the paper presented and published (in abstract book) in the 8th International "Başkent" Congresses on Physical, Social, and Health Sciences, which was held on February 04-06, 2023.

REFERENCES

Ahmad S, Munir S, Zeb N, Ullah A, Khan B, Ali J, Bilal M, Omer M, Alamzeb M, Salman M, S ve Saqib A 2019. Green nanotechnology: a review on green synthesis of silver nanoparticles — an ecofriendly approach. *Int J Nanomedicine,* 14: 5087–5107.

Baig N, Kammakakam I and Falath W 2021. Nanomaterials: a review of synthesis methods, properties, recent progress, and challenges. *Royal Society of Chemistry*. 2, 1821-1871.

Baykal B 2022. Nanoparticle synthesis using green leafy plants and dye removal efficiency. Master Thesis, Zonguldak Bülent Ecevit University Graduate School of Natural and Applied Science, Zonguldak. (in Turkish)

Brar S K, Verma M, Tyagi RD, Surampalli RY 2010. Engineered nanoparticles in wastewater and wastewater sludge -Evidence and impacts, *Waste Management*, 30, 504-520.

Çiftçi H, Çalışkan ÇR, Öztürk K and Yazıcı B 2021. Bioactive nanoparticles synthesized by green method. *Black Sea Journal of Engineering and Science,* 4 (1), 29-42. (in Turkish)

Fakhari S, Jamzad H and Fard HK 2019. Green synthesis of zinc oxide nanoparticles: a comparison. *Green Chemistry Letters and Reviews,*12 (1), 19-24.

Gandhi N, Sirisha D and Sharma VC 2014. Microwave-mediated green synthesis of silver nanoparticles using Ficus elastica leaf extract and application in air pollution controlling studies, *International Journal of Engineering Research and Applications*, 4(1), 61-72.

Gençay S N 2022. Investigation of green synthesis, structural characterization and biological activities of ZnO nanoparticles using chestnut honey. Master Thesis, Düzce University Graduate School of Natural and Applied Science, Düzce. (in Turkish)

Gour A and Jain NK 2019. Advances in green synthesis of nanoparticles. *Artificial Cells, Nanomedicine, and Biotechnology,* 47(1), 844-851.

Güven OC 2022. Synthesis and characterization of copper (Cu) nanoflowers using green synthesis method, determination of photocatalytic, antimicrobial and antioxidant activity. Master Thesis, Nevsehir Hacı Bektaş Veli University Graduate School of Natural and Applied Science, Nevşehir. (in Turkish)

Hatipoğlu A 2022. Green synthesis of silver nanoparticles and their antimicrobial effects on some food pathogens. *Süleyman Demirel University Journal of Natural and Applied Sciences,* 26 (1), 106-114. (in Turkish)

Hussain I, Singh NB, Singh A, Singh H and Singh SC 2015. Green synthesis of nanoparticles and its potential application. *Biotechnology Letters,* 38, 545–560.

Jadoun S, Arif R, Jangid N K and Meena RK 2021. Green synthesis of nanoparticles using plant extracts: a review. *Environmental Chemistry Letters,* 19, 355–374.

Kütük N and Çetinkaya S 2019. Investigation of nanomaterial production by green synthesis and usage areas. *5th International Engineering Architecture and Design Congress,* 842-848, İstanbul. (in Turkish)

Nadaroğlu H, Güngör AA and İnce S 2017. Synthesis of nanoparticles by green synthesis method, *International Journal of Innovative Research and Reviews,* 1(1), 6-9.

Rafique M, Sadaf I, Rafique MS and Tahir B M 2017. A review on green synthesis of silver nanoparticles and their applications. *Artificial Cells, Nanomedicine, and Biotechnology*, 45,7.

Srikar SK, Giri D D, Pal D B, Mishra P K and Upadhyay N 2016. Green synthesis of silver nanoparticles. *Green and Sustainable Chemistry,* 6(1), 34-56.

Şimşek UB 2015. Production of zero valent iron nanoparticles at different synthesis conditions, optimization and application for the textile dyes removal, Master Thesis, Mersin University Graduate School of Natural and Applied Science, Mersin. (in Turkish)

Umaz A and Koç A 2019. Biomedical applications of green path synthetic metal nanoparticles. Gece Library, Research and Reviews in Science and Mathematics, 77-90, M. F. Baran, A. Eren (Ed.). (in Turkish)

Wang Y, O'Connor D, Shen Z, Lo I M, Tsang DC, Pehkonen S, Pu S and Hou D 2019. Green synthesis of nanoparticles for the remediation of contaminated waters and soils: Constituents, synthesizing methods, and influencing factors. *Journal of Cleaner Production*, 226, 540-549.

Yakut Ş M and Karataş M 2021. Green engineering in nanosynthesis and its place in environmental engineering, *Düzce University Journal of Science and Technology*, 9, 1267-1281. (in Turkish)

CHAPTER 13

Investigation of the Death Effects of Four Different Chemotherapeutic Agents on Breast Cancer Cell Lines Under the Microscope

Bahar YILMAZ[1]

What is a cell?

Cells are the smallest building blocks of living things that can be seen with a microscope (1). All cells in our body have specific functions and these cells divide regularly (except muscle and nerve cells) (2). When cells get old or damaged, they die and are replaced by new cells that can renew themselves. When these cells begin to multiply uncontrollably, cancer cells, also called tumoral structures, are formed (3). As seen in Figure 1, cancer cells continue to grow and form new cells, forming an abnormal structure and leaving no room for normal cells.

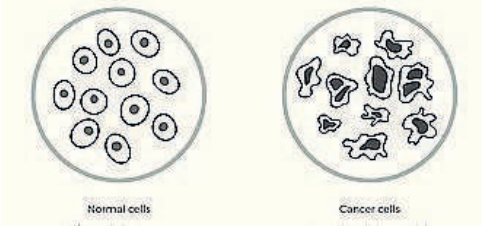

Figure 1. Normal and cancer cells

1 Karamanoglu Mehmetbey University, Faculty of Engineering, Department of Bioengineering, Karaman, Turkey, ORCID ID: 0000-0002-6315-3018, baharyilmaz@kmu.edu.tr

What is cancer cell?

Because this abnormal growth affects normal cells, it creates a complex that threatens human health (4). Cancer, a complex condition that millions of people are diagnosed with every year, is still a serious health problem from past to present (5). Despite advances in the detection of cancer cases worldwide, studies to prevent detected cancer, and modern methods of treatment, these cases still affect millions of people. This disease lowers the living standards of patients and often causes people to lose their lives. According to the records of the World Health Organization, 11 million people are diagnosed with cancer annually and it is determined that there are still around 25 million cancer patients in the world (6). When we look at the causes of death in the world, cancer is the second cause of death after coronary heart diseases (7) with a rate of 20.06%. In our country, cancer causes the most deaths after heart diseases (Table 1).

Table 1. % ratio of cancer diseases among the most common fatal diseases

Diseases	**% ratio**
Coronary heart ailments	%25,9
Cancer	%20,6
Cerebrovascular diseases	%13,7
Pneumonia	%8,0
Chronic bronchitis	%4,1
Accidents	%3,8

While the death rate due to heart diseases is 42% in Turkey, the rate due to cancer is 12.9%. In the research conducted in 2018; While 18.1 million people were diagnosed with cancer, it was determined that 9.9 million people died due to these cases (8).

Factors that cause cancer

According to researches; Many factors such as radiation, genetics, DNA mutations, stress, environment, biochemical and synthetic chemicals cause cancer formation (9). Moreover; Environmental causes such as X-rays, UV rays, pollution and chemicals, lifestyles including alcohol and smoking habits, and diets containing vitamins, antioxidant factors, fatty or fibrous foods affect the frequency of tumor formation (Figure 2) (10).

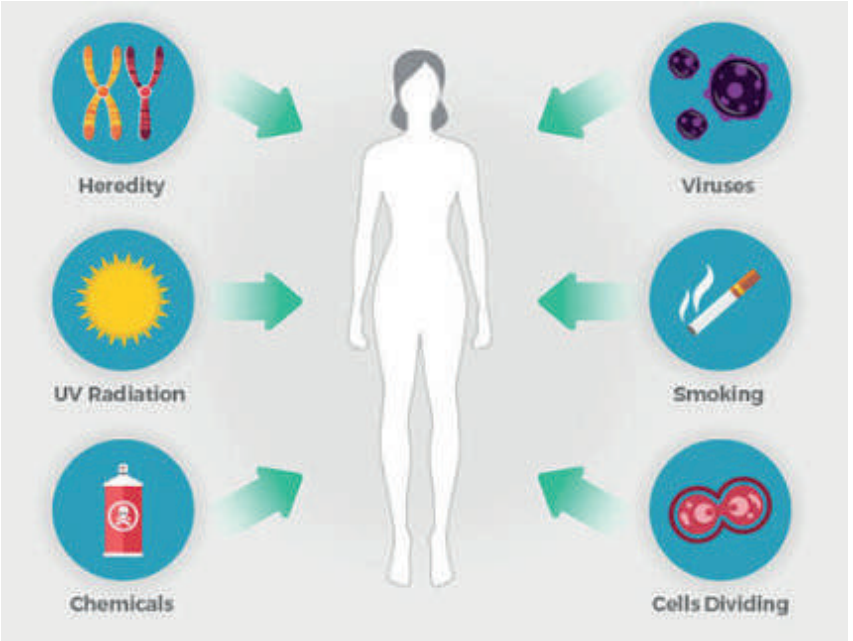

Figure 2. Factors that cause cancer

Although the incidence and mortality of cancer have increased rapidly in recent years, it threatens humanity more and more as time goes on (11). Cancer, which initially starts locally, tends to spread rapidly to other parts of the body, making the disease incurable.

Breast cancer

Breast cancer ranks first among the most common types of cancer among women (12). In the cancer rankings detected in Turkey, breast cancer is the most common type of cancer in women, and it is also identified as the leading cause of death from cancer cases in many countries. Breast cancer, which is a malignant tumor that starts in breast cells, is tumoral structures that occur with uncontrolled proliferation of cells in the mammary glands (lobular) or milk ducts (13). Breast cancer is frequently seen in women, although this type of cancer is rarely seen in men. Breast cancer, which occurs in two forms, is called ductal carcinoma (cancer arising from the milk ducts) and lobular carcinoma (cancer arising from the lobules) (12). Breast cancer, which starts mostly in duct cells, can sometimes start in lobules.

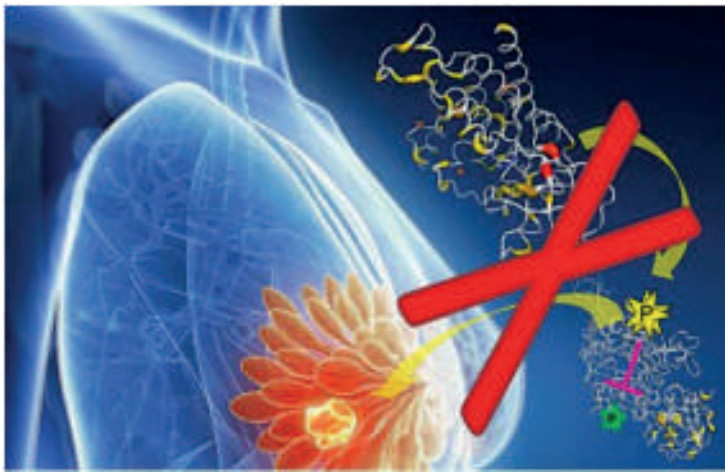

Figure 3. Breast cancer resulting from excessive FGFR4 (Fibroblast growth factor receptor 4) growth (12)

Cancer treatment methods

In cancer treatments, being aware of the methods of prevention from cancer cases, early diagnosis and obtaining positive results from the treatment lead to a decrease in the fear of cancer cases in people over time (14). Today, the treatment possibilities of many types of cancer have increased, and the life expectancy of patients is increasing compared to other years. However, cancer has not escaped being talked about as synonymous with fear and even death (15). Cancer and cancer treatment are among the most important health problems of the people of many countries. Many treatments are used to reduce the death rate and increase survival in cancer treatment (16). Among them, there are many options such as surgery, chemotherapy-hormone therapy, radiotherapy, immunotherapy, new drug types and treatment methods. Treatments such as surgery, radiotherapy, chemotherapy are limited by the accessibility of the tumor. Among these important problems that need to be solved are the early diagnosis delayed in cancer diagnosis and treatment, lack of drug compliance and use of systemic drugs that are not specific to the tumor, incomplete drug concentrations reaching the tumor site, and inability to display post-treatment responses (14-15). Cancer biotechnology focuses on the techniques and materials necessary to overcome these problems, and cancer biotechnology research activities are divided into seven categories as a result of the researches (15).

- First; early detection of cancers in the early stages and development of imaging agents to be used.

- Latter; deriving methods that can enable assessments of the effects of treatments in the region.
- Third; will transfer the therapeutic agents to the cancer area without being damaged by biological agents; develop targeted materials, devices and carriers.
- Fourth; development of agents to distinguish malignant from benign cancer cells and to observe predictive molecular changes.
- Fifth; making various observations to detect genetic conditions predisposing to cancer and developing mutations that trigger cancer.
- Sixth; development of new methods for monitoring cancer symptoms that reduce quality of life.
- Seventh; development of techniques to rapidly identify target sites and predict drug resistance in clinical therapy to support researchers.

In cancer technology research; In addition to the imaging of cancerous cells recently, it is also important to monitor the effect of drug materials applied to the tumor area (14). If drug materials can be used effectively in cancer treatment in accordance with the desired target, it is predicted that it will be one of the biggest developments in this field (16). Another important situation is; It is aimed to apply many drugs to the tumor area at the same time, and thus to eliminate or minimize the problem of drug resistance, which is one of the most undesirable problems in cancer treatment (17-18). In recent years, many chemotherapy drugs and new treatment methods have been developed for cancer treatment. There are many cancer drugs and cancer drug combinations. They have individual side effects.

Cisplatin

Cisplatin is indicated for the palliative treatment of the following diseases, either alone or in combination with other approved chemotherapeutic agents (19): Metastasized testicular tumors: In established combination therapy with other approved chemotherapeutic agents in patients with metastasized testicular tumors who have undergone appropriate surgery and/or radiotherapy (20). Established combination therapy includes cisplatin and cyclophosphamide. Cisplatin as a single agent is indicated as a secondary therapy in patients with metastatic ovarian tumors refractory to standard chemotherapy who have not previously received cisplatin therapy.

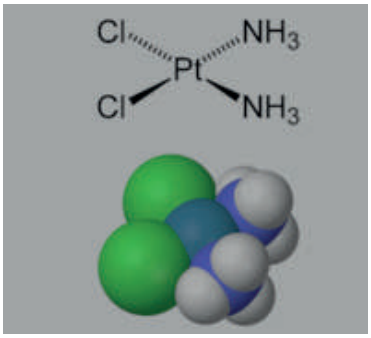

Figure 4. Cisplatin structure

Docetaxel

Docetaxel, sold under the brand name Taxotere, is a chemotherapy drug used to treat a number of cancer types. This includes breast cancer, head and neck cancer, stomach cancer, prostate cancer, and non-small cell lung cancer. It can be used alone or in combination with other chemotherapy drugs (21).

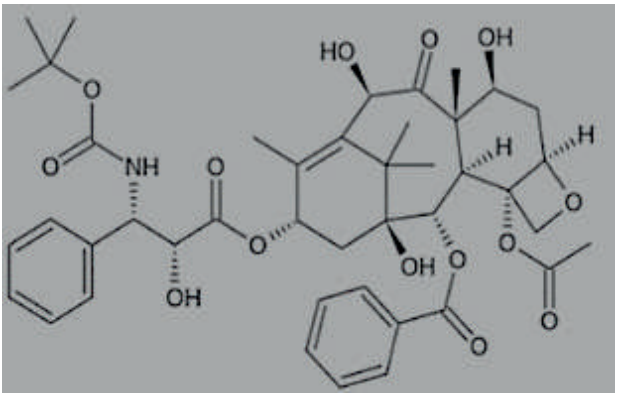

Figure 5. Docetaxel structure

Gemcitabine

Gemcitabine is a chemotherapy drug. It treats cancers such as testicular cancer, breast cancer, ovarian cancer, non-small cell lung cancer, pancreatic cancer, and bladder cancer. It is administered by intravenous infusion (22).

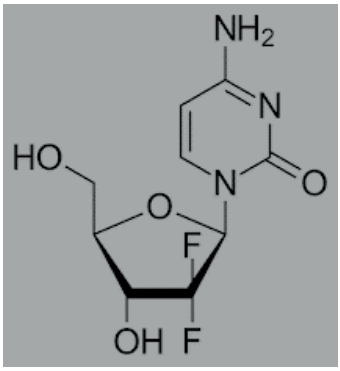

Figure 6. Gemcitabine structure

Taxol

Paclitaxel (Taxol) is a chemotherapy drug used to treat various types of cancer. This includes ovarian cancer, esophageal cancer, breast cancer, lung cancer, Kaposi's sarcoma, cervical cancer, and pancreatic cancer. It is administered by intravenous injection. There is also an albumin-dependent formulation (23).

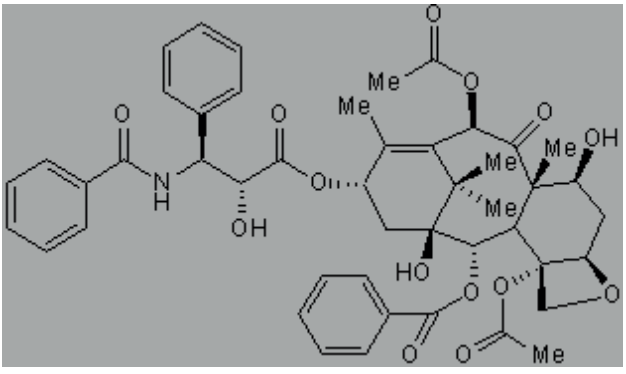

Figure 7. Taxol structure

Application Of Four Different Drugs To Breast Cancer Cell Lines

Cancer is usually called continuous and fast growing tumor cells. It is a disease characterized by uncontrolled growth and metastasis by activation of oncogenes, epigenetic modifications, and inactivation of tumor suppressors (24). Treatments are based on researched methods with the aim of minimizing tumor progression, recurrence and mortality. Generally, many treatment methods are applied, especially chemotherapy, radiotherapy and surgical

methods (25). Cytotoxic chemotherapy is most commonly used. Since these chemotherapies target all body cells, they can damage some healthy cells as well as cancer cells (26). Existing chemotherapy drugs (Docetaxol, taxol, cisplatin and gemstabin) used during the treatment are examined under the microscope for their harmful effects on cells.

In many studies, the anticancer activities of such drugs and their derivatives have been determined by examining them with a microscope. In this study, the death effects of four different drugs on breast cancer cells were examined under a microscope and compared.

Although cancer treatment, which is still a major problem in the world, is treated with three methods (surgery, radiotherapy and chemotherapy), chemotherapy, also known as drug therapy, is known as the only treatment method that can affect all parts of the body systemically (14-15). Cancer is a systemic disease that affects many organs of the body. The common feature of chemotherapy drugs used in drug treatment applications is that they damage cells with a high growth and division rate and that the tumor cell growth rate is too uncontrolled, so that these chemotherapeutic drugs are damaged by these chemotherapeutic drugs (3, 12). Because these chemotherapy drugs affect the normal cells of the body with a high rate of division as well as cancer cells, nausea, decrease in blood counts, hair loss, etc., which are common during treatment. side effects may occur (9, 23). One of the most important distinctions between these cells is that while normal cells can repair themselves over time, cancerous cells cannot fully repair themselves. Therefore, in about two to three weeks, while normal cells can recover from the effects of chemotherapy drugs, cancer cells cannot tolerate this and fail. In this case, the cells die over time (20).

All these treatment methods may become insufficient over time. While the cell becomes resistant to the drug and the death rate is expected to increase, the cell may grow further and metastasize. All these treatment methods may become insufficient over time (16). While the cell becomes resistant to the drug and the death rate is expected to increase, the cell may grow further and metastasize. Anticancer drugs used in cancer treatments show their effects mainly in five ways: apoptosis, necrosis, autophagy, mitotic catastrophe and senescence (27). In addition, two more death pathways known as necroptosis and proptosis can be activated with anticancer drugs.

Apoptosis and autophagy pathways are genetically tightly controlled mechanisms of programmed cell death. Necrosis and mitotic catastrophe are types of unscheduled and uncontrolled cell death that occur in the face of severe cellular attacks. Senescence, which is characterized by telomere

damage and activation of tumor suppressor factors, literally means cellular senescence (27).

It is expected that the development of drug active substances that are synthesized or derivatized for cancer treatments, cause the death of tumor cells by causing the above-mentioned cellular functions or mechanisms in cell lines. For this reason, macrocyclic molecules and their derivatives, especially calixarene molecules, are functionalized for many uses such as drug transport, release, solubility and preservation in cancer treatments, in vitro and in vivo studies are carried out and still being investigated.

The four different cancer drugs used have been investigated by many research groups for their anticancer activities. These drugs have multiple mechanisms of action for their anticancer properties, including enzyme inhibition, antagonism of angiogenesis, suppression of oncogenes, upregulation of tumor suppressor genes, and DNA binding. In other literature studies, it has been observed that platinum derivatives cause growth inhibition, while drug molecules in the taxol structure inhibit phosphatases such as alkaline phosphatase and tyrosine phosphatase. In addition, many studies have suggested that new cancer drugs may interact with the platelet-derived growth factor (PDGF) receptor, preventing it from interacting with PDGF and phosphorylation, resulting in an anti-angiogenic effect (28). It has been shown in many studies that cancer drugs and their equivalents can increase the activity of tumor suppressor genes by stabilizing the relevant protein.

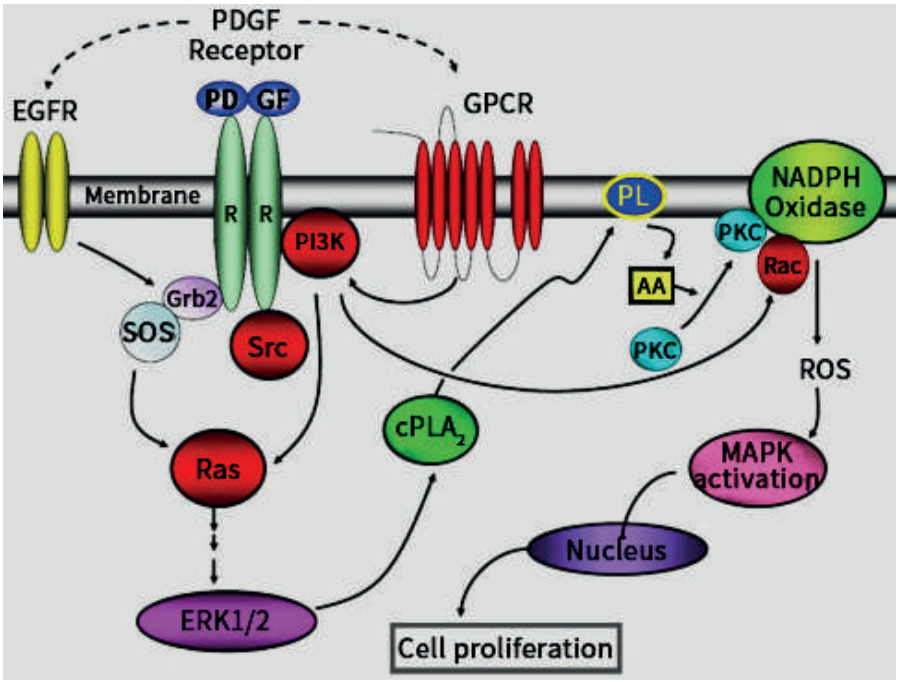

Figure 8. Growth factor (PDGF) receptor (29)

Again, as a result of research; it has been observed that gemstabin inhibits glutathione S-transferase and prevents multidrug resistance of cancer cells. It has also been proven to regulate the tumor suppressor gene and the p53 gene (30).

Drug molecules containing sulfo and/or sulfur in their structure initiate the apoptotic caspase system with the help of photodynamic therapy, thereby destroying the membrane and mitochondria. While apoptosis was expected to be preferred over the above-mentioned death pathways by metal-based anticancer drugs, other death pathways showed greater activation. It has been reported that Cisplatin, which has been used in clinical applications for years, causes cell death by apoptosis, but rarely causes necrosis (31).

Figure 9 shows images of cisplatin-treated breast cancer cells (MCF-7). When we look at the appearance of breast cancer cell before and after drug administration, it is clearly observed that cisplatin is a very effective drug.

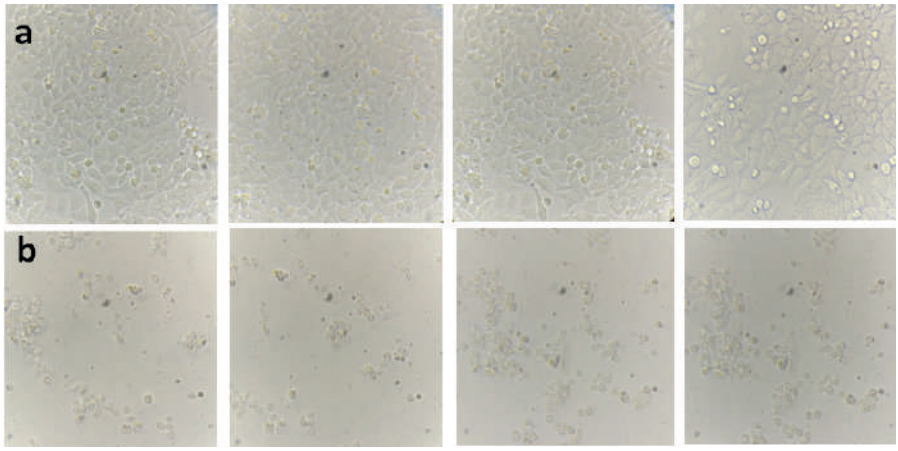

Figure 9. (a) Non-medicated and (b) Drug-administered (Cisplatin) MCF-7 cell line

As a result of researches, with the use of platinum-based Cisplatin against cancer, the search for other metal-based drug candidates that are less toxic on healthy tissues and more effective against cancer cells has accelerated.

In the light of the literature information; Gemstabin has a water-soluble structure thanks to the active groups it contains. It has been proven that this structure acts like cisplatin and inhibits DNA (genetic material) synthesis and acts against tumor cell DNA. Although not as effective as cisplatin, it has been proven to inhibit DNA synthesis of tumor cells (Figure 10). It is clearly seen that the drug molecule Gemstabin produces less toxic effects than Cisplatin (29-31).

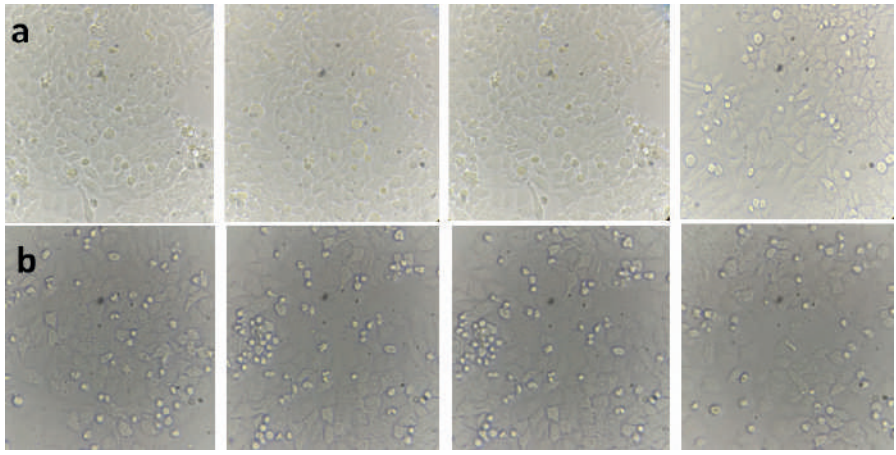

Figure 10. (a) Non-medicated and (b) Drug-administered (Gemstabin) MCF-7 cell line

These studies, thanks to the groups and structures of drug molecules and derivatives of different structures against cancer cell structures; DNA, mitochondria, growth factors and their effects on cell cycles illuminate the mechanisms in cell death.

The more cytotoxic effects of drug molecules on the cancer cell line, the effects on cell cycles, DNA structure, growth inhibition or many cell functions such as protein synthesis were better observed with microscopic images. These observed cell lines were evaluated by comparing drug treated and untreated control cells. When we look at Taxol and Docetaxel drug molecules, it is clearly observed in Figure 11 and Figure 12 that they cause similar deaths.

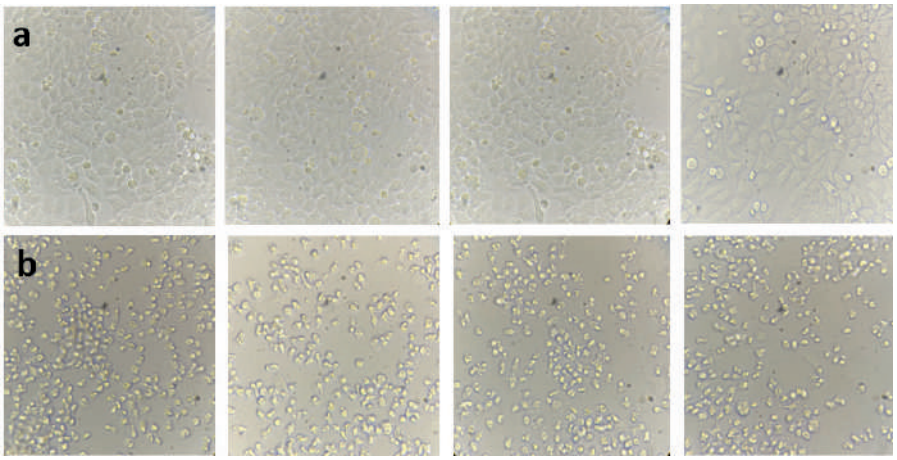

Figure 11. (a) Non-medicated and (b) Drug-administered (Taxol) MCF-7 cell line

In general, membrane integrity and cell structure were evaluated by examining the drug-administered cells. Cells with impaired membrane structure are generally observed as the cause of death due to external influence (26). Although the integrity of the membrane is preserved, the deaths observed as a result of intracellular interactions are generally considered as controlled cell death. This explains the occurrence of necrosis (self-death of the cell). It is observed that nuclear fragmentation, which also evokes an apoptic (programmed death of the cell) appearance, creates deep folds and cellular disorders in the cells (28-29). Necrosis and apoptosis processes occur more in cancer cell lines (32). As a result of microscopic images, necrosis and apoptosis processes in cancer cell lines were clearly demonstrated.

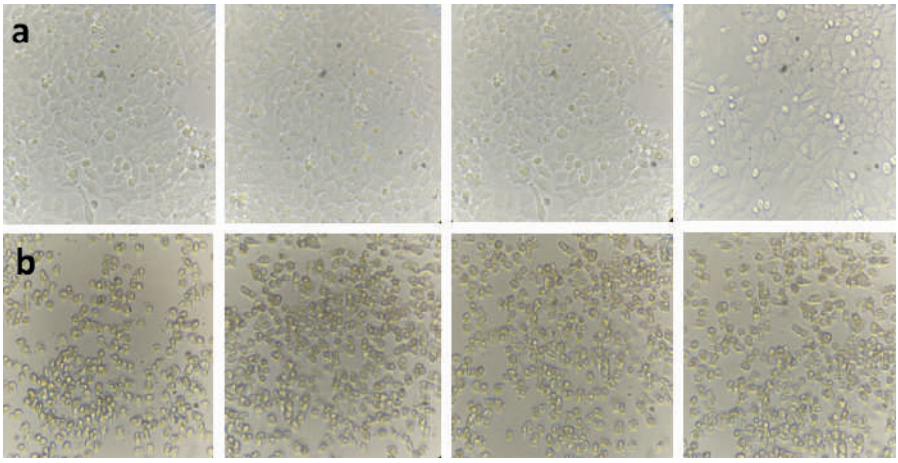

Figure 12. (a) Non-medicated and (b) Drug-administered (Docetaxel) MCF-7 cell line

In all studies, the mechanism of drug molecules against cancer cells is explained (33). Considering these mechanisms, the effects of drug molecules on cell growth and division have been studied directly and indirectly. In addition to the cytotoxic effects of drug molecules against cancer cells, it is also important that they do not harm healthy cells. In this study, the toxic effect and mechanism of 4 different drug molecules on breast cancer cell line were investigated. Binding of amine side chains of different drug molecules to single-stranded DNA can inhibit cell proliferation by causing DNA replication to be inhibited (32-33).

The drug molecules have the ability to induce apoptosis in endothelial cells and cardiomyocytes through the activation of cardiomyopathy, p53 protein, and reactive oxygen species.

REFERENCE

Brown, M. T., Munn, M., & Tyler, L. (2007). Cells.

Sulston, J. E., & Horvitz, H. R. (1977). Post-embryonic cell lineages of the nematode, Caenorhabditis elegans. *Developmental biology*, *56*(1), 110-156.

Sulston, J. E., Schierenberg, E., White, J. G., & Thomson, J. N. (1983). The embryonic cell lineage of the nematode Caenorhabditis elegans. *Developmental biology*, *100*(1), 64-119.

Sabarwal, A., Kumar, K., & Singh, R. P. (2018). Hazardous effects of chemical pesticides on human health–Cancer and other associated disorders. *Environmental toxicology and pharmacology*, *63*, 103-114.

Siegel, R., DeSantis, C., Virgo, K., Stein, K., Mariotto, A., Smith, T., ... & Ward, E. (2012). Cancer treatment and survivorship statistics, 2012. *CA: a cancer journal for clinicians*, *62*(4), 220-241.

Ginsburg, O., Bray, F., Coleman, M. P., Vanderpuye, V., Eniu, A., Kotha, S. R., ... & Conteh, L. (2017). The global burden of women's cancers: a grand challenge in global health. *The Lancet*, *389*(10071), 847-860.

Mansur, A. D. P., Favarato, D., Strunz, C. M. C., Avakian, S. D., Pereira-Barretto, A. C., Bocchi, E. A., & César, L. A. M. (2022). Sex Differences in Cardiovascular Disease Mortality in Brazil between 1996 and 2019. *International Journal of Environmental Research and Public Health*, *19*(19), 12827.

Sung, H., Ferlay, J., Siegel, R. L., Laversanne, M., Soerjomataram, I., Jemal, A., & Bray, F. (2021). Global cancer statistics 2020: GLOBOCAN estimates of incidence and mortality worldwide for 36 cancers in 185 countries. *CA: a cancer journal for clinicians*, *71*(3), 209-249.

Aitken, R. J., Baker, M. A., & Sawyer, D. (2003). Oxidative stress in the male germ line and its role in the aetiology of male infertility and genetic disease. *Reproductive biomedicine online*, *7*(1), 65-70.

Parsa, N. (2012). Environmental factors inducing human cancers. *Iranian journal of public health*, *41*(11), 1.

Adams, J. M., & White, M. (2004). Biological ageing: a fundamental, biological link between socio-economic status and health?. *The European Journal of Public Health*, *14*(3), 331-334.

Tiong, K. H., Tan, B. S., Choo, H. L., Chung, F. F. L., Hii, L. W., Tan, S. H., ... & Leong, C. O. (2016). Fibroblast growth factor receptor 4 (FGFR4) and fibroblast growth factor 19 (FGF19) autocrine enhance breast cancer cells survival. *Oncotarget*, *7*(36), 57633.

Wu, W., Hai, Y., Chen, L., Liu, R. J., Han, Y. X., Li, W. H., ... & Wu, X. R. (2016). Deguelin-induced blockade of PI 3K/protein kinase B/MAP kinase signaling in zebrafish and breast cancer cell lines is mediated by

down-regulation of fibroblast growth factor receptor 4 activity. *Pharmacology research & perspectives*, *4*(2), e00212.

Mazumdar, M., & Glassman, J. R. (2000). Categorizing a prognostic variable: review of methods, code for easy implementation and applications to decision-making about cancer treatments. *Statistics in medicine*, *19*(1), 113-132.

Sudhakar, A. (2009). History of cancer, ancient and modern treatment methods. *Journal of cancer science & therapy*, *1*(2), 1.

Safarzadeh, E., Shotorbani, S. S., & Baradaran, B. (2014). Herbal medicine as inducers of apoptosis in cancer treatment. *Advanced pharmaceutical bulletin*, *4*(Suppl 1), 421.

World Health Organization. (1979). *WHO handbook for reporting results of cancer treatment*. World Health Organization.

Guy Jr, G. P., Machlin, S. R., Ekwueme, D. U., & Yabroff, K. R. (2015). Prevalence and costs of skin cancer treatment in the US, 2002– 2006 and 2007– 2011. *American journal of preventive medicine*, *48*(2), 183-187.

Boulikas, T., & Vougiouka, M. (2004). Recent clinical trials using cisplatin, carboplatin and their combination chemotherapy drugs. *Oncology reports*, *11*(3), 559-595.

Roche, H., & Vahdat, L. T. (2011). Treatment of metastatic breast cancer: second line and beyond. *Annals of Oncology*, *22*(5), 1000-1010.

Yuan, Q., Han, J., Cong, W., Ge, Y., Ma, D., Dai, Z., ... & Bi, X. (2014). Docetaxel-loaded solid lipid nanoparticles suppress breast cancer cells growth with reduced myelosuppression toxicity. *International journal of nanomedicine*, *9*, 4829.

Fantini, M., Gianni, L., Santelmo, C., Drudi, F., Castellani, C., Affatato, A., ... & Ravaioli, A. (2011). Lipoplatin treatment in lung and breast cancer. *Chemotherapy research and practice*, *2011*.

Long, H. J. (1994, April). Paclitaxel (Taxol): a novel anticancer chemotherapeutic drug. In *Mayo Clinic Proceedings* (Vol. 69, No. 4, pp. 341-345). Elsevier.

Jabir, M. S., Taha, A. A., Sahib, U. I., Taqi, Z. J., Al-Shammari, A. M., & Salman, A. S. (2019). Novel of nano delivery system for Linalool loaded on gold nanoparticles conjugated with CALNN peptide for application in drug uptake and induction of cell death on breast cancer cell line. *Materials Science and Engineering: C*, *94*, 949-964.

Chaouki, W., Leger, D. Y., Eljastimi, J., Beneytout, J. L., & Hmamouchi, M. (2010). Antiproliferative effect of extracts from Aristolochia baetica and Origanum compactum on human breast cancer cell line MCF-7. *Pharmaceutical Biology*, *48*(3), 269-274.

Wong, C., & Chen, S. (2012). The development, application and limitations of breast cancer cell lines to study tamoxifen and aromatase inhibitor resistance. *The Journal of steroid biochemistry and molecular biology*, *131*(3-5), 83-92.

Sazonova, E. V., Petrichuk, S. V., Kopeina, G. S., & Zhivotovsky, B. (2021). A link between mitotic defects and mitotic catastrophe: detection and cell fate. *Biology Direct*, *16*(1), 1-11.

Ding, W., Knox, T. R., Tschumper, R. C., Wu, W., Schwager, S. M., Boysen, J. C., ... & Kay, N. E. (2010). Platelet-derived growth factor (PDGF)–PDGF receptor interaction activates bone marrow–derived mesenchymal stromal cells derived from chronic lymphocytic leukemia: implications for an angiogenic switch. *Blood, The Journal of the American Society of Hematology*, *116*(16), 2984-2993.

Parra, E., Maturana, J. C., & Hecht, P. (2022). Response of T98G Glioblastoma Cells Line to Wortmannin and Platelet-derived Growth Factor. *New Visions in Biological Science Vol. 10*, 38-54.

Justin, S., Rutz, J., Maxeiner, S., Chun, F. K. H., Juengel, E., & Blaheta, R. A. (2020). Chronic sulforaphane administration inhibits resistance to the mTOR-inhibitor everolimus in bladder cancer cells. *International Journal of Molecular Sciences*, *21*(11), 4026.

Fuertes, M. A., Castilla, J., Alonso, C., & Prez, J. M. (2003). Cisplatin biochemical mechanism of action: from cytotoxicity to induction of cell death through interconnections between apoptotic and necrotic pathways. *Current medicinal chemistry*, *10*(3), 257-266.

McKeague, A. L., Wilson, D. J., & Nelson, J. (2003). Staurosporine-induced apoptosis and hydrogen peroxide-induced necrosis in two human breast cell lines. *British journal of cancer*, *88*(1), 125-131.

Xu, C., Wu, A., Zhu, H., Fang, H., Xu, L., Ye, J., & Shen, J. (2013). Melatonin is involved in the apoptosis and necrosis of pancreatic cancer cell line SW-1990 via modulating of Bcl-2/Bax balance. *Biomedicine & Pharmacotherapy*, *67*(2), 133-139.

Edıtor

Dr. Öğr. Üyesi Arif Hikmet ÇAKOĞLU

1994 yılında Atatürk Üniversitesi İnşaat Mühendisliği Bölümünden mezun oldu. Vatani görevini ifa ettikten sonra çeşitli firmalarda yol ve balıkçı barınağı inşaatlarında çalıştı. Aralık 1998'de Gençlik ve Spor Bakanlığı YURTKUR Gaziantep Bölge Müdürlüğünde inşaat mühendisi olarak devlet memurluğuna başlayıp aynı kurumun Trabzon ve Samsun Bölge Müdürlüklerinde -son iki yılı inşaat ve emlak şube müdürü olmak üzere- görev yaptıktan sonra 2018 yılı Haziran ayında Sinop Üniversitesi Boyabat MYO İnşaat Teknolojisi bölümüne öğretim görevlisi olarak atandı. 2003 yılında Karadeniz Teknik Üniversitesi (KTÜ) Fen Bilimleri Enstitüsünde Yüksek Lisansını, 2021 yılında Ondokuz Mayıs Üniversitesi FBE İnşaat Mühendisliği Bölümünde Doktorasını tamamladı. Yapı Malzemesi alanında çalışmalar yapmakta olup halen Sinop Üniversitesi Boyabat İİBF Gayrimenkul Geliştirme ve Yönetimi Bölümünde Doktor Öğretim Üyesi olarak görev yapmaktadır.

Dr. Lecturer Arif Hikmet ÇAKOĞLU

He graduated from Atatürk University Civil Engineering Department in 1994. After performing his military service, he worked in various companies in the construction of roads and fishermen's shelters. He started to work as a civil engineer at the Ministry of Youth and Sports YURTKUR Gaziantep Regional Directorate in December 1998 and worked in the Trabzon and Samsun Regional Directorates of the same institution -the last two years as the manager of the construction and real estate branch-. was appointed appointed as a lecturer at Sinop University Boyabat Vocational School of Construction Technology in June 2018. He completed his Master's Degree at Karadeniz Technical University (KTU) Institute of Science in 2003, and his PhD at Ondokuz Mayıs University FBE Civil Engineering Department in 2021. He is working in the field of Building Materials and still works as a Doctor Lecturer in the Department of Real Estate Development and Management of Sinop University Boyabat Faculty of Economics and Administrative Sciences

Edıtor

Muhammet Raşit SANCAR

2015 yılında Süleyman Demirel Üniversitesi Enerji Sistemleri Mühendisliği Bölümünden mezun oldu. Üniversite yıllarında enerji geri kazanımı ve yenilenebilir enerji alanında TÜBİTAK projeleri gerçekleştirdi. 2015 yılında Enerji sistemleri Mühendisliği Proje Ve Çözüm Derneği'nin kurucu başkanı olarak göreve başladı bu kapsamda Türkiye'de enerjide dışa bağımlılığın çözümlenmesi ve enerji üretiminin yenilenebilir enerjiden sağlanması konularında çalışmalar gerçekleştirdi. Aynı yılda yüksek lisans eğitimine yine Süleyman Demirel Üniversitesi Fen Bilimleri Enstitüsün Enerji Sistemleri Mühendisliği Anabilim Dalında başladı ve bu yıl içerisinde BEC tarafından genç enerji liderleri arasında seçildi. Yüksek lisans eğitimi sürecinde derneksel alanda ve akademik anlamda çalışmalarına devam ederek 2018 yılında yüksek lisans eğitimini bitirdi ve yine Süleyman Demirel Üniversitesinde aynı anabilim dalında YÖK 100/2000 öncelikli alanlarında doktora eğitimine başladı. Üniversitelerde gerçekleşen ayrılmalar sebebiyle Isparta Uygulamalı Bilimler Üniversitesi'nde doktora eğitimine devam etmekte olan Sancar doktora sürecinde Elektrikli araçlar ve fotovoltaik sistemler üzerine akademik çalışmalar gerçekleştirmektedir.

I graduated from the Energy Systems Engineering Department of Süleyman Demirel University in 2015. During my university years, I carried out TÜBİTAK projects in the field of energy recovery and renewable energy. In 2015, I started serving as the founding chairman of the Energy Systems Engineering Project and Solution Association, where I worked on solving energy dependence in Turkey and providing energy production from renewable sources. That same year, I started my master's degree at the Energy Systems Engineering Department of the Institute of Natural Sciences of Süleyman Demirel University and was selected among young energy leaders by BEC. During my master's education, I continued my work in the association and academic fields and completed my master's degree in 2018. I then started my doctorate in the same department at Süleyman Demirel University under the priority areas of YÖK 100/2000. Due to the separations in the universities, Sancar is continuing his doctorate education at Isparta Applied Sciences University and is conducting academic studies on electric vehicles and photovoltaic systems during his doctorate process.

Versatile Approaches to Engineering and Applied Sciences:
Materials and Methods

Dr. Arif Hikmet Çakoğlu
Dr. Muhammet Raşit Sancar

ÖZGÜR YAYINLARI

ISBN 978-975-447-569-2